UNIVERSITAT DE BARCELONA

Advances in carbon nanofiber-based supercapacitors

Allan Daragmeh

ADVANCES IN CARBON NANOFIBER-BASED SUPERCAPACITORS

Advances in carbon nanofiber-based supercapacitor

Allan Daragmeh

Directors de tesi. Dr. Albert Cirera Hernández i Dr. Llorenç Servera Serapio

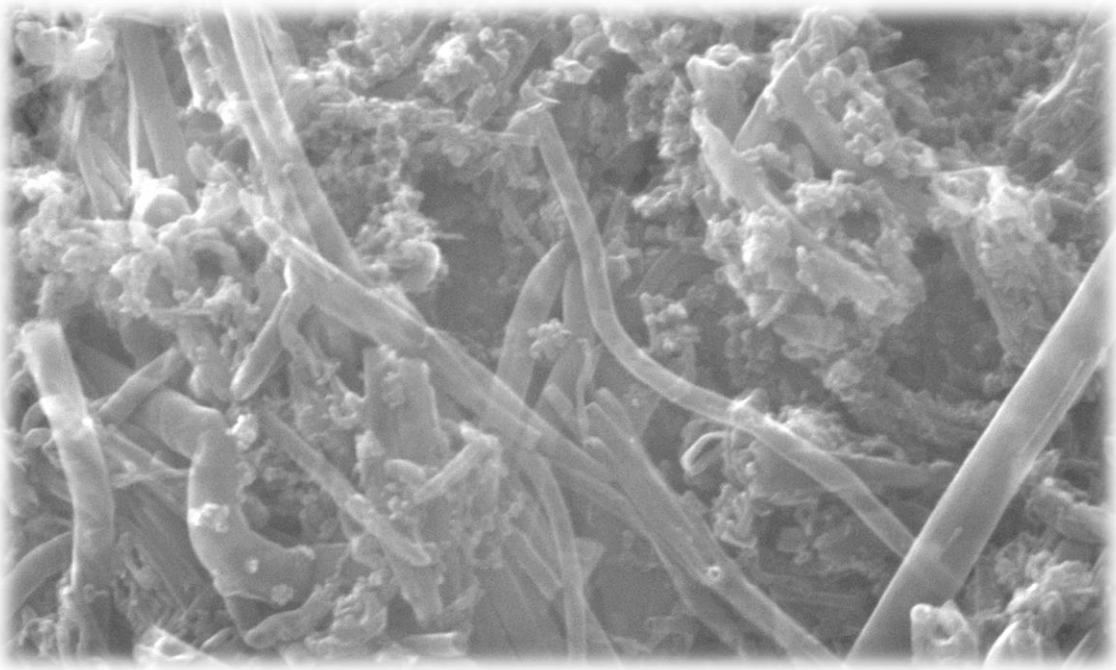

UNIVERSITAT DE BARCELONA

Advances in carbon nanofiber-based supercapacitor

MEMORIA PRESENTADA PER OPTAR AL GRAU DE DOCTOR PER LA UNIVERSITAT DE BARCELONA

UNIVERSITAT DE BARCELONA

PROGRAMA DE DOCTORAT EN NANOCIÈNCIES

Autor: Allan Daragmeh

Adreça de correu electrònic: allan.daraghmeh@ub.edu ,allan.d@najah.edu

Títol: Advances in carbon nanofiber-based supercapacitor

Universitat de Barcelona

Departament d'Enginyeria Electrònica i Biomèdica

Àrea de coneixement: Nanociències

Direcció de la tesi:

Dr. Albert Cirera Hernandez

Dr. Llorenç Servera Serapio

Juny 2017

Advances in carbon nanofiber-based supercapacitors

Summary report

Nowadays, our modern society huge challenges related to energy, savings as well as energy management, to improve and extend the standar of living to a growin population over 7000 million people, and do it with sustainable technologies becomes our main survival role play. Energy storage is a critical question to obtain a complete energy management system. Storage devices, suitably controlled by modern fast power electronic converters, may play a fundamental role in facing the challenge of global energy savings. In the present work, a new storage system based in electrochemical double layer capacitor has been developed and tested. The present doctoral thesis gives background related to energy storage based on supercapacitors. It attempts to place the supercapacitor device in context of available and future technologies for alternative energy systems management. Limitations of cells and electrodes are introduced. Ionic transport in active carbon and carbon nanofiber electrodes and possible restrictions in carbon nanostructured porous systems are studied and a novelty method to solve them are described. There are some open issues in the supercapacitor development, in this thesis the major challenges are introduced and how we can go beyond them, become the major objective. The results from the studies are presented in this thesis together with the scientific papers this thesis is based on.

Resum

Avui en dia, en les societats modernes, tenim l'important repte de fer sostenible el consum d'energia i al mateix temps salvaguardar els estàndards de qualitat de vida, en un planeta amb mes de 7.000 milions de persones, per això en l'acord de Paris (2015) es va marcar com objectiu que l'increment de temperatura mundial quedi per sota dels 2ºC, per aconseguir aquest objectiu s'han de reduir les emissions de gasos que influeixen negativament en l'efecte hivernacle.

Reduir les emissions de gasos passa per un us mes racional de les diferents fonts d'energia, prioritzant l'energia elèctrica, que ha mostrat ser la menys contaminat. Un ús eficient de l'energia elèctrica passa pel desenvolupament de nous sistemes per emmagatzemar l'energia elèctrica, tant pel seu ús en sistemes de transport com per el nou paradigma de les ciutats intel·ligents.

En aquest treball s'ha proposat:

1.- Estudiar els sistemes d'emmagatzematge elèctric basats en supercondensadors, des de les diferents parts que formen el supercondensador, s'han analitzat a fons les tres parts principals que conformen el supercondensador: Els elèctrodes, els separadors i l'electròlit. S'ha dedicat un especial esforç al estudi i disseny de nous elèctrodes, per això, s'han fet servir nanofibres de carbó, comprovant l'efecte del dopat de les nanofibres de carboni amb òxid de manganès millora de forma notable els valors de la capacitat especifica, arribant a valors de 812 F/g mesurats amb una rampa de tensió de 5 mV/s, i també, pensant en una futura industrialització del procés de fabricació, s'ha estudiat en profunditat la concentració i el tipus de polímer que es pot fer servir com a "binder" per mantindré l'estructura mecànica del elèctrode.

2.- Desenvolupar un nou sistema basat en l'ús de nano estructures carbonoses per la fabricació d'elèctrodes de supercondensadors de alta eficiència. S'ha estudiat l'efecte de fer servir nanofibres de carbó juntament amb carbó activat per millorar la resposta tant pel que fa a la capacitat especifica com a la resistència sèrie equivalent (ESR), s'han obtingut valors de capacitat especifica de 334 F/g fent servir únicament carbó activat i

de 52 F/g amb nano fibres, fent servir sempre una rampa de tensió de 5 mV/s. Pel que fa a la ESR, les nanofibres, com era d'esperar, ens proporcionen el valor mes baix (0.28 Ω) en comparació als valors obtinguts fent servir carbó activat (3.72 Ω).

Per aprofitar les millors característiques de les nano fibres i del carbó activat, s'ha estudiat quina es la millor relació entre elles: (90% de AC / 10% de CNFs) amb això el millor valor obtingut ha estat de 207 F/g.

3.- Estudiar el fenomen de la conductivitat iònica a l'interior de les estructures carbonoses dels elèctrodes i desenvolupar una millora que permeti reduir la resistència sèrie equivalent (ESR). Pensant en la sostenibilitat, s'ha dedicat un esforç especial al estudi i desenvolupament d'electròlits en base aquosa, que permetin optimitzar els valors de resistència sèrie equivalent (ESR) al mateix temps que s'ha evitat fer ús de productes nocius pel medi ambient o que requereixin de processos industrials complicats per la seva obtenció. En base a això, s'ha comprovat que el millor electròlit de base aquosa es la dissolució 1M de KOH, malgrat que aquesta es reactiva a l'alumini i complica el posterior procés d'encapsulat. Finalment s'ha optat per el sulfat de sodi (Na_2SO_4) que ha estat fet servir com ha referencia en bona part del estar del art, malgrat això, s'ha comprovat que la concentració del aigua del Mart Mort, que conté bàsicament clorurs de magnesi i potassi també dona uns resultats acceptables.

4.- Estudiar els efectes de la auto descàrrega i proposar un nou tipus de separadors que permeti millorar aquest paràmetre, seguint el model del supercondensador, seria fer que la resistència paral·lel sigui d'un valor el mes gran possible. Un dels elements constituents dels supercondesandors que ha estat poc estudiat en la literatura científica es el separador, habitualment es fa servir cel·lulosa, en aquest estudi s'ha estudiat l'efecte del separador de cel·lulosa en comparació amb un separador de fibra de vidre i per últim s'ha comprovat que les membranes conductores iòniques, que habitualment es fan servir en les bateries de flux, ens proporcionen els millors resultats pel que fa als valors de la resistència paral·lel.

Acknowledgements

This thesis is dedicated to the Palestinian people and to all people that make a lot effort to achieve scientific improvements**.** Many thanks to my advisor Dr. Albert Cirera and Dr. Llorenç Servera to lighting the path in my work. Special thanks to Dr Shazad Hussain and all the researchers in the nanoelectronics lab for their help and support. Special thanks and appreciation for committee of AVEMPACEIII/Erasmus Mundus program for giving me the chance to pursue my PhD degree at Universitat de Barcelona. This work would not have been possible without the unconditional support of my parents, brothers and sisters. Thanks to them for encouraging supporting and loving me.

Contents

List of figures

Background

To build a sustainable future, energy source needs to be non-fossil-based, ideally, it should be reliable, affordable and inexhaustible. [1] Reducing fossil fuel consumption and greenhouse gas emissions has become global objectives being recognized as an imperative for the sustainable development of economy and society. European Union has set a goal by 2020 to reduce greenhouse gas emissions by 20%, drawing 20% of energy from renewable sources, and cutting the EU-wide energy use by 20%. [2] It is essential to explore natural and renewable energy sources to take place of those classical fossil sources, encouraging us to seek greener and more efficient energy technologies to meet the increasing energy demands. Energy conversion and storage plays the key role in achieving global energy sustainability. To date, numerous energy conversion and storage technologies, such as solar cell, fly wheel, compressed air, fuel cell, supercapacitor and battery, have been developed with the goal of utilizing sustainable energy sources, such as solar, wind, geothermal, tidal or biomass energy. [1] Supercapacitors and batteries have been proven to be the most effective electrochemical energy conversion and storage devices for practical application. Briefly, supercapacitors store charge at the electrode/electrolyte interface via electrical double layer or reversible faradic reactions, while batteries directly convert chemical energy into electrical energy by exothermal redox reactions. [2] Innovative materials design lies at the heart of developing advanced energy storage devices. Further breakthroughs in electrode materials design hold the key to next-generation energy storage devices. Ideally, energy storage materials are produced by using renewable resources via simple, low cost and environmentally friendly methods, with controllable morphologies, rich porosity, modified surface chemistry and appropriate functionalities. To transform such science fantasy into reality, more efforts should be devoted to designing and synthesizing high-performance, sustainable electrode materials. Green and renewable energy supplies [3, 4], like solar energy [5], wind power [6], hydro power [7], biogas [8] and even nuclear energy [9], have attracted great attentions over the past decades. However, considerable disadvantages, like instable support (solar &wind energy), low efficiency (solar), limited life cycle of device (solar), geographic restrictions (wind & hydro power), and potential risks (nuclear energy), become obstacle. [10-12] for vast applications of these energy forms. To solve reliability

issue of the green energy supplies, energy storage systems play an important role. Such systems store and release energy whenever needed to satisfy industrial and social demands. Typically, there are mainly four types of energy storage devices -conventional capacitors, batteries, fuel cells and electrochemical supercapacitor. [3] Conventional capacitors. [13] Store and retrieve energy by achieving non-Faradaic accumulation and releasing opposite charges electrostatically on the surfaces of two electrodes separated by vacuum space or dielectric layer. The charge/discharge cycle is highly reversible. Batteries [14] provide (or "provide/restore" for rechargeable batteries) energy by outputting (or "outputting/inputting") Faradaic current, generated by reduction or oxidation of some chemical substrates at electrodes with phase change. Fuel cells [15] convert chemical energy directly to electrical energy by reduction of oxidant and oxidation of fuel through internal electrolyte, usually with help of high efficient catalyst (Pt). To some degree, it is more precise to use "energy generator" to describe fuel cells, rather than "energy storage device". Supercapacitors, which are also called electrochemical capacitors or ultracapacitors, have attracted much attention in recent years because of their pulse power supply, long cyclic life (>100 000 cycles), simple operational mechanism, and high dynamics of charge propagation. [15,16] Supercapacitors have a high-power capability and relatively large energy density compared to the conventional capacitors, which have already enabled supercapacitors to be applied in a variety of energy storage systems. For example, they are already used in memory back-up systems, consumer electronics, industrial power supplies, and energy management. [17] A more recent application is the use of supercapacitors in emergency doors on Airbus A380, highlighting their safe and reliable performance. [18] In such cases, supercapacitors are coupled with primary high energy batteries or fuel cells to serve as a temporary energy storage device with a high-power capability. Electrochemical rechargeable batteries are energy storage devices. A variety of rechargeable batteries is now available commercially. As an example, lithium batteries are quite popular because of their excellent properties like weight/energy ratio and low self-discharge rates [19, 20]. Scientists are interested in supercapacitors because they offer solutions to energy storage and delivery applications in systems where a high-power output is required, such as in fully electric cars. They present a low energy density and a high-power density, as compared to batteries which have high energy density and low power density. Moreover, supercapacitors provide a long cycle life [19, 20] and quick ability to discharge and

charge. Other advantages include simple operating principles and modes of construction as well as cheap materials. Supercapacitors are likely to show an equal importance as batteries for future energy storage systems. The energy storage density and power delivery capability of various systems are summarized in a Ragone plot shown as Figure 1.1. Typical supercapacitors can store up to 1-10 Wh kg^{-1} of energy and deliver up to 10^5 W kg^{-1} of power. In comparison, the specific energy contained in conventional capacitors and batteries amount to less than 0.1 and up to a few hundred Wh kg^{-1} respectively. Likewise, conventional capacitors can deliver up to 10^7 W kg^{-1} of power, whereas batteries have up to about 10^3 W kg^{-1} of specific power capability. The plot area covered by supercapacitors overlaps at both ends with that of capacitors (at the high power, low energy end) and that of batteries (at the high energy, low power end). More importantly, the information provided in Ragone plots for supercapacitors and batteries most often only refer to the capability of the active materials. Actual device performance may be quite significantly lower, as in those cases the weight of the electrolyte, current collectors and device housing, need to be considered.

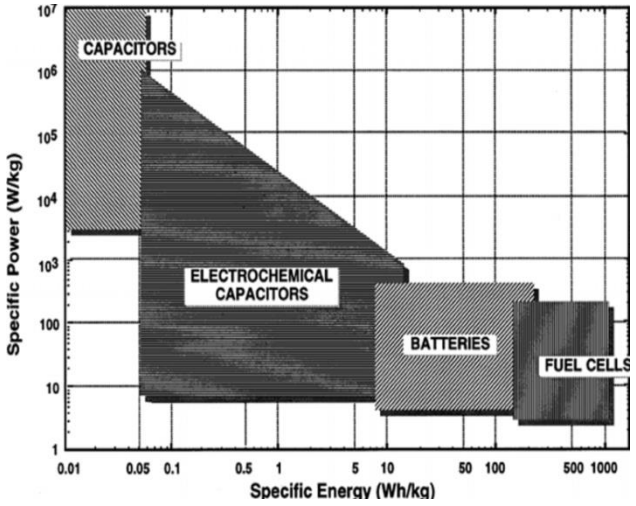

Figure 1.1(b) Ragone plot of various energy storage and conversion devices. Figure from Winter and Brodd. [18]

Supercapacitors do not function as the sole power source component; more often they are used together with other devices to form hybrid systems. For example, the battery-supercapacitor hybrid. [21] The fuel cell-supercapacitor hybrid. [22] and the fuel cell-battery-supercapacitor hybrid [23, 24] have been investigated for use in electric vehicles. The application of supercapacitors in hybrid or electric vehicles is currently an extremely active area for research. [25-27] but these examples also highlight that none of the

individual batteries, supercapacitors or fuel cell units could perform up to the required energy and power standards in cars. In these cases, owing to the high-power capability of supercapacitors, energy and current is drawn preferentially when the vehicle requires acceleration, while batteries or fuel cell units can be used during constant speed cruising as they store more energy and therefore prolong the drive distance. Supercapacitors have also been used in vehicles for regenerative braking, with braking energy recovery close to 70 %.5. The difference between renewable energy sources is presented in table 1.A supercapacitor is a specially designed capacitor which has a very large capacitance. Supercapacitor combine the properties of capacitor and batteries into one device. Supercapacitor can store hundreds or thousands of times more energy than conventional capacitors but still low energy density than batteries. Due to the fast charging discharging time of supercapacitors can be used to operate low power equipment such as mobile devices component toward high-power equipment such as power supply.

Table 1.1 Comparison of the performances for battery, capacitor and supercapacitor [28].

	Battery	Capacitor	Supercapacitor
Discharge time	0.3 - 3 hrs	10-3 to 10-6 sec	0.3 - 30 sec
Charge time	1 - 5 hrs	10-3 to 10-6 sec	0.3 - 30 sec
Energy density (Wh/kg)	10 - 100	< 0.1	1 - 10
Power density (W/kg)	50 - 200	> 10,000	1000 - 2000
Charge/discharge efficiency	0.7 – 0.85	≈1	0.85 – 0.98
Cycle life	500 - 2000	> 500,000	> 100,000

Objective of thesis

The present doctoral thesis gives background related to energy storage based on supercapacitors. It attempts to place the supercapacitor device in context of available and future technologies for alternative energy systems management. Limitations of cells and electrodes, ionic transport in active carbon and carbon nanofiber electrodes and possible restrictions in carbon nanostructured porous systems and key challenges in the supercapacitor development are introduced, how we can go beyond it's the major objective of this work.

- learn about supercaps in depth: important parameters, technologies, how to test it
- design a procedure to test supercaps
- design a procedure for long live cycling test
- define a single cell supercap test prototype
- test different carbon nanofibres tapes and separators and select the best
- Test different binder polymer and study the effect of binder concentration.
- Study the effect of pressure force smaller to higher for the preparation of electrodes.
- modify carbon nanofibers with MnO_2 (and maybe other oxides) and select best procedure and concentration
- Test CNFs and Activated carbon (AC) alone
- Prepare electrode based on mixture of CNF and AC to increase the capacitance and decrease ESR and enhance the power and energy density.
- Considering the significant effects of pore structure on the capacitance performance of supercapacitor electrodes.
- Study the surface area, pore size distribution, morphology and structure for each sample by Brunauer–Emmett–Teller method, SEM and TEM.
- Improve the cycle stability of the electrode material.
- Study the effect of the electrode thickness on performance

The results from the studies are presented in this thesis together with the scientific research papers.

Structure of thesis

Chapter 1

Provides a theoretical background of supercapacitors and presents a comprehensive literature review on the working principle of supercapacitors and the electrode materials for supercapacitors.

Chapter 2

Describes the electrochemical techniques and material characterization methods employed in this thesis

Chapter 3.

This chapter reports the use of flexible tape casting of dense carbon nanofiber (CNFs) alone and in hybrid structure with MnO_2 for supercapacitor applications. Different electrolyte concentrations of potassium hydroxide (KOH) were tested and it was founded that mild concentrated electrolyte provides higher specific capacitance. Afterwards a novel, fast and simple method is adopted to achieve a hybrid nanostructure of CNFs/MnO_2 with various $KMnO_4$ ratios. SEM, TEM, BET and Raman analysis were performed to study the morphology, surface area, porous structure and quality of material. Electrochemical characterization was performed to study the supercapacitor properties.

Chapter 4

In this chapter preparation of symmetric supercapacitors by carbon nanofibers (CNF) and activated carbon (AC) using similar proportions of binder PVDF polymer in an aqueous electrolyte has been demonstrated. SEM, TEM, BET analysis was performed. The prepared electrodes were tested electrochemically.

Chapter 5

This chapter discuss the impact of binder PVDF concentration (5, 10 and 20 wt.%) and pressure force (3, 7, 14 and 20 ton) for the fabrication of electrodes based on Carbon nanofibers (CNFs) for supercapacitors. The surface area, pore size distribution and morphology were characterized by Brunauer–Emmett–Teller method, SEM and TEM. The two-electrode system tested in aqueous solution to study the electrochemical properties.

Chapter 6

This chapter discuss the mixture of active carbon with carbon nano fiber as electrode for supercapacitors with same concentration of binder PVDF. all sample tested in 6M KOH aqueous solution. The surface area, pore size distribution and morphology were characterized by Brunauer–Emmett–Teller method, SEM and TEM.

Chapter 7

Conclusions.

References

[1] Tarascon JM. Key challenges in future Li-battery research. Phil Trans R Soc A. 2010;368:3227–3241.

[2] Conway BE. Electrochemical science and technology. Transition from “supercapacitor” to “battery” behavior in electrochemical energy storage. J Electrochem Soc. 1991;138:1539–1548

[3] C. W. J. Van Koppen, "The potential of renewable energy sources," Resources and Conservation, vol. 7, pp. 17-36, 1981.

[4] B. Sorensen, "Renewable Energy - A Technical Overview," Energy Policy, vol. 19, pp. 386-391, May 1991.

[5] S. Baron, "Solar-Energy - Will It Conserve Our Non-Renewable Resources," Transactions of the American Nuclear Society, vol. 30, pp. 9-10, 1978.

[6] B. Sorensen, "Energy and Resources: A plan is outlined according to which solar and wind energy would supply Denmark's needs by the year 2050," Science, vol. 189, pp. 255-60, 1975.

[7] S. P. Simonovic and L. M. Miloradov, "Potential hydroenergy production by optimization,"Journal of Water Resources Planning and Management-Asce, vol. 114, pp. 101-107, Jan 1988.

[8] M. Balat and H. Balat, "Biogas as a Renewable Energy SourceA Review," Energy Sources Part a-Recovery Utilization and Environmental Effects, vol. 31, pp. 1280-1293, 2009.

[9] W. D. Harkins, "The neutron, the intermediate or compound nuclous, and the atomic bomb," Science (New York, N.Y.), vol. 103, pp. 289-302, 1946 Mar 1946.

[10] X. F. Zheng, C. X. Liu, Y. Y. Yan, and Q. Wang, "A review of thermoelectrics research – Recent developments and potentials for sustainable and renewable energy applications," Renewable & Sustainable Energy Reviews, vol. 32, pp. 486-503, Apr 2014.

[11] Z. Hameed, Y. S. Hong, Y. M. Cho, S. H. Ahn, and C. K. Song, "Condition monitoring and fault detection of wind turbines and related algorithms: A review," Renewable & Sustainable Energy Reviews, vol. 13, pp. 1-39, Jan 2009.

[12] M. T. Dunham and B. D. Iverson, "High-efficiency thermodynamic power cycles for concentrated solar power systems," Renewable & Sustainable Energy Reviews, vol. 30, pp. 758-770, Feb 2014.

[13] B. E. Conway, Electrochemical Supercapacitors. Scientific Fundamentals and Technological Applications. New York, Boston, Bordrecht, London, Moscow: Kluwer Academic/Plenum Publishers, 1999.

[14] R. J. Brodd, K. R. Bullock, R. A. Leising, R. L. Middaugh, J. R. Miller, and E. Takeuchi, "Batteries, 1977 to 2002," Journal of the Electrochemical Society, vol. 151, pp. K1-K11, Mar 2004.

[15] W. E. Winsche, K. C. Hoffman, and F. J. Salzano, "Hydrogen: Its Future Role in the Nation's Energy Economy," Science (New York, N.Y.), vol. 180, pp. 1325-32, 1973 Jun 1973.

[16] A. Du Pasquier, I. Plitz, J. Gural, S. Menocal, and G. Amatucci, "Characteristics and performance of 500 F asymmetric hybrid advanced supercapacitor prototypes," Journal of Power Sources, vol. 113, pp. 62-71, Jan 2003.

[17] A. Burke, J. Power Sources, 2000, 91, 37.

[18] M. Winter and R. J. Brodd, Chem. Rev., 2004, 104, 4245.

[19] Ping Liu, Mark Verbrugge, Souren Soukiazian, Influence of temperature and electrolyte on the performance of activated-carbon supercapacitors, Journal of Power Sources 156 (2006) 712–718.

[20] H. Gualous, R. Gallay, A. Berthon, Utilisation des supercondensateurs pour les stockages de l'énergie embarquée: applications transport, Revue de l'électricité et de l'électronique (2004); 8:82,83-90.

[21]. B. Frenzel, P. Kurzweil and H. Roennebeck, J. Power Sources, 2011, **196**, 5364-5376.

[22]. R. Kotz, S. Muller, M. Bartschi, B. Schnyder, P. Dietrich, F. N. Buchi, A. Tsukada, G. G. Scherer, P. Rodatz, O. Garcia, P. Barrade, V. Hermann and R. Gallay, in Batteries and Supercapacitors, 2003, pp. 564-575.

[23]. A. K. Shukla, C. L. Jackson and K. Scott, Bull. Mater. Sci., 2003, **26**, 207-214.

[24]. G. Pede, A. Iacobazzi, S. Passerini, A. Bobbio and G. Botto, J. Power Sources, 2004, **125**, 280-291.

[25]. M. Mastragostino and F. Soavi, J. Power Sources, 2007, **174**, 89-93.

[26]. D. Iannuzzi and Ieee, in Iecon 2007: 33rd Annual Conference of the Ieee Industrial Electronics Society, Vols 1-3, Conference Proceedings, Ieee, New York, 2007, pp. 539-544.

[27]. D. Iannuzzi and P. Tricoli, in SPEEDAM 2010 International Symposium on Power Electronics, Electrical Drives, Automation and Motion, Pisa, Italy, 2010.
[28] - S. Bose, T. Kuila, A. K. Mishra, R. Rajasekar, N. H. Kim, and J. H. Lee, "Carbon-based nanostructured materials and their composites as supercapacitor electrodes," Journal of Materials Chemistry, vol. 22, pp. 767-784 201

Chapter 1: Supercapacitor

1.1. Overview.

Supercapacitors are called with several names such as electrochemical capacitors, ultra-capacitors and electrochemical double-layer capacitors. In 1957 Becker suggested a capacitor based on porous carbon material with high surface area to store electrical energy for practical purposes. The principle involved was charging of the capacitance, C_{dl}, of the double layer, which arises at all solid/electrolyte interfaces, such as metal, semiconductors and colloid surfaces. After Becker, the Sohio Corporation in Cleveland, Ohio, also utilized the double layer capacitance of high-area materials in a non-aqueous solvent containing a dissolved tetra-alkyl ammonium salt electrolyte [1]. In late 70's and 80's, Conway and coworkers made a great contribution to the capacitor research work based on RuO_2, which has high specific capacitance and low internal resistance. In the 90's, supercapacitors received much attention in the context of hybrid electric vehicles.

Commercial productions of supercapacitors in nowadays markets are basically from the high surface area porous carbon materials as well as noble metal oxides systems. For instance, Matsushita Electric Industrial (Panasonic, Japan) developed gold capacitors, as high-performance supercapacitors for military applications that were produced by Pinnacle Research (USA). The commercial supercapacitors are widely used as power sources for activators, elements for long time constant circuits, standby power for random access memory devices, and hand phone equipment. Batteries are typically low power devices compared to conventional capacitors that have power densities as high as 10^6 Wk/g, but low energy densities. From this point of view, supercapacitors (Ultracapacitors) combine the properties of high power density and higher energy density, and show long life cycles due to the absence of chemical reactions [2]. A graphical taxonomy of the different classes and subclasses of supercapacitors is presented in (figure 1.1-b).

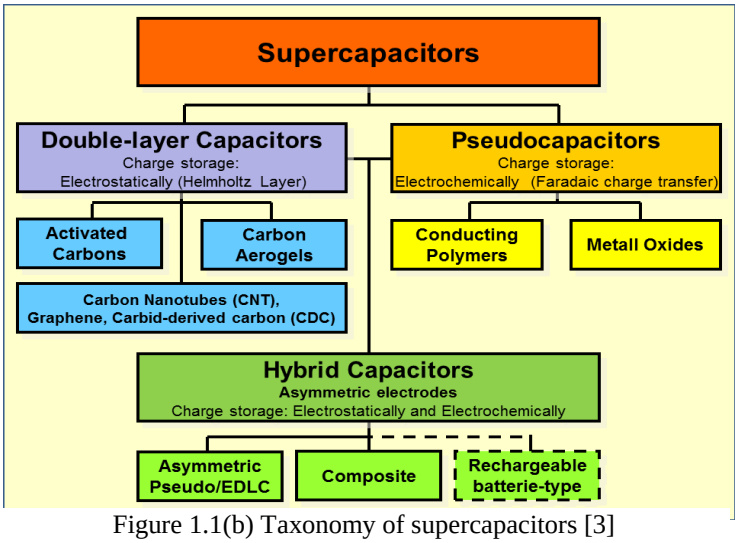

Figure 1.1(b) Taxonomy of supercapacitors [3]

Carbon materials are mostly used for capacitor as it provides large surface area. The capacitance value of EDLC is dependent on adsorption of the ions, which moves from the electrolyte to the electrode surface. Therefore, charge storage in EDLC is highly reversible with high cycling stabilities [4]. In addition, the performance of the EDLC can be adjusted by using different type of electrolytes. EDLC can also operate with either an aqueous or organic electrolyte or ionic electrolytes. Aqueous electrolytes, such as sulfuric acid (H_2SO_4) and potassium hydroxide (KOH) normally presents lower equivalent series resistance (ESR) and lower minimum pore size requirement compared to organic electrolyte. However, aqueous electrolytes also provide narrow window of voltage ranges. Thus, the trade-off between the capacitance, ESR and window of voltage range should be considered in the use of electrolyte. [5, 6], Figure 1.1 illustrates the key technology for the EDLC.

1.2 Principle of supercapacitor

Supercapacitors are made of two electrodes immersed in an electrolyte solution, with one separator between them. The process of energy storage is associated with buildup and separation of electrical charge accumulated on two conducting plates spaced some distance apart.

Conventional capacitors based on two conducting electrodes of equal area A and separated by a distance d in vacuum. When a voltage is applied to a capacitor, opposite

charges build up on the surfaces of each electrode. The charges are kept separate by the dielectric, thus producing an electric field that allows the capacitor to store energy. In a plane capacitor with a pair of plates of equal area, capacitance C is given by (equation 1.1),

$$C = \frac{A}{4\pi d} \tag{1.1}$$

If the plates are separated by a dielectric medium the capacitance is given by (equation 1.2).

$$C = \frac{A\varepsilon}{4\pi d} \tag{1.2}$$

Supercapacitors store energy in a similar way, but the charge does not accumulate on two conductors separated by a dielectric. Instead, the charge accumulates in the electric double layer at the interface between the surface of a conductor and an electrolyte solution. When charged, the negative ions in the electrolytes will diffuse to the positive electrode, while the positive ions will diffuse to the negative electrodes [2].

A typical supercapacitor consists of three basic components, the electrodes, the electrolyte, and the separator (figure 1.2). The overall performance of supercapacitors is determined by the physical properties of both the electrode and the electrolyte materials. However, the electrode is one of the most basic constituent for charge storage/delivery, and plays an important role in determining the energy and power densities of a supercapacitor. The electrochemical performance of a supercapacitor can be characterized by cyclic voltammetry and galvanostatic charge–discharge measurements. The capacitance (*C*) is determined from the constant current discharge curves according to (equation 1.3).

$$C = \frac{I}{\left(dv/dt\right)} \tag{1.3}$$

Where *I* is the discharge current and dv/dt is calculated from the slope of the discharge curve. Then, the specific capacitance (C_{SP}) for one electrode in a supercapacitor can be calculated using the following (equation 1.4):

$$C_{sp}(Fg^{-1}) = \frac{4C}{M} \tag{1.4}$$

Where *C* is the measured capacitance for the two-electrode cell and *m* is the total mass of the active materials in both electrodes.

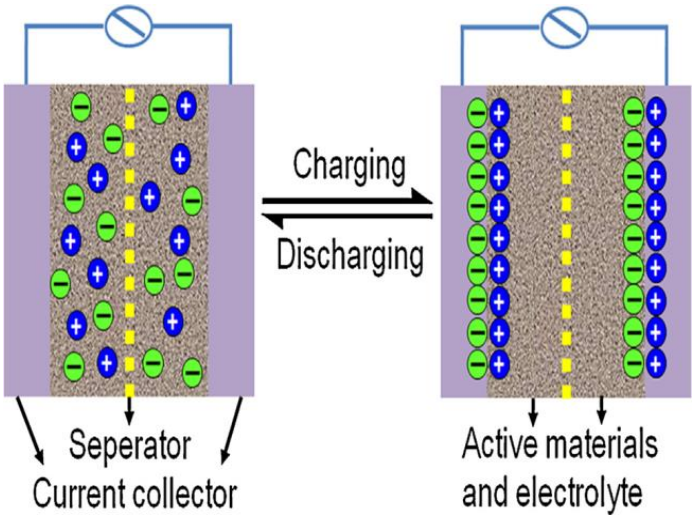

Figure 1.2 Schematic illustration of the charging/discharging process in a supercapacitor [7].

The stored energy (*E*) and the power density (*P*) in a supercapacitor can then be calculated from (equations 1.5, 1.6) respectively.

$$E = \frac{(CV^2)}{2} \tag{1.5}$$

$$P = \frac{V^2}{(4R_s)} \tag{1.6}$$

Where *C* (*F/g*) is the total capacitance of the cell, V is the cell voltage, and R_S is the equivalent series resistance [8].

Capacitors can be classified as film-type (dielectric), electrolytic and supercapacitors. Electrolytic capacitors based on aluminum foils and liquid electrolytes are well-known for many decades. In them a thin film (thickness in the order of micrometers) of aluminum oxide prepared by electrochemically oxidizing the Al foils serves as dielectric film. Their

specific energy is of the order of some hundredths Wh/L [2]. Due to different energy storage mechanisms, supercapacitors could be differentiated into two categories: electrical double-layer capacitors (EDLCs) and pseudocapacitors. EDLCs could demonstrate 1 to 5 % pseudocapacitance out of its total capacitance due to the Faradaic reactivity of the surface functional groups, on the surface of carbon material. The pseudocapacitors usually show 5-10 % electrostatic double-layer capacitance, which is proportional to the electrochemically accessible interfacial area [1].

1.2.1 Electric double layer

Electrical double layer results from strong interactions between the ions/molecules in the solution and the electrode surface. At a metal-solution interface, there is a thin layer of charge on the metal surface that results from an excess or deficiency of electrons. On the other hand, near the electrode surface, there is an opposite charge in solution due to an excess of either cations or anions. Thus, the electrical double layer is made up of the whole array of charged species and oriented dipoles existing at the metal-solution interface [2].

The electrochemical process for the double-layer capacitor can be written as;

Positive electrode

$$E_s{}^{+} + A^{-} \leftrightarrow E_s{}^{+} \,//\, A^{-1} + e^{-1} \tag{1.7}$$

Negative electrode

$$E_s{}^{-} + C^{+} + e^{-} \leftrightarrow E_s{}^{-} \,//\, C^{+} \tag{1.8}$$

Overall reaction

$$E_s{}^{+} + E_s{}^{-} + C^{+}A^{-} \leftrightarrow E_s{}^{+} \,//\, A^{-1} + E_s{}^{-} \,//\, C^{+} \tag{1.9}$$

Where *E* represents the carbon electrode surface, // represents the double layer where charges are accumulated on the two sides of the double layer and *C* and *A* represent the cation and the anion of the electrolyte, respectively. As shown in (equations. 1.7 and 1.8), during the charge, electrons are forward from the positive electrode to the negative electrode through the external power sources; at the same time, positive and negative ions are separated from the bulk electrolyte and moved to the electrode surfaces. During the

discharge, electrons move from the negative electrode to the positive electrode through the load, and ions are released from the electrode surface and moved back into the bulk of the electrolyte. As shown in the overall reaction, the salt (C^+A^-) in the electrolyte is consumed during charge, so the electrolyte can also be considered as an active material [9]. In view of this, only electrons would be transported to and from the electrode surfaces through the external circuit, and anions and cations of the electrolyte moved within the solution to the charged surfaces. Theoretically, no chemical or phase changes are involved or no charge transfer takes place on the interface of electrode and electrolyte [10]. Due to the purely physical formation of the EDL without electrochemical reactions, the charging of EDL capacitors (*EDLCs*) is very rapid. This fundamentally differs from batteries, where energy is stored through redox processes. *EDLCs* can deliver very high-power densities (~15 kW/kg) compared to, for example, Li-ion batteries (up to about 2 kW/kg). [7]

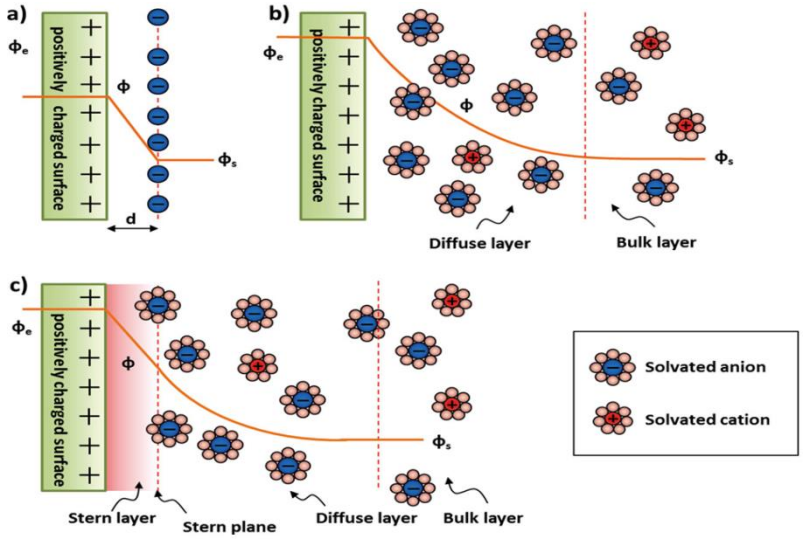

Figure 1.3 (a) Helmholtz, (b) Gouy-Chapman, and (c) Stern model of the electrical double-layer formed at a positively charged electrode in an aqueous electrolyte. The electrical potential, ∅, decreases when transitioning from the electrode, φ e , to the bulk electrolyte infinite away from the electrode surface, ∅ **s** . The Stern plane marks the distance of closest approach of the ions to the charged surface. Note the absence of charges/ions in the Stern layer. The diffuse layer starts in the range of 10 – 100 nm from the electrode surface. [7]

As shown in (figure 1.3) the charge accumulation is established across the double-layer, which is composed of a compact layer (Helmholtz layer) with the thickness about 0.5-0.6 nm, equivalent to the diameters of the solvent molecules and ions reside on it, and a wider region of diffuse layer with dimensions over 1 to 100 nm, depending on the concentration of the electrolyte. It is just owing to the small thickness of the compact molecular interfacial layer that a quite larger *SC* could arise for an EDLC, compared to that of a conventional capacitor, where the separation distance is within the micro meter range. The energy is stored within the electrochemical double-layer at the electrode-electrolyte interface using the charge separation mechanism. The electrochemical capacitor has two electrodes made from porous, high surface area materials immersed in an electrolyte and separated by a semi permeable separator which permeable to only ions in electrolyte. When voltage is applied, there will be a charge on the electrode and electrolyte due to excess or deficiency of electrons. This charge resides in a very thin layer (<0.1 Å) on the surface. The charge in solution is an excess of either cations or anions near the electrode surface. A whole array of oppositely charged ions exists at the electrode electrolyte interface and hence the electrochemical capacitor is also called double layer capacitor. The electrical double-layer mechanism, which arises from the electrostatic attraction between the surface charges of activated carbon and ions of opposite charge, plays the major role in carbon/carbon supercapacitors. The Helmholtz model [11] describes the charge separation at the electrode/electrolyte interface when an electrode of surface area **A** is polarized. Under this condition, ions of opposite sign diffuse through the electrolyte to form a condensed layer with a thickness of a few nanometers in a plane parallel to the electrode surface ensuring charge neutrality. This accumulation of charges is called electrical double layer (EDL). The potential near the electrode then decreases when the distance d (m) between the ions and the electrode increases (Figure 1.3. a). This simplified Helmholtz double-layer (DL) can be regarded as an electrical capacitor of capacitance C_H defined by Equation (1.10).

$$C_H = \in_r \in_0 \frac{A}{d} \qquad (1.10)$$

Where $\in_r$ and $\in_0$ are the dielectric constants of the electrolyte and vacuum, respectively, and *A* is the specific surface area of electrode/electrolyte interface (accessible surface area). And d is the effective thickness of the D_L, often approximated as the Debye length.

Considering the very large specific surface area of porous carbon electrodes (up to 3000 m^2 /g) and a Debye length in the range of <1 nm, the resulting capacitance of D_L's will be much higher than for flat plate capacitors. Helmholtz model does not take into account several factors such as the diffusion of ions in the solution and the interaction between the dipole moment of the solvent and the electrode, Gouy and Chapman proposed a diffuse model of the EDL in which the potential decreases exponentially from the electrode surface to the fluid bulk (Figure1.3 a). [12] Gouy-Chapman model is insufficient for highly charged double-layers, however, the Gouy & Chapman model overestimated the capacitance arising from charged ions close to the electrode surface. In 1924, Stern. [13] Suggested a model combining the Helmholtz and Gouy-Chapman models by accounting for the hydrodynamic motion of the ionic species in the diffuse layer and the accumulation of ions close to the electrode surface (Figure1.3 c). These two layers are equivalent to two capacitors in series, $\boldsymbol{C}_H$ (Helmholtz layer) and $\mathbf{C}_D$ (diffuse layer), and the total capacitance of the electrode (C_{DL}) is given by Equation (1.11) :

$$\frac{1}{C_{DL}} = \frac{1}{C_H} + \frac{1}{C_D} \qquad (1.11)$$

1.2.2 Pseudocapacitors

In contrast to EDLCs, that store charge electrostatically, pseudocapacitors store charge faradaically through the transfer of charge between electrode and electrolyte. This is accomplished through electrosorption, reduction-oxidation reactions, and intercalation processes. The pseudocapacitors may be allowed to achieve greater capacitance properties and energy densities than EDLCs by presence of Faradaic processes. Two types of electrode materials are served to store charge in pseudocapacitors: (i) metal oxides and (ii) conducting polymers [14]. Pseudocapacitance is Faradaic in origin, involving charge transfer across the double-layer, which is the same as in the charging and discharging of batteries, but such capacitance originates due to some specific applied thermodynamic conditions, the electrode potential (V) is some continuous function of the charge (q) that passes through the electrode, so that a derivative dq/dV exists, which is tantamount to and measurable as the capacitance. The capacitance possessed by such systems is referred to as pseudocapacitance since it arises in a quite different way from

that exhibited by an EDLC, where ideally no charge transfer takes place and capacitance originates in an electrostatic way [10].

1.3 Electrode materials for supercapacitors

Based upon the chemical composition, several types of supercapacitor electrode materials have been intensively investigated that include different type of carbon materials, e.g. carbon aerogel, activated carbon, carbon nanofibers, grapheme and CNTs as well as electrically conducting metal oxides, e.g. RuO_2, IrO_2, Fe_2O_3, Fe_3O_4, MnO_2, NiO, conducting polymers, e.g. polythiophene, polypyrrole (PPy), polyaniline (PANI) and their derivatives. [14]

1.3.1. Carbon material for supercapacitors

Carbon materials are considered as attractive electrode materials for supercapacitor industrial applications due to their advantages of low cost, high specific surface area, good electronic conductivity, good chemical stability, non-toxicity, abundance, high temperature stability and easy processing. The performance of carbon materials depends on structure, textures, and its form. Figure 1.4 shows most important forms of carbon: CNTs, activated carbon, graphene, and carbon nanofibers. [15,16] AC carbon is one of the cheapest materials as they originate from diverse easily available sources such as charred coconut husk and is extensively studied in for the supercapacitor applications. Activated carbons are carbons made of small hexagonal rings organized into graphene sheets with high surface area and high porosity. A wide distribution of pore sizes was found in activated carbons. Typical Brunauer, Emmett, and Teller (BET) surface areas for activated carbon are 1000 to 3000m^2g^{-1}. [17,18] Regarding the porosity, there is a general trend of increased capacitance with increased specific surface area (SSA); however, the carbon structure including pore shape, surface functional groups, and electrical conductivity should be considered as well. The capacitance of AC is improved by activation through several treatments such as CO_2 or KOH. The treatment increases the capacitance of AC by increasing the surface area by opening pores that are closed or obstructed. Indeed, a high surface area or large pore volume limits energy density or high power, and a very high porosity directly translates to low volumetric density resulting in moderate to low volumetric power and energy performance [18].

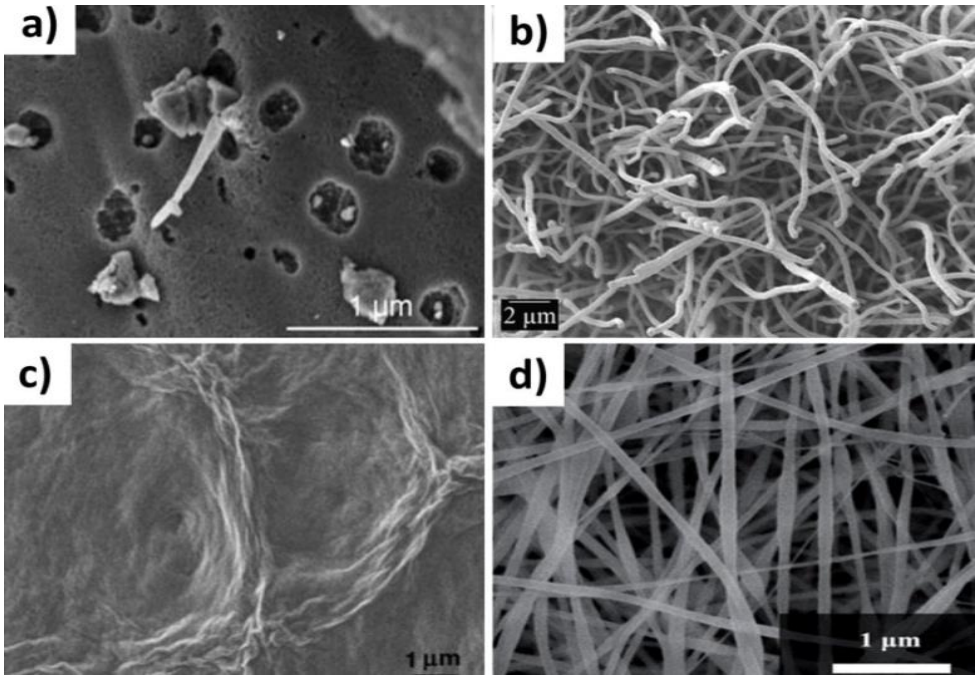

Figure 1.4. SEM images of a) activated carbon, b) multi-walled carbon nanotubes, c) graphene, and d) carbon nanofibers . [18]

The International Union of Pure and Applied Chemistry (IUPAC) define pores according to their size as follows:

• Macropores: larger than 50 nm

• Mesoporous: between 2 and 50 nm

• Microporous: smaller than 2 nm

Usually, specific capacitance of EDLC capacitance has linear dependence with specific surface area calculated from Brunauer-Emmett-Teller (BET) method. This correlation is valid for small BET values, but when the surface area is higher than 1200-1500 m^2g^{-1} value the capacitance becomes almost constant. The BET method often overestimates the SSA for carbons. The electrosorption and insertion of a certain ion in pores of different sizes does not necessarily lead to the same capacitance, even not for materials of comparable BET values. In fact, the capacitance will be controlled by the relationship between the average pore size and the effective size of ions. Such processes can be studied by means of cyclic voltammetry and in the case where the average pore size is slightly smaller than the size of the ions, it is possible to force their insertion into the pores by

slowing down the scan rate applied. In this case, ion sieving also results in increased, yet reversible swelling of the pore network.

In the case of solvent based aqueous or organic electrolytes, the effective ion size is larger due to the solvation shell as compared to the ion itself. Pores too small for ions to enter are to be avoided for the rational design of porous carbon electrodes in EDLCs. For templated carbons, the capacitance is proportional to the ultra-micropore volume (pores smaller than 0.7 – 0.8 nm) measured by CO_2 gas sorption, in both aqueous and organic media. The ion sieving effect is more important for the negative electrode, where the cations are trapped, than for the positive one meaning that the cell capacitance is essentially controlled by the negative electrode. Apart from capacitance limitations, too narrow pores may also contribute to an increased ESR, and consequently a decrease of power; especially if the carbon is exclusively microporous, the equivalent resistance is rather high. Hence, carbons with subnanometer-sized pores are recommended for enhancing ions trapping, but a small proportion of mesoporous (i.e., pores between 2 and 50 nm) is necessary to reduce the diffusion resistance.

Besides tailoring the pore size and total pore volume, the achievable maximum capacitance of conventional EDLCs remains limited, and high energy density supercapacitors require different technological solutions. One strategy to increase the capacitance is related to pseudocapacitive phenomena at the electrode/electrolyte interface. Transition metal oxides are also considered as attractive materials to achieve high energy storage in supercapacitors. The capacitance can also be increased significantly by using diverse faradaic reactions originating from oxygen and nitrogen heteroatoms in the carbon network. Such pseudocapacitive effects accompany the typical electrical double-layer charging and they can relate to either quick faradaic reactions of functional groups or also with a local modification of the electronic structure of the doped carbon. In this case, the decrease of gap between the conduction and valence bands enhances the electrical conductivity and, in turn, the ion sorption due to an increased number of local free electrons. [7] Introducing oxygenated functionalities in the carbon network can greatly enhance the capacitance. [19] Nitrogen enriched carbons can be obtained by nitrogen plasma. [20]

1.3.2. Activated carbons (ACs)

ACs is the materials employed in commercial EDLCs with capacitances of 200 F/g in aqueous electrolyte and 100 F/g in organic electrolyte. [21] AC is the preferred material due to its unique combination of very high surface area (~3500 m^2 /g), stable supply, well-established fabrication procedures, and decent conductivity. [22] Structurally, AC is comprised of discrete fragments of curved graphene sheets, in which pentagons and heptagons (defects) are distributed randomly throughout hexagon networks. [23] AC can be fabricated from cheap materials, such as fruit and plant components and it is carried out in two steps. [24] The first step is carbonization, during which the carbon-rich organic precursor undergoes heat treatment to remove the non-carbon elements. Subsequently, to increase surface area, the carbon material is physically or chemically activated using oxidizing gases or oxidizing agents (e.g. KOH, ZnCl2, H_3PO_4), respectively. [25-27]

. Physical activation gasifies the char (the interstices) in steam to enhance the pores and chemical activation uses dehydrating agents to inhibit the formation of tar and enhance the yield of carbon (Figure 1.5). [25]

. Chemical activation is advantageous because it involves only one step and lower pyrolysis temperatures, it produces higher carbon yield of high surface area, and microporosity can be developed and controlled. [24, 26] Factors influencing the materials characteristics during activation are shown in Figure 1.5, from which the carbonization temperature is essential, because as temperature increases, the surface area decreases. Activation of carbon is a well-developed process that provides the ability to control, to some extent, the resulting properties of the material. On the downside, the pore size distribution is not uniform, limiting the exposure of the developed area to the electrolyte. [21]

. AC electrode preparation is generally carried out by mixing the active material with conductivity enhancer and binder in a solvent and coating the mixture onto the current collector (CC), or by pressing the dry mixture into pellets without the loss of AC porosity. [28].

. Electrodes prepared by the former method with olive pits-derived and KOH-high temperature activated carbon showed a specific capacitance of up to 260 F /g 29. Doctor blade coated AC electrodes derived from rice husk and activated with KOH showed a

capacitance of 250 F/g. [30] AC electrodes prepared by pressing pellets with apricot shell-derived carbon, activated with NaOH, showed a capacitance of 339 F/g. [31]

Coke-derived, KOH-activated carbon electrodes showed a capacitance of up to 350.96 F/g. [32] and free-standing binder-free AC/carbon nanotubes (CNT) (95% AC) paper electrodes prepared by a filtration method showed a maximum capacitance 267.7 F/g. [33]

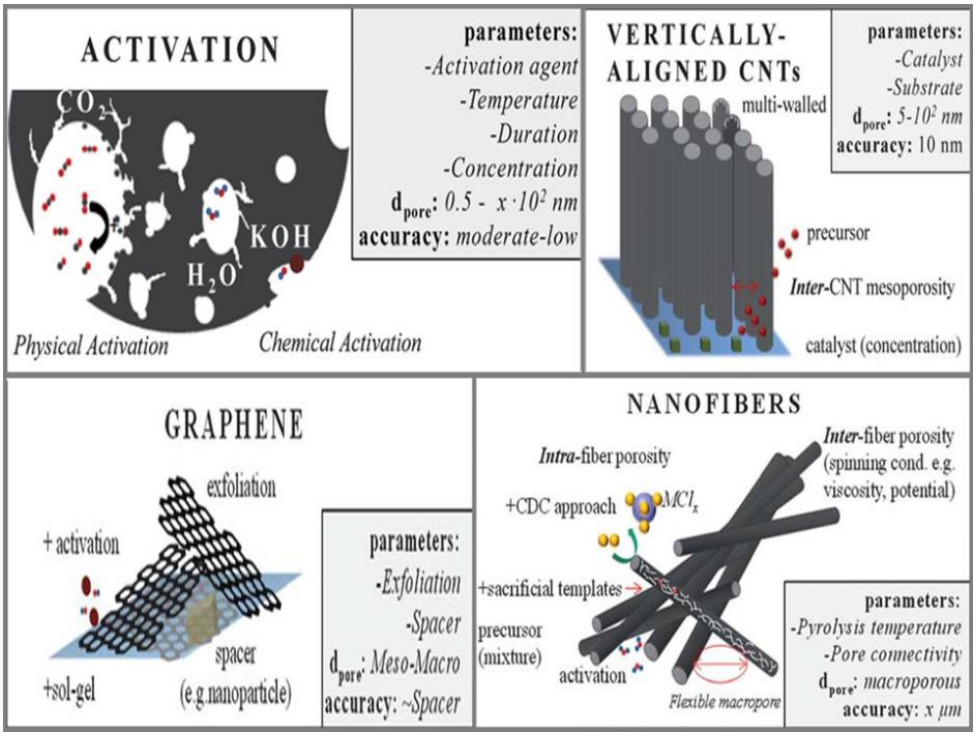

Figure 1.5 Different carbon nanostructures and parameters affecting the material properties. [27,34]

Activation consists of creating porosities so that electrolyte ions can move. For example, anthracite, common or high-performance carbon fibers have been chemically or physically activated [35]. The best result was a capacitance of 320 F/g by chemically activating anthracite in the form of powder with KOH. Carbon activated powders can also be used and a capacitance value of 290 F/g can be reached [36]. The problem with carbon powder is that capacitance is limited by the contact resistance between particles which appeared to be critical in decreasing the overall electrode electrical conductivity.

1.3.3. Carbon nanofibers (CNFs)

Carbon fibers represent an important class of graphite related materials that are closely related to carbon nanofibers. Regarding structure and properties carbon fibers have been studied scientifically since the late 1950s and fabricated industrially since 1963. They are now becoming a technologically and commercially important material in the aerospace, construction, sports, electronic device and automobile industries. The global carbon fiber market has now grown to about 12500 t/y of product, after 40 years of continuous R&D work [37–39]. Carbon fibers are defined as a filamentary form of carbon with an aspect ratio (length/diameter) greater than 100. Probably, the earliest documented carbon fibers are the bamboo char filaments made by Edison for use in the first incandescent light bulb in 1880. With time, carbon fibers were replaced by the more robust tungsten filaments in light bulb applications, and consequently carbon fiber R&D vanished at that early time. But in the late 1950s, carbon fibers once again became important because of the aggressive demand from aerospace technology for the fabrication of lightweight, strong composite materials, in which carbon fibers are used as a reinforcement agent in conjunction with plastics, metals, ceramics, and bulk carbons. The specific strength (strength/weight) and specific modulus (stiffness/weight) of carbon fiber-reinforced composites demonstrate their importance as engineering materials, due to the high performance of their carbon fiber constituents.

Carbon nanofibers could be defined as sp^2-based linear filaments with diameter of ca. 100 nm that are characterized by flexibility and their aspect ratio (above 100). Materials in a form of fiber are of great practical and scientific importance. The combination of high specific area, flexibility, and high mechanical strength allow nanofibers to be used in our daily life as well as in fabricating tough composites for vehicles and aerospace. However, they should be distinguished from conventional carbon fibers [37–39] and vapor-grown carbon fibers (VGCFs) [40–46] in their small diameter. Conventional carbon fibers and VGCFs have several micrometer-sized diameters. In addition, they are different from well-known carbon nanotubes. [41, 47–50] Carbon nanofibers could be grown by passing carbon feedstock over nanosized metal particles at high temperature [40-46], which is very like the growth condition of carbon nanotubes. However, their geometry is different from concentric carbon nanotubes containing an entire hollow core, because they can be visualized as regularly stacked truncated conical or planar layers along the filament length

[51–53]. Such a unique structure renders them to show semi- conducting behavior [54] and to have chemically active end planes on both the inner and outer surfaces of the nanofibers, thereby making them useful as supporting materials for catalysts [55], reinforcing fillers in polymeric composites [56], hybrid type filler in carbon fiber reinforced plastics [57– 59], and photocurrent generators in photochemical cells [60, 61]. Alternatively, carbon nanofibers could be fabricated by the right combination of electrospinning of organic polymers and thermal treatment in an inert atmosphere. The electro-spinning technique has been one of the advanced fiber formation techniques from polymer solution by using electrostatic forces. [62– 65] Electrospun-based nanofibers exhibited noticeable properties, such as nanosized diameter, high surface area and thin web morphology, which make them applicable to the fabrication of high-performance nanocomposites, tissue scaffolds and energy storage devices [66, 67].

CNFs usually exhibit diameters of 100−300 nm and length of up to 200 μm. They can be classified in highly graphitic (high electrical conductivity, low specific surface area) and lowly graphitic CNFs (lower electrical conductivity, higher surface area, less crystalline). [68] CNFs are synthesized using CVD methods or from polymeric fibers such as rayon or polyacrylonitrile. [69] They can be used directly as electrode without the need for binder, achieve high electrical conductivities (200 – 1000 S/cm), and high surface area (once activated: 1000-2000 m^2/g). This material has been studied for flexible electrodes, although their cost still restricts its application in commercial devices. Coal based nanofibers and nitrogen-doped hollow activated CNFs were prepared by electrospinning, carbonization, and activation. Electrodes showed a specific capacitance of 230 F/g and N-doped CNFs achieved 197 F/g .[70] Amorphous CNFs activated in KOH lead to new microporus and larger surface areas as well as a higher content of basic oxygen groups, enhancing the specific capacitance. Supercapacitor electrodes processed as cylindrical pellets with binder attained values as high as 255 F/g. [68] Mesoporous carbon nanofibres (CNFs) were prepared from furfuryl alcohol precursor coupled with a mesoporous silica template by vapor deposition polymerization strategy. [71] A specific capacitance of 222 F/g was obtained with electrodes prepared by mixing CNFs, conductivity enhancer and binder and pressing the mixture onto a nickel grid. [48] Other important carbon materials include carbon aerogels (CAs), hydrogels, and carbide-derived carbon. The first group is a large class of gels composed of particles with sizes in the nanometer range covalently bonded together. They have very high porosity (over 50%, with pore diameter under 100

nm) and high surface areas ranging between 400–1,000 m^2/g .[15,21] The three-dimensional mesoporous materials with interconnected ordered pore structure can provide efficient diffusion of electrolyte ions and electrons, leading to promising applications in supercapacitors .[49] CAs are prepared from the sol-gel route by the condensation reaction of resorcinol and formaldehyde and subsequent pyrolysis .[10] Capacitances of up to 150 F/g (aqueous) have been obtained with this material .[72] and due to its very low density and therefore poor volumetric capacitance, it has been of less interest for supercapacitor applications.

1.3.4. Carbon nanotubes (CNTs)

CNTs are often referred to one dimension owing to the electronic transport uniquely along the tube axis and they exist as either single- or multi-layers of carbon and have diameters ranging from 1 to 50 nm. In comparison MWCNTs are much cheaper and have greater capillarity force than single-wall carbon nanotubes (SWCNTs). Several reasons why MWCNTs-based electrodes may ultimately outperform activated carbon in supercapacitors are well-established. These include the fact that nanotubes have extraordinary mechanical properties, high conductivity, surface area of $120m^2g^{-1}$ to $400m^2g^{-1}$, good corrosion resistance, high temperature stability, percolated pore structure, and can be functionalized to optimize their properties. One of the primary benefits of percolated MWCNTs electrodes over-activated carbon electrodes is the opened mesoporous formed by the accessible interconnected network of nanotubes. However, the BET surface area of MWCNTs-based active materials is sometimes not as high as in activated carbon. Despite this, the porosity of MWCNTs is more accessible to the ions of the electrolytes than that of an activated carbon. [14]

1.3.5. Graphene

Graphene is the well-known two-dimensional carbon monolayers composed of all-sp2-hybridized carbons with some of the most intriguing properties, i.e., lightweight, high electrical and thermal conductivity, highly tunable surface area (up to 2675 m^2/g), strong mechanical strength (~1 TPa) and chemical stability. These outstanding properties enable graphene and graphene-based materials to find applications in high performance structural nanocomposites, electronics, and environmental protection and energy devices including both energy generation and storage. The combination of these outstanding

physical, mechanical and chemical properties make graphene-based materials more attractive for electrochemical energy storage and sustainable energy generation, i.e., Li-ion batteries, fuel cells, supercapacitors, and photovoltaic and solar cells. For instance, the theoretical specific capacitance of single layer- graphene is ~21 uF/cm^2 and the corresponding specific capacitance is ~550 F/g when the entire surface area is fully utilized. However, the practical capacitive behavior of pure graphene is lower than the anticipated value due to the serious agglomeration during both the preparation and application processes. Therefore, boosting the overall electrochemical performance of graphene-based materials still remains a great challenge. Graphene-based materials have been extensively investigated as a conducting network to support the redox reactions of transition metal oxides, hydroxides and conducting polymers. Indeed, these nanohybrid electrodes consisting of graphene and nanoparticles of transition metal oxides/hydroxides or conductive polymers show the superior electrochemical performance, as a result of the synergistic effect which graphene

Layers facilitate the dispersion of metal oxide/hydroxide nanoparticles, and act as a highly conductive matrix for enhancing the electrical conductivity, and the metal oxide/ hydroxide/conducting polymers offer the desired pseudocapacitance. [73]

1.3.6. Carbide-derived carbons

Carbide-derived carbons are attractive because they are produced through one of the most accurate synthesis strategies to control micropore size with sub-Ångstrom accuracy based on the selective removal of metal atoms out of metal carbide matrices using gaseous halogens, primarily chlorine. [74] The extraction of metal atoms serves for the creation of micropores and takes place under full conservation of the original shape of the carbide allowing for a precise control over the resulting pore size, which depends on the used precursor. Their specific surface area exceeds 3000 m^2/g 74 and in this case, higher temperatures usually lead to an increase in the pore size due to the self-organization of the highly mobile carbon atoms. [75,76]

1.4. Pseudo-capacitive contributions

In addition to typical electrostatic interactions in the electrical double-layer, quick faradic redox reactions with electron transfer on the electrode/electrolyte interface may also contribute to the charge storage process and energy enhancement. Since the electrode potential (U) varies proportionally to the charge transferred (Q) as in capacitor, $dQ = C\,dU$, the process is referred to as pseudo-capacitance. [77,78]

However, the typical faradic origin of these processes is associated with a slow kinetic of the heterogeneous reaction (limited mainly by the diffusion of the involved electrochemical species) and with a moderate cycle life (connected with changes of the material structure undergoing the oxidation or reduction process). Metal oxides such as RuO_2, MnO_2, NiO, as well as electronically conducting polymers such as polyaniline and polypyrrole, have been extensively investigated. Among them, RuO_2 presents the highest theoretical capacitance values (about 1400 F/g). However, due to its low cost, environmental friendliness, and, more importantly, its Faradic response with rectangular voltammograms, MnO_2 appears to be more suitable for high power applications [79]. Regarding the oxidation/reduction mechanism in MnO_2 pseudocapacitors, Toupin et al. suggested that H+ and C^+ (Na^+, K^+, La^+) are intercalated and deintercalated upon reduction and oxidation in the bulk of MnO2, and C+ is adsorbed on the surface of MnO_2. [80]

This procedure includes a redox reaction between Mn3+ and Mn4+ oxidation states. Since only the surface is involved in the charge storage mechanism, a thinner film of MnO_2 shows a higher capacitance than a thicker one. However, a compromise must be achieved to obtain the optimum thickness since usually a thinner layer of manganese dioxide undergoes mechanical instability and, as a result, delivers poor energy density. Therefore, for supercapacitor applications, it is important that the electrode material possesses high surface area and high porosity, as well as very low electrical resistance. A suitable configuration is CNTs/MnO_2 composite electrodes, in which a thin layer of MnO_2 provides high pseudocapacitance due to Faradic redox reactions taking place on large surface area electrodes. CNTs provide high electrical conductivity and mechanical stability to the 3D electrode. Although the highest reported capacitance obtained with such composite electrodes, in which MnO_2 is deposited on the outer surface of CNTs, is

as high as 790 F/g, it is still well below the theoretical value for MnO_2 (about 1370 F/g) .[81]

Regarding the oxidation/reduction mechanism in MnO_2 pseudocapacitors, Mathieu Toupin et al. suggested that H^+ and C^+ (Na^+, K^+ , La^+) are intercalated and de-intercalated upon reduction and oxidation in the bulk of MnO_2 and C^+ adsorbed on the surface of MnO_2 as shown by (equations 1.12 and 1.13) [82].

$$MnO_2 + H^+ + e^- \leftrightarrow MnOOH \quad (1.12)$$

Or

$$MnO_2 + C^+ + e^- \leftrightarrow MnOOC \quad (1.13)$$

This procedure includes a redox reaction between Mn^{3+} and Mn^{4+} oxidation states. [81]

Pseudocapacitance in carbon materials has been revealed as an efficient way to increase their capacitance by adding this effect to the EDLC. In carbon materials, pseudocapacitance can have several origins: i) fast redox reactions involving oxygen- or nitrogen-containing surface functionalities and the electrolyte; ii) reversible electrochemical hydrogen storage taking place when a negative polarization is applied to an activated carbon electrode iii) redox-active electrolytes at the carbon/electrolyte interface, such as iodide/iodine, vanadium/vanadyl, quinone/hydroquinone additive to aqueous electrolytes, bromide species , etc.[83]

1.4.1 Conducting polymers

In addition to metal oxides the materials which give pseudocapacitance are various conducting polymers, polyaniline (PANI), polypyrrole (PPy) and derivatives of polythiophene (PTh). PANI has been the most studied because of its relatively easy preparation, low cost, high conductivity and stability. So far, the reported specific capacitance of pure PANI modified electrodes varies from 160 to 815 F/g.84 The main concern in using of conducting polymers is their poor cycling stability due to volumetric changes during doping/dedoping. [85,86]

On the other hand, these materials present relatively low power performance because of the slow diffusion of ions within electrode bulk. Another disadvantage of conducting polymers is their narrow stability potential window. Therefore, current research efforts

with conducting polymers for supercapacitor applications are directed towards hybrid Systems. [87,88]

1.5. Electrolyte

The capacitance of supercapacitor is greatly influenced by the choice of electrolyte. In the case of electrochemical capacitors of the double layer type, the behavior of dielectric of the capacitor has a special significance since it is the solvent of electrolyte provides shells of ions in medium. Double layer at an electrode/solution interface consist of one real, electronically conducting plate (semiconductor, metal oxide or activated carbon) and a second plate that is the inner interfacial limit of a conducting electrolyte solution phase. The double layer distribution of a compact layer having dimensions of about 0.5 to 0.6 nm corresponding to the dimensions of solvent molecules and ions that occupy it and a wider region of thermally distributed ions over 1 to 100nm, depending on ionic concentration. It is because of this very small thickness of the compact molecular inner layer, very large specific capacitance of 20 to 40 uF/cm^2 can be obtained. The choice of electrolyte in supercapacitor is as important as the choice of electrode material. The attainable cell voltage of a supercapacitor will depend on the breakdown voltage of the electrolyte, and hence the possible energy density (which is dependent on voltage) will be limited by the electrolyte. Power density is dependent on the cell's ESR, which is strongly dependent on electrolyte conductivity. There are currently two types of electrolyte for supercapacitors: organic and aqueous. Organic electrolytes are the most commonly used in commercial devices, due to their higher dissociation voltage. Cells using an organic electrolyte can usually achieve voltages in the range of 2 – 2.5 V. The resistivity of organic electrolytes is relatively high, however, limiting cell power. Aqueous electrolytes have a lower breakdown voltage, typically 1.1 V, but have better conductivity than organic electrolytes. [89]

The ability to store charge is dependent on the accessibility of the ions to the porous surface-area, so ion size and pore size must be optimal. The best pore size distribution in the electrode depends upon the size of the ions in the electrolyte, so both electrode and electrolyte must be chosen together. [15]

1.5.1. Aqueous Electrolytes

Until recently, the most commonly used aqueous electrolytes were 1 mol L^{-1} H_2SO_4 and

6 mol L^{-1} KOH [90]. Compared with non-aqueous electrolytes, the aqueous medium provides a much higher conductivity leading to higher power density. The conductivity (25 C) of 6mol L^{-1} KOH exceeds 600 mS/cm while it is only 20 mS/cm for tetraethylammonium tetrafluoroborate in propylene carbonate and ~10 mS/cm for typical room temperature ionic líquids. [91] On the other hand, low cost and easy manipulation could be further advantages for aqueous electrolytes. Unfortunately, the lower voltage of aqueous medium is restricted via the thermodynamic window of water at 1.23 V. When the voltage is higher than 0.8 V, the potential of one of the electrodes may be beyond the thermodynamic limit resulting in the water decomposition. It is much lower than in non-aqueous electrolytes (e.g., 2.7 V- 2.8 V for the organic medium) resulting in much lower energy and power stored. Interestingly, it has been demonstrated that neutral aqueous electrolytes such as alkali sulfates could achieve higher voltages with symmetric carbon/carbon capacitors than generally obtained in acidic or basic medium. In previous work from CRMD, a stability potential window around 2.0 V has been demonstrated with activated carbon in 0.5 mol L^{-1} Na_2SO_4. As a result, a practical voltage of 1.6 V has been attained during 10,000 reversible charge/discharge cycles in symmetric carbon/carbon systems [92]. The electrochemical analysis of seaweed carbons in 0.5 mol L^{-1} Na_2SO_4, demonstrated that the nature of the electrode material and the electrolyte pH influence both the capacitance values and the stability potential window; due to the presence of nitrogenated functionalities in these carbons, the potential window reached 2.4 V in 0.5 mol L^{-1} Na_2SO_4 Qu *et al.* reported that the migration rate of hydrated ions in the bulk electrolyte and within the inner pores of activated carbon increase in the order of Li+ < Na+ < K+, and that the rate performance improves in the order $Li_2SO_4 < Na_2SO_4 < K_2SO_4$. The highest operating voltage of 2.2 V with an exceptional cycling stability has been demonstrated in Li_2SO_4; Fic *et al.* have suggested that the stronger hydration of Li^+ compared to Na^+ and K^+ ions is responsible for larger voltage in Li_2SO_4 solution.Those findings have opened a new door for the aqueous medium. Although acidic and basic solutions has been reported mainly due to their high electrochemical activity, their corrosive properties severely hinder large-scale commercialization because of the high price of corrosion-resistant current collectors such as gold or platinum .Therefore, neutral-pH aqueous electrolytes appear as a more promising choice from industrial point of view, according to the pragmatic rule “supercapacitors will see growth only when their costs fall”. [93]

1.6. Membrane separator

The purpose of membrane separator in an electrochemical capacitors was to separate the two electrode to prevent short circuit, which can trigger the conversion of chemical energy to heat and cause irreversible damage to electrochemical capacitors devices. In the meantime, membrane contained numerous pores and tunnels to enable free pass through diffusion of ions and electrolyte molecules. The important parameters of a membrane separator are thickness, permeability, absorbency, chemical stability, pore sizes, puncture resistance, tensile strength, and thermal properties.

The membrane should have good permeability because the internal resistance was proportional to the permeability. The permeability reflected how easily ions and molecules moving through it. Absorbency is the ability to absorb electrolyte, which directly reveal the wetting ability of membrane separator to electrolyte. Good absorbency could substantially reduce internal resistance. Moreover, membrane separator should have good chemical stability in different electrolyte and cycling stability under high potential, which had great influence on ES and battery life. There were requirements on thickness, tensile strength and puncture resistance for membrane separators. Electrodes and current collectors were not smooth and the rough edges were strong enough to pierce separator if it was not thick enough. However, thickness of membrane separator had influence to internal resistance and permeability. So the thickness must be chosen after testing. Polymer or paper separators can be used with organic electrolytes, and ceramic or glass fiber separators are often used with aqueous electrolytes .[93,94]

References

[1]. B. E. Conway, Electrochemical Supercapacitors; Scientific Fundamentals and Technological Applications, Kluwer Academic/ Plenum Publishers, NewYork, NY,USA, 1999.

[2]. Meisam Valizadeh Kiamahalleh and _Sharif Hussein Sharif Zein, Multiwalled carbon nanotubes based nanocomposites for supercapacitors: areview of electrode materials, Department of Chemical Engineering University Sains Malaysia, 14300 Nibong Tebal Pulau Pinang, Malaysia.

[3]. Chuang Peng, Shengwen Zhang, Daniel Jewell, George Z. Chen, Carbon nanotube and conducting polymer composites for supercapacitors, Progress in Natural Science, Volume 18, Issue 7, 10 July 2008, Pages 777–788.

[4]. L.-Z. Fan and J. Maier, "High-performance polypyrrole electrode materials for redox supercapacitors," Electrochemistry Communications, vol. 8, pp. 937-940, 2006.

[5] D. Yu and L. Dai, "Self-assembled graphene/carbon nanotube hybrid films for supercapacitors," The Journal of Physical Chemistry Letters, vol. 1, pp. 467-470, 2009.

[6] A. Lewandowski, K. Skorupska, and J. Malinska, "Novel poly(vinyl alcohol)– KOH–H2O alkaline polymer electrolyte," Solid State Ionics, vol. 133, pp. 265-271, 2000.

[7]. F. Béguin, V. Presser , A. Balducci , and E. Frackowiak, Carbons and Electrolytes for Advanced Supercapacitors, Adv. Mater. 2014, DOI: 10.1002/adma.201304137

[8]. Tao Chen and Liming Dai, Carbon nanomaterials for highperformance Supercapacitors, Center of Advanced Science and Engineering for Carbon (Case4Carbon), Department of Macromolecular Science and Engineering, Case Western Reserve University, 10900 Euclid Avenue, Cleveland, OH 44106, USA

[9]. J. P. Zheng, J. Huang, b and T. R. Jowt, The Limitations of Energy Densily for Electrochemical Capacitors, Army Research Laboratory, Sensors and Electron Devices Directorate, Fort Monmouth, New Jersey 07703-5 601, USA

[10]. Yaohui Wang, Manganese dioxide based composite electrodes for electrochemical supercapacitors, Open Dissertations and Theses, McMaster University, wang322@mcmaster.ca

[11]. H. Helmholtz , Ann. Phys. 1853 , 89 , 211 .

[12] L. G. Gouy , J. Phys. Theor. Appl. 1910 , 9 , 457 .

[13] O. Stern , Zeitschrift für Elektrochemie and Angewandte Physikalische Chemie 1924 , 30 , 508 .

[14]. Bakheet Awad Alresheedi, Supercapacitors based on carbon nanotube fuzzy fabric structural composites, The Degree of Doctor of Philosophy in Materials Engineering, UNIVERSITY OF DAYTON, Dayton, Ohio, December, 2012

[15]. Frackowiak, E.; Béguin, F., Carbon materials for the electrochemical storage of energy in capacitors. Carbon 2001, 39, (6), 937-950.

[16]. Chen, S.-M.; Ramachandran, R.; Mani, V.; Saraswathi, R., Recent advancements in electrode materials for the high-performance electrochemical supercapacitors: a review. Int. J. Electrochem. Sci 2014, 9, 4072-4085.

[17]. Suheda isikli ,B.SC ,M.SC ,Quinone - based orgànic redox compounds for electrochemical energy Storage devices ,doctor of philosoph from Autonomous university of Madrid, 2013

[18].Margarita Rosa Arcila Vélez, Design and synthesis of polymer, carbon and composite electrodes for high energy and high power supercapacitors, Doctor of PhilosophyChemical Engineering, Clemson University

[19].S Hussain,R Amade, E Jover and E Bertran, Functionalization of carbon nanotubes bywater plasma, Nanotechnology 23 (2012) 385604 (8pp).

[20]. Shahzad Hussain, Roger Amade , Eric Jover, Enric Bertran, Nitrogen plasma functionalization of carbon nanotubes for supercapacitor applications, August 2013 Springer Science+Business Media New York 2013

[21]. Simon, P., Taberna, P., Béguin, Supercapacitors: Materials, Systems, and Applications. First ed.; Wiley-VCH Verlag GmbH & Co.: Weinheim, Germany, 2013.

[22]. Pandolfo, T., Ruiz, V., Sivakkumar, S., Nerkar, J., Supercapacitors: Materials, Systems, and Applications. First ed.; Wiley-VCH Verlag GmbH & Co.: Weinheim, Germany, 2013.61

[23].. Harris, P. J. F., New Perspectives on the Structure of Graphitic Carbons. Critical Reviews in Solid State and Materials Sciences 2005, 30, (4), 235-253.

[24].. Al Bahri, M.; Calvo, L.; Gilarranz, M. A.; Rodriguez, J. J., Activated carbon from grape seeds upon chemical activation with phosphoric acid: Application to the adsorption of diuron from water. Chemical Engineering Journal 2012, 203, 348-356.

[25]. Caturla, F.; Molina-Sabio, M.; Rodríguez-Reinoso, F., Preparation of activated carbon by chemical activation with ZnCl2. *Carbon* **1991,** 29, (7), 999-1007.

[26].Sevilla, M.; Mokaya, R., Energy storage applications of activated carbons: supercapacitors and hydrogen storage. *Energy & Environmental Science* **2014,** 7, (4), 1250-1280.

[27].Wang, J.; Kaskel, S., KOH activation of carbon-based materials for energy storage. *Journal of Materials Chemistry* **2012,** 22, (45), 23710-23725.

[28]. Sevilla, M.; Mokaya, R., Energy storage applications of activated carbons: supercapacitors and hydrogen storage. *Energy & Environmental Science* **2014,** 7, (4), 1250-1280

[29].Redondo, E.; Carretero-González, J.; Goikolea, E.; Ségalini, J.; Mysyk, R., Effect of pore texture on performance of activated carbon supercapacitor electrodes derived from olive pits. Electrochimica Acta 2015, 160, 178-184.

[30].. Xu, H.; Gao, B.; Cao, H.; Chen, X.; Yu, L.; Wu, K.; Sun, L.; Peng, X.; Fu, J., Nanoporous Activated Carbon Derived from Rice Husk for High Performance Supercapacitor. Journal of Nanomaterials 2014, 2014, 7.

[31].. Xu, B.; Chen, Y.; Wei, G.; Cao, G.; Zhang, H.; Yang, Y., Activated carbon with high capacitance prepared by NaOH activation for supercapacitors. Materials Chemistry and Physics 2010, 124, (1), 504-509.63

[32]. Roldán, S.; Villar, I.; Ruíz, V.; Blanco, C.; Granda, M.; Menéndez, R.; Santamaría, R., Comparison between Electrochemical Capacitors Based on NaOHand KOH-Activated Carbons. Energy & Fuels 2010, 24, (6), 3422-3428.

[33]. Xu, G.; Zheng, C.; Zhang, Q.; Huang, J.; Zhao, M.; Nie, J.; Wang, X.; Wei, F., Binder-free activated carbon/carbon nanotube paper electrodes for use insupercapacitors. Nano Research 2011, 4, (9), 870-881.

[34]. Borchardt, L.; Oschatz, M.; Kaskel, S., Tailoring porosity in carbon materials for supercapacitor applications. *Materials Horizons* **2014,** 1, (2), 157-168.

[35] Graeme A. Snook, Pon Kao, Adam S. Best, Conducting-polymer-based supercapacitor devices and electrodes, Journal of Power Sources 196 (2011) 1–12.

[36] M.J. Bleda-Martinez, J.A. Macia-Agullo, D. Lozano-Castello, E. Morallon, D. Cazorla-Amoros, A. Linares-Solano, Role of surface chemistry on electric double layer capacitance of carbon materials, Carbon 43 (2005) 2677–2684

[37]. J.B. Donnet, R.C. Bansal: Carbon Fibers (MarcelDekker, New York 1984)

[38]. L.H. Peebles: Carbon Fibers (CRC, Boca Raton 1994)

[39]. D.D.L. Chung: Carbon Fiber Composites (ButterworthHeinemann, Boston 1994)

[40]. M.S. Dresselhaus, G. Dresselhaus, K. Sugihara,I, L. Spain, H.A. Goldberg: Graphite Fiber and Filaments(Springer, Berlin Heidelberg 1988)

[41]. A. Oberlin, M. Endo, T. Koyama: Filamentous growthof carbon through benzene decomposition, J. Cryst. Growth 32, 335–349 (1976)

[42]. R.T.K. Baker: Catalytic growth of carbon filaments, Carbon 27, 315–323 (1989)

[43]. G.G. Tibbetts: Why are carbon filaments tubular?,J. Cryst. Growth 66, 632–637 (1984)

[44]. M. Endo: Grow carbon fibers in the vapor phase,Chem. Technol. 18, 568–576 (1988)

[45]. N.M. Rodriguez: A review of catalytically grown carbonnanofibers, J. Mater. Res. 8, 3233–3250 (1993)

[46]. G.G. Tibbetts: Vapor-grown carbon fibers: Status and prospects, Carbon 27, 745–747(1989)

. [47]. S. Iijima: Helical microtubules of graphitic carbon, Nature **354**, 56–58 (1991)

[48]. M.S. Dresselhaus, G. Dresselhaus, P. Eklund: *Scienceof Fullerenes and Carbon Nanotubes* (Academic, NewYork 1996)

[49]. R. Saito, G. Dresselhaus, D.S. Dresselhaus: *PhysicalProperties of Carbon Nanotubes* (Imperial CollegePress, London 1998)

[50]. T.W. Ebbesen: *Carbon Nanotubes: Preparation andProperties* (CRC, London 1997)

[51]. N.M. Rodriguez, A. Chambers, R.T.K. Baker: Catalyticengineering of carbon nanostructures, Langmuir 11,3862–3866 (1995)

[52].M. Endo, Y.A. Kim, T. Fukai, T. Hayashi, K. Oshida,M. Terrones, T. Yanagisawa, S. Higaki, M.S. Dresselhaus:
Structural characterization of cup-stackedtype nanofibers with an entire hollow core, Appl.Phys. Lett. 80, 1267–1269 (2002)

[53]. S.H. Yoon, C.W. Park, H.J. Yang, Y. Korai,I. Mochida, R.T.K. Baker, N.M. Rodriguez: Novel carbonnanofibers of high graphitization as anodicmaterials for lithium ion secondary batteries, Carbon42, 21–32 (2004)

[54]. Q.F. Liu, W.C. Ren, Z.G. Cheng: Semiconductingproperties of cup-stacked carbon nanotubes, Carbon47, 731–736 (2009)

[55].M. Endo, Y.A. Kim, M. Ezaka, K. Osada, T. Yanagisawa,T. Hayashi, M. Terrones, M.S. Dresselhaus:Selective and efficient impregnation of metalnanoparticles on cup-stacked-type nanofibers,Nano Lett. 3, 723–726 (2003)

[56]. Y.K. Choi, Y. Gotoh, K.I. Sugimoto, S.M. Song,T. Yanagisawa, M. Endo: Processing and characterizationof epoxy nanocomposites reinforced bycup-stacked carbon nanotubes, Polymer 46, 11489–11498 (2005)

[57]. T. Yokozeki, Y. Iwahori, S. Ishiwata: Matrix crackingbehaviors in carbon fiber/epoxy laminates filledwith cup-stacked carbon nanotubes (CSCNTs), Compos.A: Appl. Sci. Manuf. 38, 917–924 (2007)

[58]. T. Yokozeki, Y. Iwahori, S. Ishiwata, K. Enomoto:Mechanicalproperties of CFRP laminates manufacturedfrom unidirectional prepregs using CSCNT-dispersedepoxy, Compos. A: Appl. Sci. Manuf. 38, 2121–2130(2007)

[59]. T. Yokozeki, Y. Iwahori, M. Ishibashi, T. Yanagisawa,K. Imai, M. Arai, T. Takayashi, K. Enomoto: Fracturetoughness improvement of CFRP laminates by dispersionof cup-stacked carbon nanotubes, Compos.Sci. Technol. 69, 2268–2273 (2009)

[60]. K. Saito, M. Ohtani, F. Fukuzumi: Electron-transferreduction of cup-stacked carbon nanotubes affordingcup-shaped carbons with controlled diameterand size, J. Am. Chem. Soc. 128, 14216–14217 (2006)

[61]. T. Hasobe, H. Murata, P.V. Kamat: Photoelectrochemistryof stacked-cup carbon nanotube film:

Tube-length dependence and charge transfer withexcited porphyrin, J. Phys. Chem. C 111, 16626–16634(2007)

[62]. S. Ramakrishna, K. Fujihara, W.-E. Teo, T.-C. Lim,Z. Ma: An Introduction to Electrospinning and Nanofibers (World Scientific, Singapore 2005)

[63].D.H. Renecker, A.L. Yarine, H. Fong, S. Koombhongse:Bending instability of electrically charged liquid jets of polymer solutions in electrospinning,J. Appl. Phys. 87, 4531 (2000)

[64].Y.M. Shin, M.M. Hohman, G.C. Martin: Processingand microstructural characterization of porous biocompatibleprotein polymer thin films, Polymer 40,7397–7407 (1999)

[65]. I.D. Norris, M.M. Shaker, F.K. Ko, A.G. MacDiarmid:Electrostatic fabrication of ultrafine conductingfibers: polyaniline/polyethylene oxide blends,Synth. Met. 114, 109–114 (2000)

[66].F. Ko, Y. Gogotsi, A. Ali, N. Naguib, H. Ye, G. Yang,C. Li, P. Willis: Electrospinning of continuous carbonnanotube-filled nanofiber yarns, Adv. Mater.15, 1161–1165 (2003)

[67]. R. Bacon: Production of graphite whiskers, J. Appl.Phys. 31, 283–290 (1960)

[68].. Barranco, V.; Lillo-Rodenas, M. A.; Linares-Solano, A.; Oya, A.; Pico, F.; Ibañez, J.; Agullo-Rueda, F.; Amarilla, J. M.; Rojo, J. M., Amorphous Carbon Nanofibers and Their Activated Carbon Nanofibers as Supercapacitor Electrodes. The Journal of Physical Chemistry C 2010, 114, (22), 10302-10307.

[69].. Boskovic, B. O.; Stolojan, V.; Khan, R. U. A.; Haq, S.; Silva, S. R. P., Large-area synthesis of carbon nanofibres at room temperature. Nature Materials 2002, 1, (3), 165-168.66

[70].. McArthur, M. A.; Hordy, N.; Coulombe, S.; Omanovic, S., A binder-free multiwalled carbon nanotube electrode containing oxygen functionalities for electrochemical capacitors. *Electrochimica Acta* **2015,** 162, 245-253.

[71].. Su , D. S.; Schlögl, R., Nanostructured Carbon and Carbon Nanocomposites for Electrochemical Energy Storage Applications. ChemSusChem 2010, 3, (2), 136-168.

[72].Wu, X.-L.; Xu, A.-W., Carbonaceous hydrogels and aerogels for supercapacitors. Journal of Materials Chemistry A 2014, 2, (14), 4852-4864.

[73]. Qingqing Ke, John Wang, Graphene-based materials for supercapacitor electrodes, /J Materiomics 2 (2016) 37e54

[74].. Presser, V.; Heon, M.; Gogotsi, Y., Carbide-Derived Carbons – From Porous Networks to Nanotubes and Graphene. Advanced Functional Materials 2011, 21, (5), 810-833.

[75]. Gogotsi, Y.; Dash, R. K.; Yushin, G.; Yildirim, T.; Laudisio, G.; Fischer, J. E., Tailoring of Nanoscale Porosity in Carbide-Derived Carbons for Hydrogen Storage. Journal of the American Chemical Society 2005, 127, (46), 16006-16007.

[76].. Borchardt, L.; Oschatz, M.; Kaskel, S., Tailoring porosity in carbon materials for supercapacitor applications. Materials Horizons 2014, 1, (2), 157-168.

[77] B. E. Conway, V. Birss, J. Wojtowicz. The role and utilization of pseudocapacitance for energy storage by supercapacitors. J Power Sources 66 (1997) 1-14.

[78] B. E. Conway, W. G. Pell. Double-layer and pseudocapacitance types ofelectrochemical capacitors and their applications to the development of hybrid devices. J Solid State Electrochem. 7 (2003) 637-644.

[79] K. Fic, E. Frackowiak, and F. Beguin, “Unusual energy enhancement
in carbon-based electrochemical capacitors,” Journal ofMaterials Chemistry, vol. 22, pp. 24223–24213, 2012.

[80] M. Toupin, T. Brousse, and D. B´elanger, “Charge storagemechanism ofMnO2 electrode used in aqueous electrochemicalcapacitor,” Chemistry ofMaterials, vol. 16, no. 16, pp. 3184–3190,2004.

[81]. Shahzad Hussain, Roger Amade, Eric Jover, and Enric Bertran, Water Plasma Functionalized CNTs/MnO2Composites for Supercapacitors, Hindawi Publishing CorporationThe ScientificWorld JournalVolume 2013, Article ID 832581, 8 pages

[82]. M. Toupin, T. Brousse, and D. B´elanger, “Charge storage mechanism ofMnO2 electrode used in aqueous electrochemical capacitor,” *Chemistry ofMaterials*, vol. 16, no. 16, pp. 3184–3190, 2004.

[83]. Qiang Gao, Optimizing carbon/carbon supercapacitors in aqueous and organic electrolytes, Docteur de l’université d’Orléans, Le 08 Juillet 2013

[84] H. L. Li, J. X. Wang, Q. X. Chu, Z. Wang, F. B. Zhang, S. C. Wang. Theoretical and experimental specific capacitance of polyaniline in sulfuric acid. J Power Sources 190(2009) 578-586.

[85] Y. Zhang, H. Feng, X. B. Wu, L. Z. Wang, A. Q. Zhang, T. C. Xia, H. C. Dong, X. F.Li, L. S. Zhang. Progress of electrochemical capacitor electrode materials: a review. Int JHydrogen Energy 34 (2009) 2467-2470

[86] V. Khomenko, E. Frackowiak, F. Béguin. Determination of the specific capacitance of conducting polymer/nanotubes composite electrodes using different cell configurations.Electrochim. Acta 50 (2005) 2499-2506.

[87] A. Laforgue, P. Simon, C. Sarrazin, J-F. Fauvarque. Polythiophene-based supercapacitors. J Power Sources 80 (1999) 142-148.

[88] M. Mastragostino, C. Arbizzani, F. Soavi. Conducting polymers as electrode materialsin supercapacitors. Solid State Ionics 148 (2002) 493-498.

89 R. Kötz and M. Carlen, “Principles and applications of electrochemical capacitors,” *Electrochem. Acta 45*, vol. 45, pp. 2483–2498, Dec. 2000.

[90] M. Toupin, D. Bélanger, I. R. Hill, D. Quinn. Performance of experimental carbon blacks in aqueous supercapacitors. J Power Sources 140 (2005) 203-210.

[91] P. J. Hall, M. Mirzaeian, S. I. Fletcher, F. B. Sillars, A. R. Rennie, G. O. Shitta-Bey,G. Wilson, A. Cruden, R. Carter. Energy storage in electrochemical capacitors: designing functional materials to improve performance. Energy Environ. Sci. 3 (2010) 1238-1251.

[92] L. Demarconnay, E. Raymundo-Piňero, F. Béguin. A symmetric carbon/carbon supercapacitor operating at 1.6 V by using a neutral aqueous solution. Electrochem. Commun. 12 (2010) 1275-1278.

[93].Qiang Gao, Optimizing carbon/carbon supercapacitors in aqueous and organic electrolytes

[94] Schneuwly, A., & Gallay, R., "Properties and applications of supercapacitors: From state-of-the-art to future trends," presented at PCIM 2000, 2000.

Materials Characterization and Electrochemical Techniques

The experimental work was performed in the laboratory, followed by characterizations of the obtained materials and evaluation of their electrochemical properties. In the following part of this chapter, experimental technicalities are presented, including the materials and chemicals used in the research project, typical materials, basic materials characterization techniques, cell assembly details, and electrochemical testing specifications.

2.1. Materials and Chemicals

A list of the names of materials, chemicals and equipment used in the research project, along with their formula and supplier, is shown below in Table 2.1

Table 2.1 materials, chemicals and equipment used in the research project

Materials	Formula	Supplier
Distellat water	H_2O_2	
Poly(vinylidene difluoride) (PVdF)	$(CH_2CF_2)n$	
Potassium hydroxide	KOH	
Potassium permanganate	$KMnO_4$	
Acetone	C_3H_6O	
Carbon nano fiber	C	
Active carbon	C	
Gamry 600 potentiostat	-	
glass microfiber filter	MFV5	
Swagelok cell	-	
Ethanol	CH3CH2OH	
agate mortar	-	
Hot Plate & Magnetic stirrer	-	
Ultrosonicator	-	
hydraulic press	-	
agate ball mill	-	

2.2. Materials Characterization Techniques

The following materials characterization techniques were implemented in the research project to identify the phases, present the textural features, and determine the compositions of the as-prepared materials**.**

2.2.1 Brunauer-Emmett-Teller Surface Area and Barrett-Joyner-Halenda Pore Size and Volume Analysis

Brunauer-Emmett-Teller (BET) and Barrett-Joyner-Halenda (BJH) are analysis theories for determining surface area, pore size and pore volume of the desired materials. The abbreviated terms of BET and BJH are named from the initials of the family names of those developers. BET analysis examines the external area and pore area of the materials to determine the total specific surface area in m^2 /g by nitrogen multilayer adsorption isotherms. BJH analysis can also be employed to determine pore area and specific pore volume using nitrogen adsorption and desorption techniques to characterize pore size distribution of the sample. Both BET surface area and BJH pore size distribution can be derived from the nitrogen adsorption and desorption isotherms obtained from a surface area analyzer as shown in Fig. 2.1. The BET theory applies to systems of multi layer adsorption, and usually utilizes probing gases that do not chemically react with material surfaces as adsorbates to quantify specific surface area. Nitrogen is the most commonly employed gaseous adsorbate used for surface probing by BET methods. For this reason, standard BET analysis is most often conducted at the boiling temperature of N_2 (77 K). Further probing adsorbates are also utilized, albeit with lower frequency, allowing the measurement of surface area at different temperatures and measurement scales. [1]

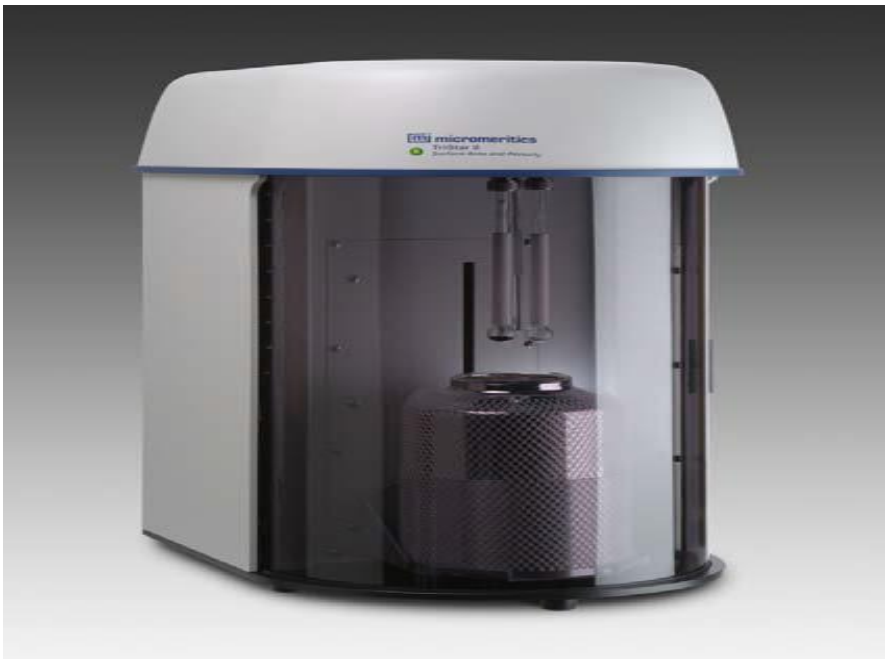

Figure 2.1. Micromeritics TriStar 3000 V6.04 A

The BET equation has been developed to calculate the surface area of a finely divided solid.. The total amount of nitrogen taken up at a pressure of 1 atm and a temprature of 77K gives the total pore volume. The Barrett-Joiner_Halenda procedure assumes capillary condensation of the liquid nitrogen within the pores and calculates from the relative pressures and the amount of nitrogen taken up at a given relative perssure of the sorption isotherm taking into account the adsorbed layer of nitrogen and the capillary condensed nitrogen the pore size distribution. That the procedure is not well founded apperars from the fact that the adsorption and the desortpion branch lead to different pore size distributions. Therefore the desoption branch is usually employed. The adsorption isotherms generally follow one of the six forms, five of which were originally assigned by Brunauer in1940[2] as given in Figure 2.6. Based on the IUPAC classification, Type I isotherms are observed for microporous solids having relatively small external surfaces, the limiting uptake being governed by the accessible micropore volume rather than by the internal surface area. The reversible Type II isotherm is the normal form of isotherm observed for a non-porous or macroporous adsorbent with unrestricted monolayer-multilayer adsorption. Point B in figure 2.2 (a) II, the beginning of the almost linear middle section of the isotherm, is often taken to indicate the stage at which monolayer coverage is complete and multilayer adsorption about to begin. Types III and V arise under conditions where gas molecules have more affinity for one another than for the

adsorbent. Type VI isotherm that is rarely observed, indicates non porous samples with completely uniform surface[2-4]. The Type IV isotherms are characterized by hysteresis loop which is associated with capillary condensation at mesopores limiting uptake to a high partial pressure. Although the effect of various factors on adsorption hysteresis is not fully understood, the shapes of hysteresis loops have often been used to identify the specific pore structures. Hysteresis loops observed at higher partial pressures of adsorption isotherm are associated with capillary condensation in mesopore structures. H1 type loop has two branches are almost vertical and nearly parallel over an appreciable range of gas uptake. On the other hand, the branches remain nearly horizontal and parallel over a wide range for H4 loop. Types H2 and H3 are regarded as intermediate between these two extremes. The steep region of the desorption branch leading to the lower closure point occurs at a relative pressure depending on adsorbate (for Nitrogen, p/p° - 0.42) and is almost independent of the nature of the porous adsorbent. According to IUPAC.[4], Type H1 represents porous materials consisting of agglomerates or compacts of approximately uniform spheres and narrow distributions of pore size. Type H2 loops represent a wide distribution of pore size and shape is not welldefined and at times were attributed to a difference in mechanism between condensation and evaporation processes occurring in pores with narrow necks and wide bodies ('inkbottle' pores). The Type H3 loop observed with aggregates of plate-like particles giving rise to slit-shaped pores. Similarly, the Type

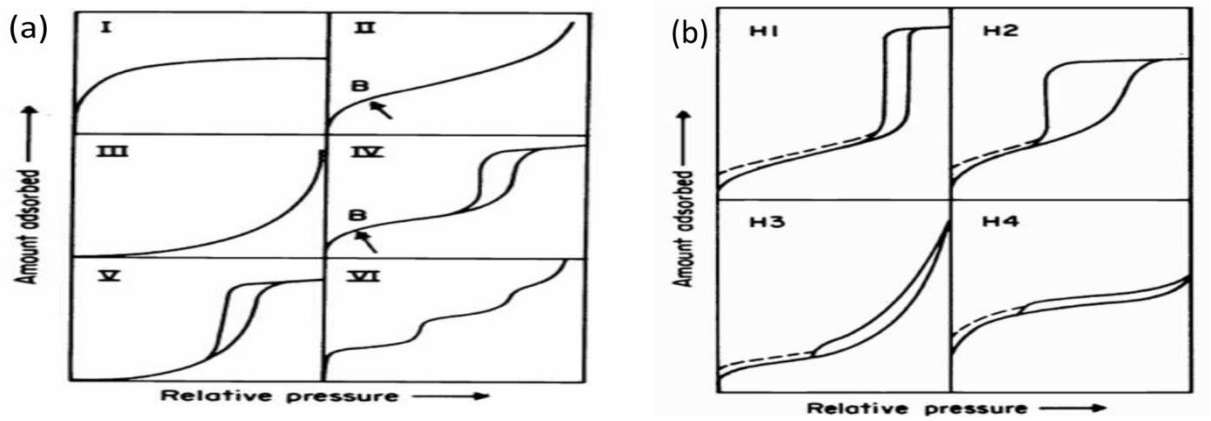

Figure 2.2. Basic types of physical adsorption isotherms and (b) types of hysteresis loops [4,5]

H4 loop is often associated with narrow slitlike pores with significant microporosity. [1]

2.2.2. Scanning Electron Microscopy and Transmission Electron Microscopy

Electron diffraction is a characterization technique used to study matter by firing a beam of accelerated electrons to a sample to obtain the interference pattern. Electron diffraction is usually performed in a scanning electron microscope (SEM) and a transmission electron microscope (TEM) to study the crystal structure of solids and examine their specific morphology.

2.2.2.1. SEM

An SEM images a sample by scanning it in a raster scan pattern with the excited electron beam. The atoms that make up the sample produce signals during each scan to deliver information about the sample's surface topography, composition, and other properties such as electrical conductivity. A Field Emission SEM (FE-SEM) is equipped with a field emission cathode in the electron gun to provide enhanced resolution and to minimize the charge issues and sample damage. [6,7], Fig. 2.3displays a typical FE-SEM facility

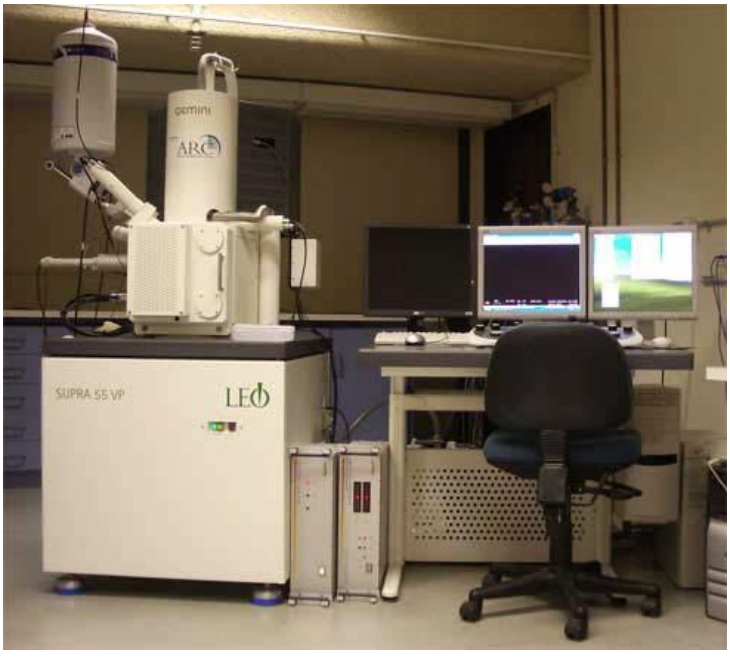

Figure 2.3. FE-SEM facility (Jeol J-7100). [7]

2.2.2.2. TEM

Before measurement, the sample was dispersed in ethanol and then dripped and dried on a copper grid. In the operation of TEM, an electron beam is focused on a specimen and

part of the electron beam is transmitted. This transmitted portion is focused by objective lens into an image and the image is passed down through enlarge lenses and a projector lens, being enlarged all the way. In the experiment, the TEM was used to characterize the internal structure of particles and the TEM images were obtained on a JEOL 2011 and JEM 2010F transmission electron microscope operated at an acceleration voltage of 200 kV. Fig 2.4, as shown below, presents a commercial TEM setup (. JEOL 2011) [7]

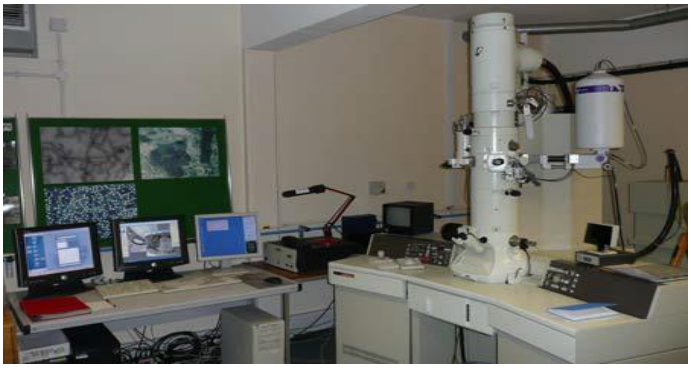

Figure 2 Commercial TEM setup (.JEOL 2011)

2.2.2.3 Raman Spectroscopy

Raman spectroscopy is a non-destructive spectroscopic technique used to study vibrational, rotational, and other low-frequency modes in a molecular system. The laser light in the Raman Microscope focuses on the test sample and interacts with its vibrations or excitations at a molecular level, generating shifted laser photons, which are immediately recorded on a Raman spectrum. The resolution of the Raman spectra can be enhanced by accumulated scans with a longer exposed time. Fig.2.5 **shows** a lab RAM HR Microscope. [6,7]

Figure 3. LAB RAM HR Raman Microscope. [6]

2.3 Electrochemical Testing

The electrochemical characterization (Cyclic Voltammetry, Galvanostatic charge discharge and Impedance spectroscopy) of electrode in this thesis, was made in a Swagelok cell as shown in fig 2.6, using a Gamry 600 potentiostat. The glass microfiber filter (MFV5) was used as a separator.

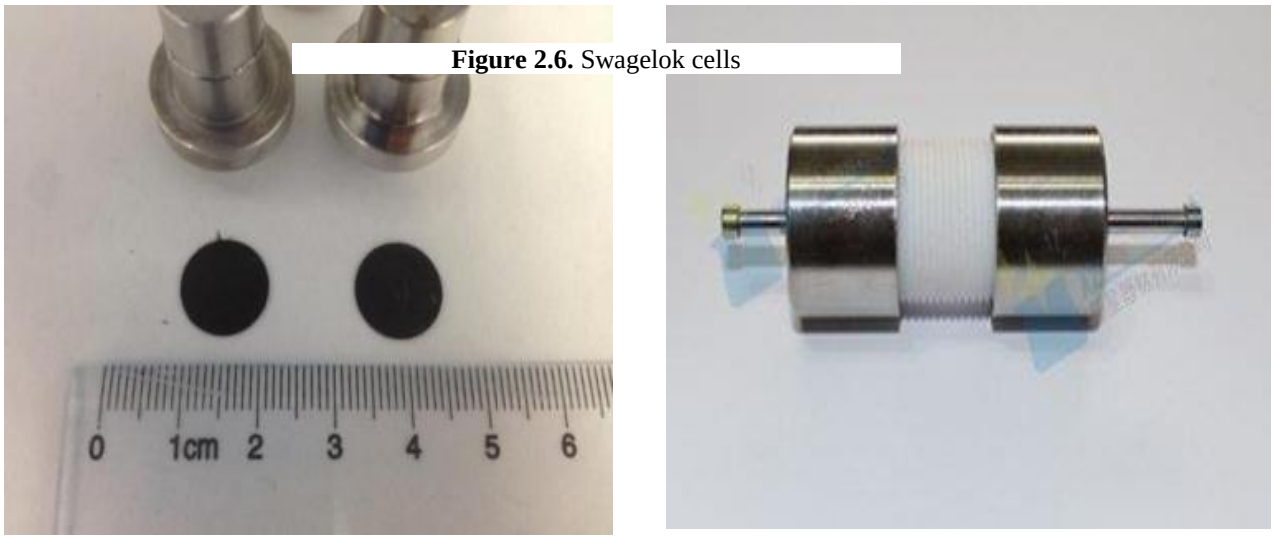

Figure 2.6. Swagelok cells

2.3.1. GAMRY Reference 600

Figure 4. Gamry Instrument [8]

The Reference 600 is a high performance Potentiostat/Galvanostat/ZRA for demanding electrochemical applications. It is ideal for fundamental electrochemical studies in areas as diverse as physical electrochemistry, corrosion measurement, batteries, coatings, supercapacitor, nanotechnology, and sensor development. Gamry offers a complete library of electrochemical application software for the Reference 600. Electrochemical experiments are performed in the Gamry Framework and the data are analyzed in the GamryEchem Analyst Gamry potentiostats (as well as some others) are all 4- probe instruments. This means that there are 4 relevant leads that need to be placed in any given experiment. Two of these leads—Working (green) and Counter (red)—carry the current, and the other two— Working Sense (blue) and Reference (white)—are sense leads which measure voltage (potential).as shown in fig 2.7 Two-electrode experiments are the simplest cell setups, but often have far more complex results, and corresponding analysis. In a two-electrode setup, the current carrying electrodes are also used for sense measurement. The physical setup for two-electrode mode will have the current and sense leads connected: Working (W) and Working Sense (WS) are connected to a (working) electrode and Reference (R) and Counter (C) are connected to a second (aux, counter, or quasi- /pseudo-reference) electrode. A diagram of 2- electrode cell setup can be seen in Figure 2.8. [8]

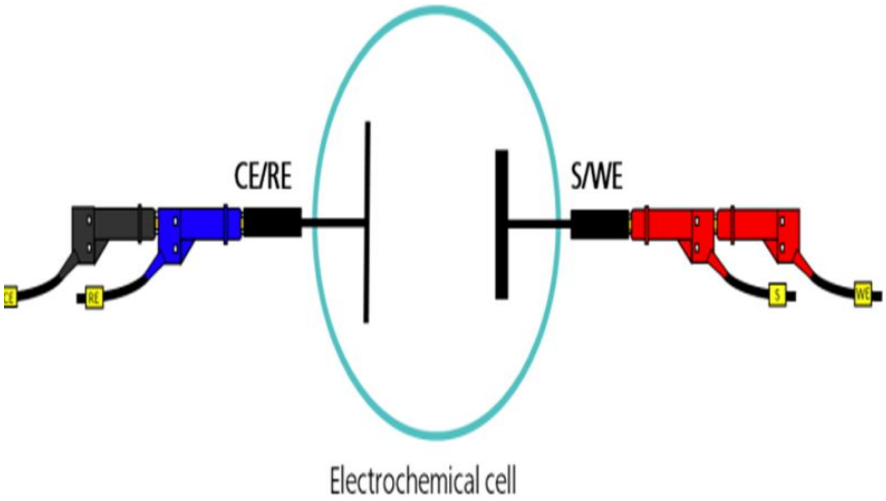

Figure 5. Schematic view of the 2-electrode setup

Two-electrode experiments measure the whole cell, that is, the sense leads measure the complete voltage dropped by the current across the whole electrochemical cell: working electrode, electrolyte, and counter electrode

2.3.1.1. PHE200™ Physical Electrochemistry Software

The PHE200 provides a complete library of electrochemical techniques, such as cyclic voltammetry, CD, for characterizing electrochemical reaction mechanisms and studying the electrode interface.

2.3.1.2. EIS300™ Electrochemical Impedance Spectroscopy

EIS is a powerful tool for a variety of applications. Using our unique Sub-Harmonic Sampling, Gamry has civilized EIS – it's easy to use, it's compact, and it's very affordable. Gamry offers the widest range of EIS techniques, including potentiostatic, galvanostatic, and hybrid great for batteries and fuel cells, supercaps

2.3.1.3. PWR800 Electrochemical Energy Software

Gamry Instruments' PWR800 Electrochemical Energy Software is a tool for testing advanced electrochemical devices. It works with a Gamry Instruments Potentiostat to

automate electrochemical testing in energy research. The PWR800 includes both simple, easy-to-use standard techniques and powerful sequencing tools for complicated tests Electrochemical cells used in energy technology include:

1-Fuel Cells 2- Batteries 3- Solar Cells 4-Super-Capacitors

The PWR800 runs a wide range of techniques on all these cells. It can test: a half-cell in a 3-electrode setup, small test cells, packaged cells, and series-connected cell stacks.

The PWR800 includes a flexible system for limit testing that terminates an experiment step when a limit condition is true. Possible limit tests parameters include:

1-Voltage 2-Current 3- Temperature 4-Power 5-Capacity 6-Energy 8-Step Time

Limit tests include under- and over- conditions and may allow for rate-of-change or absolute value calculations before the test. All common recharge protocols for commercial batteries and supercaps are possible using these limit tests.

Techniques in the PWR800 include:1-Cyclic Voltammetry (CV) 2-Cyclic Charge Discharge (CCD) 3-Discharge in Three Modes: Constant Current, Constant Power and Constant Load Resistance 4-Constant Current Charge 5-Polarization Curve

6-Simple Potentiostatic and Galvanostatic Tests 7-CCD with EIS Spectra in Each Charge State

1-Cyclic Voltammetry (CV)

Electrochemical testing on a new chemical system begins with Cyclic Voltammetry. The PWR800 CV technique is a simplified version of CV in Gamry's PHE200 Physical Electrochemistry Software. In CV, a cyclic linear voltage ramp is applied to an electrochemical cell and the cell current is plotted versus cell potential. The user has control of the ramp's Initial Potential, Final Potential and two Vertex Potentials. Potentials can be specified as relative to a measured open-circuit voltage or relative to a reference electrode voltage. CV scan rates can vary from a few microvolts per second to more than 1000 volts per second. Current range selection may be specified as auto-ranging or fixed.CV analysis includes peak location, base line correction, and integration

2-Cyclic Charge-Discharge (CCD)

The Cyclic Charge-Discharge is used in the study of secondary batteries and supercapacitors as they store and then release energy. A CCD test starts with a charge or

discharge step and repeats the charge-discharge process through many cycles. The test can end early if a Loop End test becomes true.

CCD can measure:

1-Capacity Fade 2-Energy Efficiency 3-Coulombic Efficiency 4-Imbalance in Cell Stacks

CCD uses constant current charging with optional voltage finish. CCD discharge is done at constant current, constant power or constant resistance. The discharge step ends after a set time or after a Stop At test becomes true

In CCD users can save selected "raw" charge and discharge curves. If the test uses the AE option, the raw data file will include AE voltages CCD data is analyzed with Gamry'sEchem Analyst. By default, a CCD file plots with Cycle Number of the X-axis and both Discharge and Charge Capacity on the Y-axis. Axis transforms in the Echem Analyst allow calculations on CCD data. The X axis can be transformed from cycle number to time.Y axis transforms include: 1-Charge Capacity 2- Capacitance 3- % Capacity 4- Coulombic Efficiency 5-Energy 6-EnergyEfficiency 7-Step Duration

AE data from a CCD test is plotted using the Echem Analyst's.[8]

3-CCD with EIS

The PWR800 combines Cyclic Charge-Discharge with EIS (Electrochemical Impedance Spectroscopy). EIS spectra can be recorded after charge, after discharge, or after both. Galvanostatic spectra are recorded with zero DC current and selectable AC current

EIS can be useful in determining capacity fade mechanisms. Comparison of EIS spectra at different points in a battery's lifetime can detect increases in electrolyte resistance, loss of active electrode area, and changes in reaction kinetics (to name only a few). CCD with EIS will not operate unless the system includes an EIS300 software license. With the AE option the PWR800 can simultaneous measure the current is applied to all cells, so an AC voltage measurement is sufficient for calculation of the complex impedance of the cells.

A simple electrochemical cell consists of two electrodes and an electrolyte. An electrode is the interface at which dissolved substrates may pick up or lose electron(s). An electrolyte is needed to provide electrical conductivity between the two electrodes. . [8]

2.4. Electrochemical measurements

The Techniques for testing electrodes are 1-cyclic voltammetry (CV) 2- galvanostatic charge /discharge (GCD) 3-impedance spectroscopy(EIS)

2.4.1. Cyclic voltammetry (CV)

Cyclic voltammetry (CV) is a quick screening procedure for identifying potential capacitor materials [22]. In CV tests, the voltage is swept between two values at a constant scanning rate ($s = \pm dV/dt$). The resulting current (I) is recorded as a function of time. For an ideal EDLC, the shape of the CV is rectangular, indicating that the current is independent of the potential. The capacitance is determined as $C = I/s$. However, for those non-ideal EDLCs and pseudocapacitors, the rectangular shape is distorted. In these cases, the current, I(t), is a function of time, and the capacitance is determined as according to the equation 2.1 CV has become a major method for evaluating performance of SCs because it is convenient for determining the cycle life, in addition, through an analysis of the shapes of the voltammograms as a function of s, the information on internal resistance effects and the consequent dissipative losses can be revealed.

$$C_S = \int \frac{IdV}{\mathrm{Sm}\Delta\mathrm{V}} \qquad (2.1)$$

Where I is the average current and ΔV THE the voltage window, S is the scan rate mV/s , m the total mass of active material of electrode

For a reversible electrochemical process, the shap of EDLCs should be close to the rectangular shape, while faradaic capacitors have shape a curved with anodic and cathodic peak for a reversible electrochemical process, as shown in fig 2.9

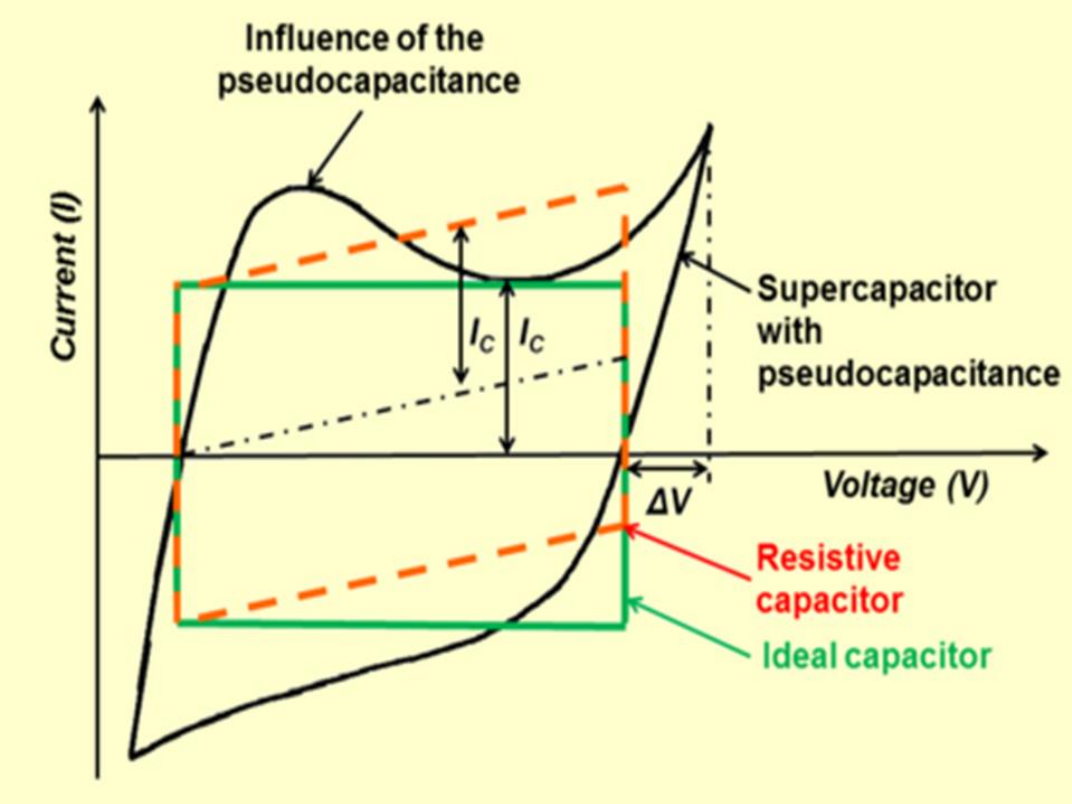

Figure 6. Schematic of typical electrochemical capacitor showing the differences between static capacitance (rectangular) and faradaic capacitance (curved)

Reversible electrochemical process, the CV plots should have peak voltage difference between the anodic and current cathodic peak of 59 m V. The peak positions do not change as a function of scan rate, the ratio of the peak currents should also be unity for reversible electrochemical process. [9,10]

2.4.2. Constant Current Techniques

Constant current charge/discharge experiment can be performed as a complementary procedure to the CV experiment. The experiment is carried out by applying

a constant current between the working and references electrodes and recording the potentialbetween the working and reference electrodes. Charging or discharging the cell at constant current results in a voltage response as opposed to the CV technique. The charge/discharge capacity (Q) can be calculated by integrating the current with respect to time. The discharge capacitance (C) was estimated from the slope (*dV/dt*) of the linear portion of the discharge curve using equation 2.2

$$C_s = \left(\frac{2I}{(dV/dt).m}\right) \qquad (2.2)$$

Constant current techniques also help to construct a Ragone plot. In this plot the energy density and power density are plotted against each other. Using this energy-power relation, different electrochemical power sources can be compared. The usual curve of galvanostatic charge- discharge process. [10]

1- The cell behavior during charging 2- the cell behavior during discharge 3- the initial process and 4- ohmic potential drop

2.4.3. Electrochemical Impedance Spectroscopy (EIS)

EIS is an important electrochemical technique used to obtain information about the characteristic frequency responses of supercapacitors and the capacitive phenomena occurring in the composite electrodes. EIS technique consists of the application of a small potential perturbation between a frequencies range at a given DC potential. A common impedance plot, also known as Nyquist plot, displays real and imaginary components of impedance on x and y axis respectively. It depicts a low frequency semi-circle and a high-frequency straight line combined with a 45^{o} line between these two regions as shown in (Fig.2.10).[11]

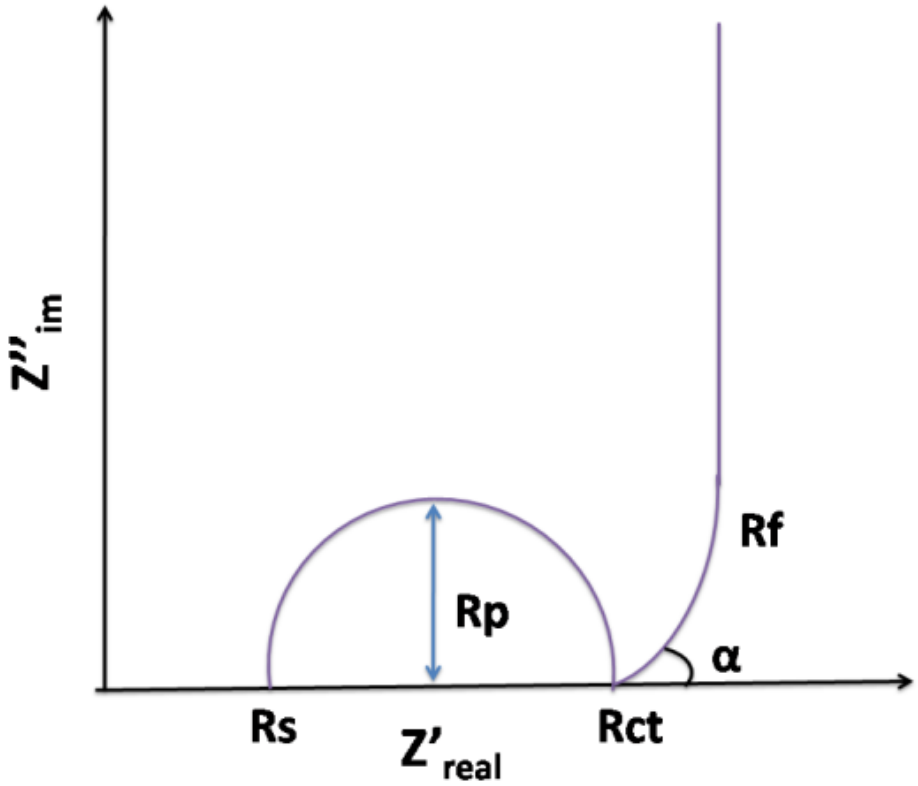

Figure 7. Components of a Nyquist plot for a supercapacitor

At the high frequency region, this semi-circle type behaviour is likely to appear because of the charge-transfer process and/or the different contact resistances and double layer capacitance. At lower frequencies, the straight line shows the diffusive processes, and is

at 90^{o} for an ideal supercapacitor. These two regions are generally combined with a 45^{o} inclined mid-frequency line which is consistent with the porous nature of the electrode when saturated with the electrolyte. At high frequencies, the resistance characteristics of the different supercapacitors are expressed by the so-called electric series resistance (Rs or ESR), which includes electrolyte resistance, collector/electrode contact resistance, and the resistance of the electrode/electrolyte interface. [11, 12] The radius of the semi-circle expresses the polarization resistance (R_p) which gives information about the electrolyte access into the pores. R_{ct} is the charge transfer or electrolyte resistance and lastly, R_f isthe contact resistance between thin electrode and current collector. Impedance spectra were recorded with 10 mV AC perturbation in the frequency range of 100 kHz to 10 mHz at 0V OCV for the supercapacitor test (two electrodes test) .[12] the specific capacitance of one electrodes was determined using the equation (2.3) :

$$C_s = 4\left(-(1/2\pi f z'' m)\right) \tag{2.3}$$

Where *f* is the lowest frequency, z'' is the imaginary impedance at *f* and *m* is the weight of one electrode. The EIS data as a function of the frequency were analyzed using equations (2.4), (2.5) and (2.6):

$$C(\omega) = C'(\omega) - jC''(\omega) \tag{2.4}$$

$$C''(\omega) = Z'(\omega) / \omega \left| Z(\omega) \right|^2 \tag{2.5}$$

$$C'(\omega) = -Z''(\omega) / \omega \left| Z(\omega) \right|^2 \tag{2.6}$$

where *Z(ω)* is equal to 1/*jωC(ω), C'(ω)* is the real capacitance, *C'' (ω)* is the imaginary capacitance, *Z'(ω)* is the real impedance and *Z'' (ω)* is the imaginary impedance. [13]

A relaxation time can be calculated from knee frequency in the real and imaginary plot according to the equation 2.7. [13]

$$\tau_0 = {}^{1}/_{f_k} \qquad (2.7)$$

Where f_k is the knee frequency at phase shift 45º

References

[1] - Sudhakar Jagannathan, PROCESS, STRUCTURE AND ELECTROCHEMICAL PROPERTIES OF CARBON NANOTUBE CONTAINING FILMS AND FIBERS, PhD Thesis, Georgia Institute of Technology August 2009

[2] Webb PA, Orr C. Analytical methods in fine particle technology. Micromeritics

Instruments Corp , Norcross, Georgia. 1997.

[3] Lowell S, Shields JE, Thomas MA, Thommes M. Characterization of porous solids and powders: Surface area, pore size and density. Kluwer Academic Publishers,

Dordrecht/Boston/London. 2004.

[4] Sing KSW, Everett DH, Haul RAW, Moscou L, Pierotti RA, Rouquerol J, et al.

Reporting physisorption data for gas/solid systems with special reference to the determination of surface area and porosity. Pure & Appl Chem. 1985;57(4):603.

[5] Brunauer S, Deming LS, Deming WE, Teller E. On a Theory of the van der

Waals Adsorption of Gases. Journal of the American Chemical Society. 1940;62(7):1723-32.

[6] Bei Wang, B. Sc., M. Eng, Graphene-based Nanocomposite Materials for High-performance Supercapacitors and Lithium Rechargeable Batteries, Doctor of Philosophy, University of Technology Sydney ,2012

[7] http://www.rothamsted.ac.uk/pbcs/bioimaging/Equipment_EMs_TEMs.php

[8] Reference 600™ Potentiostat/Galvanostat/ZRA Operator's Manual, Copyright © 2012–2015 Gamry Instruments, Inc. Revision 6.01

[9] Katlego Makgopa, effect of carbon nano materails on performance of symmetric pesedocapaccitors , PHD thesis ,University of Pretoria,May 2016

[10] Kuttipillai, Padmanaban Sasthan, "Performance evaluation of a novel asymmetric capacitor using a light-weight, carbon foam supported nickel electrode", Master's Thesis, Michigan Technological University, 2011.

[11] SUHEDA ISIKLI, QUINONE –BASED ORGANIC REDOX COMPOUNDS FOR

ELECTROCHEMICAL ENERGY STORAGE DEVICES, DOCTOR OF PHILOSOPH FromAUTONOMOUS UNIVERSITY OF MADRID, **2013**

[12] F. Lufrano and P. Staiti, Energy & Fuels, 2010, **24**, 3313–3320.

[13] C. Portet, O.L. Taberna, P. Simon, E. Flahaut and C. Laberty Robert, Electrochim. Acta, 50 (2005) 4174.

Chapter 3: Flexible supercapacitors based on low-cost tape casting of high dense carbon nanofibers

3.1. Introduction

The wearable devices that intercommunicate with each other are growing rapidly [1]. One of the major challenges is to relate the energy storage system with mechanical flexibility and easy to integrate into wearable devices. Various studies are trying to develop flexible structures to obtain a fast recharge, durable and safe supercapacitors. Different carbon structures have been used to manufacture the electrode for supercapacitors, such as activated carbon [2], carbon nanotube (CNT) [3-5], carbon nanofibers (CNF) [6], graphene [7] and carbon aerogel [8, 9]. Batteries and supercapacitors perform their operations on the ion-exchange and the reduction-oxidation reactions at the surface of the electrode. A key factor to capture a large number of ions in the interface between the electrode and the electrolyte is the specific surface of the electrode. The specific surface is directly proportional to the capacity to accumulate electric charges. Nevertheless, the specific surface must be accessible for the ions, to develop porous surfaces, where ion kinetics is enhanced by the porosity [10]. The carbon material which has good combination of high microporosity, well maintained mesoporous structure and active nitrogen functional groups can show better properties for supercapacitor applications [8,

9]. The combination of porosity and porous size has to be adapted to the ions size, which will be carried by the electrolytic solution.

According to the mechanism used to store the electric charge, the electrochemical capacitors can be classified into two types: (1) Electric Double Layer Capacitors (EDLCs) works based on an electrostatic attraction between the ions and the surface of the electrode. (2) Pseudo-capacitors exhibit charge transfer reactions (similar to batteries where the only difference is the transferred charge is proportional to voltage and its reversible). Moreover, pseudocapacitors exhibit higher energy density than the EDLCs because of the involvement of redox active material in storing charges both on the surface as well as in sub-surface layer [11]. Usually metal oxides are the suitable materials for pseudo-capacity. Generally, pseudocapacitance is associated with reversible Faradic redox processes in various oxidation states of transition metal oxides (RuO_2, V_2O_5, MnO_2, NiO, and IrO_2). Among these oxide materials, MnO_2 has been recognized as a promising pseudocapacitive material since MnO_2 has a lower cost and is considered environment friendly than other metal transition oxides [3, 12]. However, the poor conductivity of MnO_2 (10^{-5}-10^{-6} S/cm) limits the charge/discharge rate for high power applications [13]. Recently, CNFs have gained much interest because of high surface area, mechanical stability, flexibility and relatively higher conductivity. Thus, the CNFs and metal oxide based nanocomposite can be engineered as a flexible supercapacitor. There are several studies on the fabrication of flexible supercapacitors based on the carbon material [14-19]. C Ma, et al. assembled electrospun phenolic-based nanofibers and performed chemical treatment with KOH to obtained higher surface area [14]. In the study of Liu et al. flexible porous carbon nanofibers exhibits a specific capacitance of 104 F/g at a current density of 0.2 A/g [15]. M Zhi et al. showed that addition of acetylacetonate in CNFs increase their surface area. The composite of acetylacetonate/CNFs/MnO_2 electrode delivers specific capacitance of 311 F/g at a scan rate of 2 mV/s [16]. Y Huang et al. reported that multi material (CNFs/Co_3O_4/MnO_2) nanocomposite flexible electrode exhibits specific capacitance of 840 F/g at scan rate 5 mV/s based on the mass of MnO_2 [17]. D Zhou prepared hybrid nanostructured of MnO_2/Porous CNF electrode which presents high specific capacitance 520 F/g at 0.5 A/g [18]. Yang et al. shown a simple method to introduce micropores without damaging a 3D mesoporous carbon nanonetwork structure [10] S. K. Nataraj et al. manufactured flexible thin film nanocomposited supercapacitor by in situ coprecipitation of 2D MnO_2 nanosheet in the presence of CNFs.

They claimed a gravimetric capacitance of 142 F/g for CNFS-MnO_2 electrode interfaced with PVA-H4SiSiW12O40.nH_2O with slow scan rates [19]. Q Liu et al. fabricated flexible supercapacitor sheets based on diverse materials such as carbon nanotubes, silicon, titanium oxide particles and graphene flakes, incorporated into the conducting polymer polyaniline to form nanocomposite which presents specific capacitance of 477.1 F/g [20]. These reports suggest that flexible electrodes based supercapacitors are potential candidate for portable, wearable equipment. As far as we know there is no work in literature related to the use of low casting high dense carbon nanofiber alone and as in composite structure with MnO_2 for supercapacitors.

In the present work, a novel and flexible electrode based in carbon nanofibers has been developed. Various aqueous electrolyte concentrations were tested to obtain higher specific capacitance of flexible CNFs. The fast, easy and simple chemical treatment methods was used to treat CNFs with $KMnO_4$. Moreover, the effect of loading mass of MnO_2 deposited on the CNFs for supercapacitor were studied.

3.2. Experimental setup

Commercially available carbon nanofibers (CNFs), synthesized by CVD floating technique, developed by Grupo Antolín S.A., is used [21]. The diameters of the fibers are ranging from 30 to 80 nm and lengths up to several μm. For the preparation of electrodes, carbon nanofibers were casted by tape casting. This is a well-known process at industry in

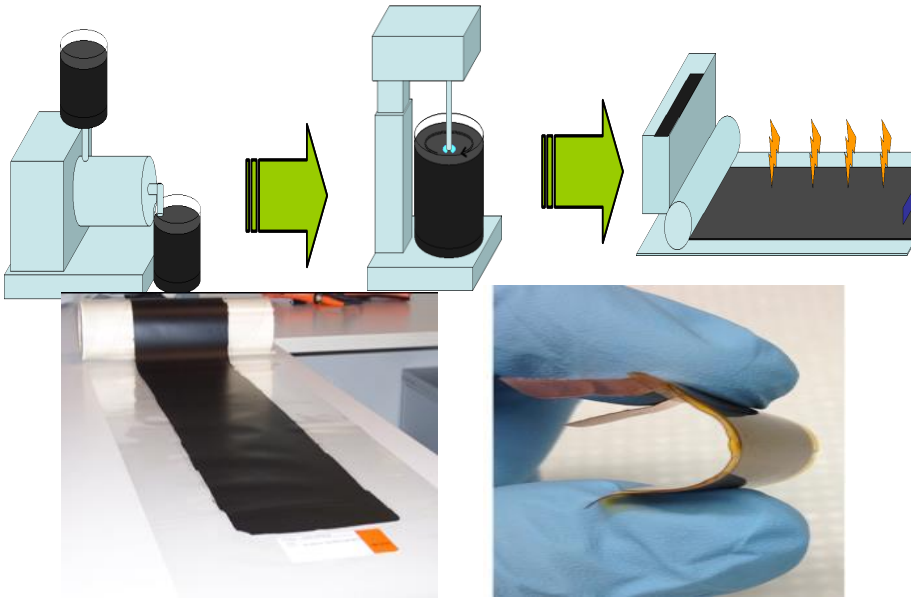

which powders are mixed with polymers and vehicle (organic or water) and later casted in a band for further processes [22, 23]. For the tape casting process, samples of carbon nanofibers where mixed with polymer in water as depicted in Figure 3.1.

Figure 3.1. (top) schematics of the tape casting process including slurry formulation and tape cast, (bottom left) image of the casted carbon nanofibers in a rolled tape, (bottom right) flexibility of the CNF tape.

In the first step the CNFs were gently dispersed in water in a pearls mill; in the second step, a slurry was formulated by mixing the water dispersed CNFs and a copolymer PE-PVAc (Celanese, Mowilith 1081 LDM) in a mechanical mixer under vacuum conditions. Different polymer concentration has been tested, a weight ratio 1:1 polymer to CNFs was considered for this work. Once the slurry was ready, the material was deposited using doctor blade system on a mylar © carrier and dried. The doctor blade carrier system and drying features were a CAM-H series Tape Casting Machine from KEKO equipment. The obtained tape is a homogeneous band without defects and pinholes of 500 mm wide and 75 μm thick. The optimized process produces 0.3 meters per hour [24]. Carrier was withdrawn prior to be used in supercapacitors.

The MnO_2/CNFs composite were synthesized via a direct redox reaction between $KMnO_4$ and CNFs based tape casting. The tape cast was cut into 10 mm diameter and immersed into a chemical treatment using $KMnO_4$ with different concentrations of 100, 450 and

1000 mg dissolved in 20 ml distilled water. The $KMnO_4$ solution was heated until the temperature reaches 47 °C. Afterwards, a 10 mm disc of CNFs was immersed in the solution for 10 minutes and was dried for 1h at room temperature. The deposited loading masses of MnO_2 were 0.3, 0.41 and 0.6 mg for $KMnO_4$ concentrations 100, 450 and 1000 mg respectively. These loading masses were designated as S1, S2 and S3 respectively. The samples were tested using a two-electrode test cell. The electrochemical characterization (Cyclic Voltammetry, Galvanostatic charge discharge and Impedance spectroscopy) of CNFs alone and chemically treated with $KMnO_4$ CNFs, a disc was made in a Swagelok cell, using a Gamry 600 potentiostat. The glass microfiber filter (MFV5) was used as a separator. The surface morphology of CNFs and CNFs/MnO_2 composite electrode were studied by using scanning electron microscopy (SEM) (Jeol J-7100)and higher resolution transmission electron microscopy (HR-TEM) (JEOL JEM-2100, Japan).Raman spectroscopy measurement was performed to analyze the difference in the structure of CNFs and CNFs/MnO_2 using micro-Raman spectroscopy (HORIBA LabRam HR800, Japan. A green laser of wavelength 532 nm, 0.5 mW and a 50 LWD objective was used during the measurements. The specific surface area and pore size distribution of CNFs alone and in nanocomposite (CNFs/MnO_2) for samples S1, S2 and S3 were obtained by the N_2 adsorption/desorption isotherm using Micromeritics TriStar 3000 V6.04 A system.

3.3. Results and discussion

The electrochemical properties of CNFs as electrodes for supercapacitors were analyzed by using various concentrations of KOH (3, 6 9 and 12 M) as a suitable electrolyte for supercapacitors. In order to evaluate the supercapacitor performance, numerous methods

were applied such as cyclic voltammetry, charge/discharge and impedance spectroscopy. First cyclic voltammetry was performed in the voltage window from 0 to 1 V. The specific capacitance per unit mass for one electrode was calculated using equation (3.1).

$$C_s = 4 * C/m \quad (3.1)$$

$$C = \frac{q_a + |q_c|}{\Delta V} \quad (3.2)$$

Where C_s is the specific capacitance in F/g, C is the measured capacitance for the two-electrode cell by equation 3.2 and m is the total mass of the active material in both electrodes [25]. In double layer capacitors it is important to achieve rectangular shaped cyclic voltammograms (CVs) for all scan rates. Figure 3.2(a) shows the comparison of different concentrations of KOH as electrolyte at a scan rate 5 mV/s. The mass of one electrode in each measurement was ~ 0.0094 g. The rectangular shape CV is desirable for ideal double layer supercapacitor. However in our case the CV profiles for different concentrations presents irreversible cathodic hump at scan rate. This is possibly

characteristic of Ni catalyst used in synthesis of CNFs and surface oxygen groups observed by EDX not shown here.

Figure 3.2. (a) Cyclic voltammogram comparison at a scan rate 5 mV/s for different concentration of KOH, (b) Specific capacitance comparison at different scan rates, (c) Cyclic voltammogram at different scan rates of (5, 10, 20, 25, 50 and 100 mV/s) for 6 M KOH as electrolyte, (d) Capacitance retention as a function of bending numbers.

The integrated scan area for 9 M is higher than others. Figure 3.2(b) shows the specific capacitance comparison over a wide range of scans for all KOH concentrations. It can be

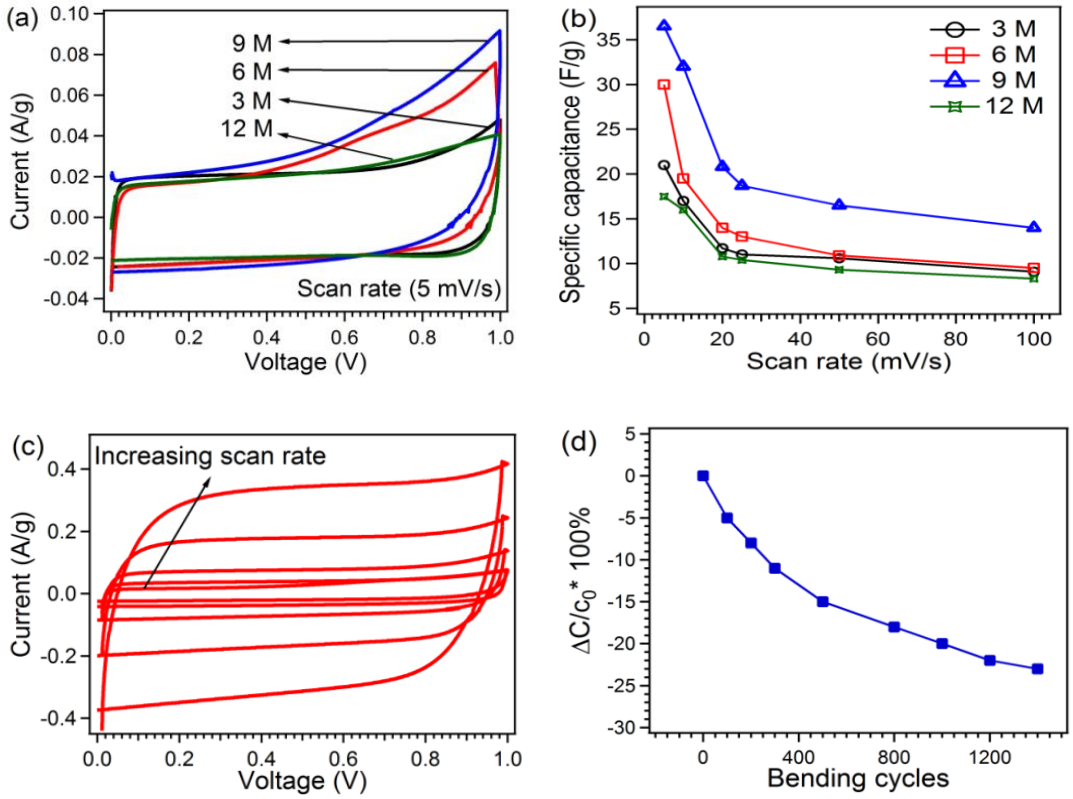

seen that the calculated specific capacitance increases from 18 to 38 F/g for 3 M to 9 M respectively, and decreases for 12 M at a scan rate 5 mV/s. It exhibits the higher electrolyte concentration provide higher ion concentration resulting in enhanced ion accessibilities onto the double layer surfaces [26]. But for much higher concentration of 12 M, capacitance is lower from all other electrolyte concentrations. These results interpret that very high electrolyte concentration 12 M may reduce the ion activity due to less water hydration, thus resulting in decrease in mobility [27]. Another reason could be that the KOH only can be dissolved in the water up to a certain limit. In supersaturation

state excess amount of KOH will remain in the state of solid as undissolved salt crystal in the solution. This solid-state crystals disturb the conductive path of the solution hence decrease the conductive pathways of the electrolyte.

Figure 3.2(c) shows the CVs at different scan rates for 6 M concentration. At the entire scan rates CV curves exhibit almost rectangular shapes, fast current response to the change of voltage sweep directions indicates the highly capacitive nature with good ion response. Therefore, we can say that the contribution of pseudo capacitance to total capacitance of the supercapacitor is negligible; the overall specific capacitance is mainly associated to double layer capacitance. The supercapacitor is flexible and stretchable. It can be bent in any direction without degradation in performance. The specific capacitance remained at 74% after 1200 bending cycle shown in Figure 3.2(d).

The electrochemical characteristics of the electrode and electrolyte were further realized by impedance spectroscopy. The impedance measurements were carried out at AC with 10 mV amplitude over a frequency range between 100 kHz to 0.1 Hz. Figure 3 shows the Nyquist plot of the CNFs with different electrolyte solution concentrations.

The equivalent circuit of a supercapacitor based on porous electrodes and electrolyte presents a complex combination of capacitance (C) and resistance (R) components. The interfacial impedance of a supercapacitor is associated with a double-layer capacitance C_{dl}, pseudocapacitance C_p, Faradaic charge-transfer resistance R_f, the sum of the electrolyte resistance, the electrode resistance, the contact resistance between the electrode and the current collector R_s [28, 29].

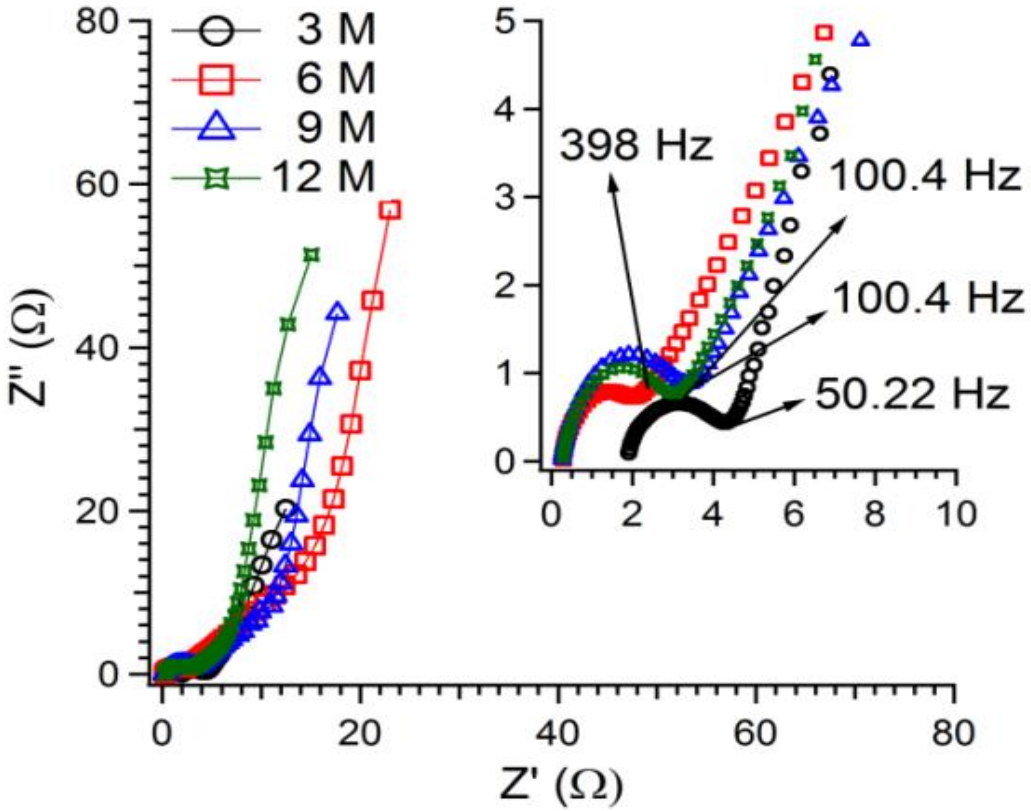

Figure 3.3.Nyquist plot at different electrolyte concentrations of KOH.

The Nyquist plots consist of a high-frequency intercept on the real Z_{Re} axis, a semicircle in the high-to-medium-frequency region, and a straight line at the very low-frequency region. The solution resistance R_s for 3 M was about 1.9 Ω higher than other concentrations which are about 0.1 Ω for all others. The semicircle from high to medium frequency which corresponds to Faradaic charge transfer resistance (R_f) of electrode material was 4.3, 2, 3 and 2.9 Ω for 3, 6, 9 and 12 M KOH concentrations respectively. This indicates that the moderated concentrated solution increases the ionic conductivity in the porous structure of the electrode. It can be seen that a semicircle in the high frequency region and almost a straight line parallel to Z_{img} axis, tells that the supercapacitors have a resistive behavior at high frequencies and a capacitive behavior at low frequencies. The knee frequency represents the maximum frequency where the capacitive behavior is dominant as well as power capability of the supercapacitor. The highest knee frequency 398 Hz was obtained for 6 M, which explains exactly polarized system as shown in Figure 3.3. These electrochemical characterization demonstrate that

relatively higher capacitance with lower ESR can be obtained with 6 M KOH. The optimized KOH electrolyte concentration with lower charge transfer resistance, small ESR and moderate specific capacitance was 6 M. Therefore, further experiments for nanocomposites of manganese and CNFs, 6 M KOH electrolyte solution were chosen.

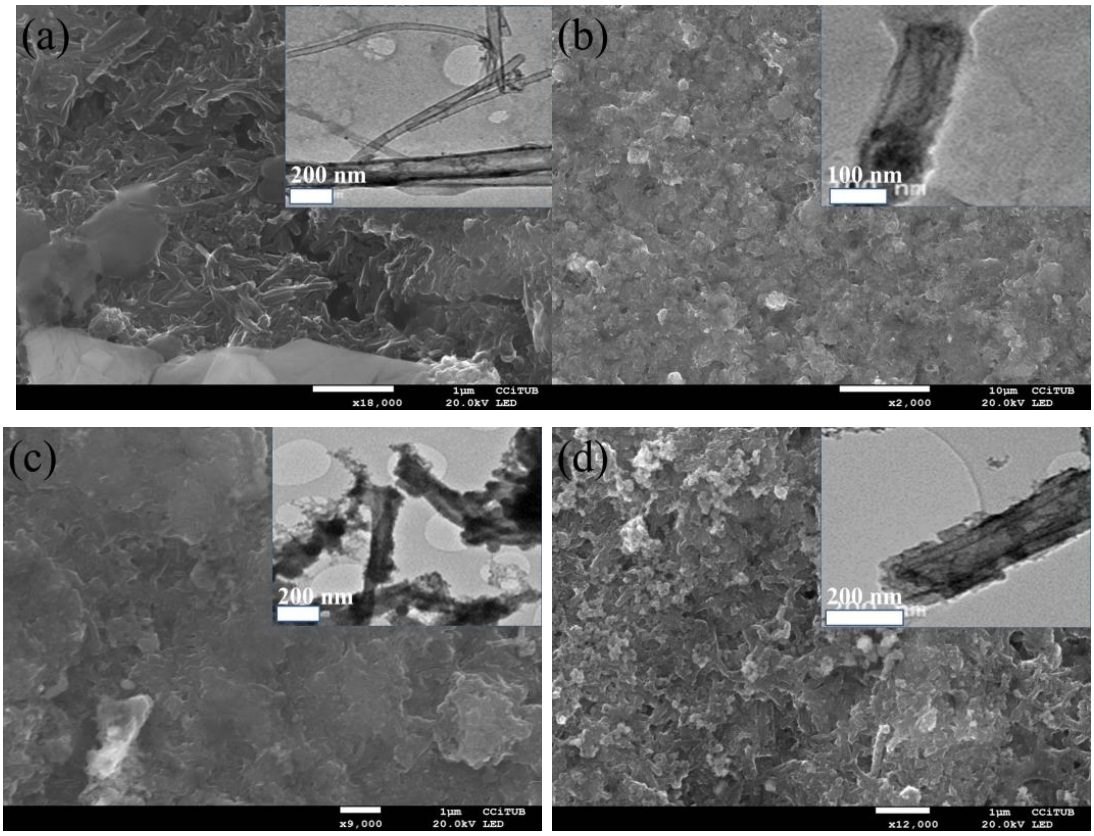

Figure 3.4. SEM images and TEM images (inset) for (a) CNFs, (b) S1, (c) S2 and (d)S3.

The surface morphology of CNFs and CNFs/MnO_2 composite electrode were studied by using SEM and TEM Figure 3.4. Figure 3.4(a) shows the structure of the entangled CNFs as received. Figure 3.4(b) corresponds to S1 sample, where MnO_2 is homogeneously distributed as a thin layer uniformly covering the surface of CNFs. It is very important to achieve a conformal coating of MnO_2 on the surface of CNFs without losing the electronic and ionic conductivity through the electrode. Figure 3.4(c) S2 sample shows that deposited MnO_2 layer on CNFs is thicker than for S1. Figure 3.4(d) S3 shows that MnO_2 is randomly deposited as a thick film and as well as nanosphere-like structures at different places.TEM images show significantly altered CNFs structure after the treatment with KMnO4 Figure 3.4 (insets). MnO_2nanoclusters (thin film) around CNFs for S1 are barely

visible because of small thickness. However, with increase in loading mass for S2 and S3 the thickness of MnO_2 is increased.

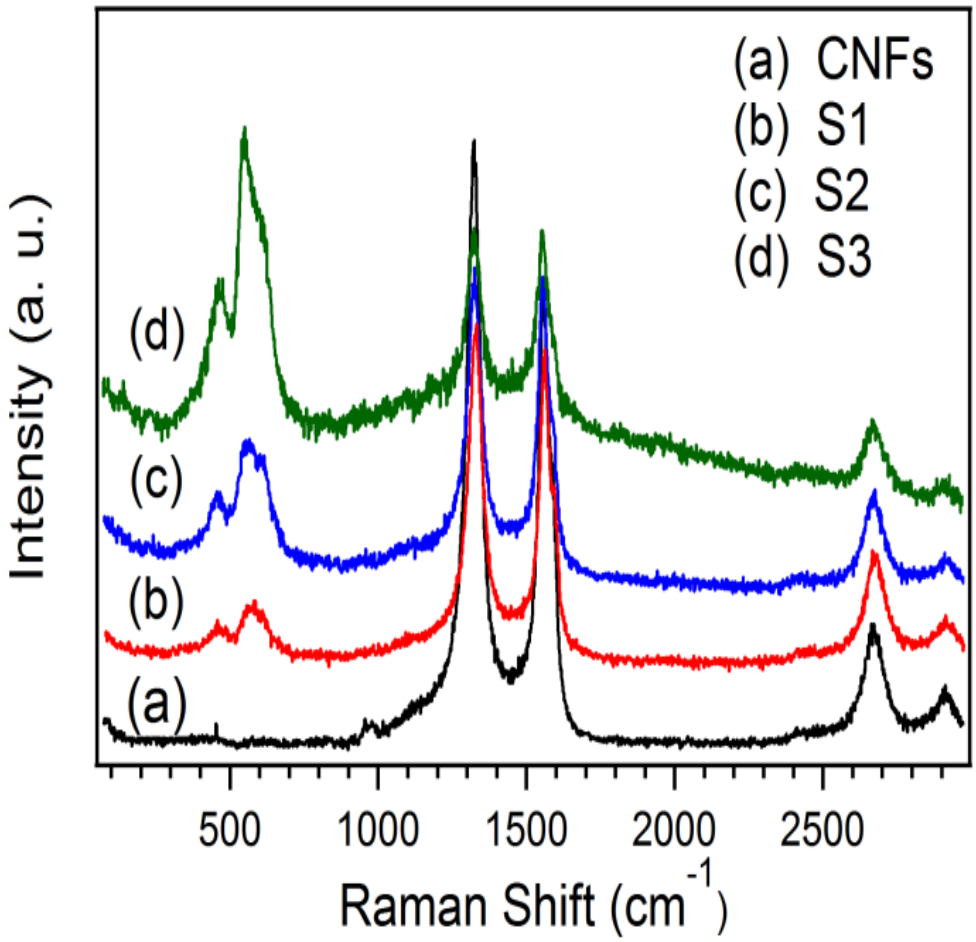

Figure 3.5.Raman spectra of CNFs, S1, S2 and S3

.

Raman spectroscopy measurement was performed to analyze the difference in the structure of CNFs and CNFs/MnO_2 composite. Figure 3.5 shows very well pronounced distinct peaks for MnO_2/CNFs sample at 490, 560, and 640 cm^{-1} are whose positions are similar to those described in the literature for MnO_2 Raman spectra [12, 30, 31]. The locations (~1365 cm^{-1}) and (~1580 cm^{-1}) are attributed to the D and G bands of carbon, corresponding to the defect and disorder induced structures and the vibrations of carbon atoms with sp^2 electronic configuration in CNFs respectively .[32]

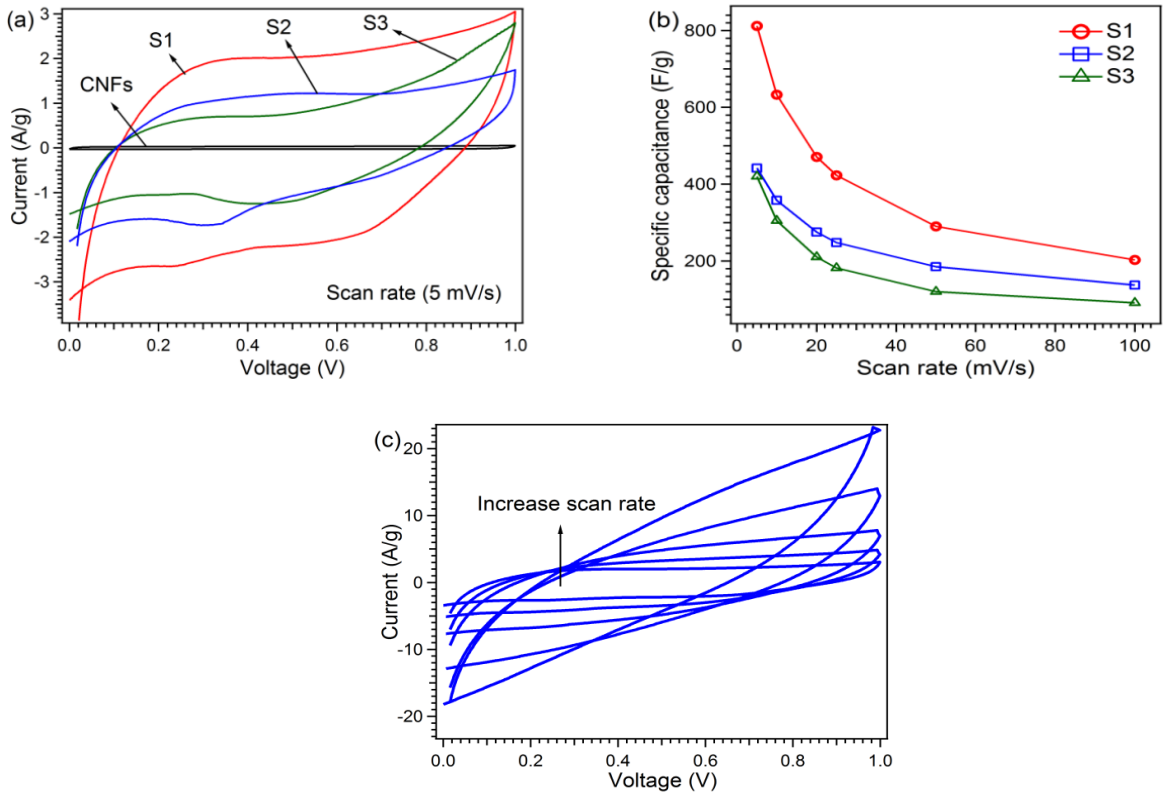

Figure 3.6. (a) Cyclic voltammetry comparison between various samples at 5 mV/s scan rate, (b) Specific capacitance comparison at different scan rates, (c) Cyclic voltammograms at different scan for S1 (5, 10, 20, 25, 50 and 100 mV/s).

Figure 3.6(a) shows the cyclic voltammograms comparison at a scan rate of 5 mV/s between CNFs and nanocomposite of CNFs/MnO_2. CVs of nanocomposites (S1, S2 and S3) are little deviated from the rectangular shape with humps at different potentials from 0.2-0.7 V. The CV deviation is related to the slow diffusion of ions on the surface and into the bulk of the material. The peaks are due to reversible Faradaic reactions in various oxidation states of manganese. The appearance of these peaks describes that the charge storage mechanism is transferred from double layer to pesudocapacitance because of redox reactions of MnO_2 [19]. The specific capacitance was calculated by using the equation 3.1 and considering the deposited mass of MnO_2 as an active material [3, 12].The electrochemical kinetics of an electrode defines the power characteristics of an electrode material. It was observed that S1 provides the larger specific current and specific capacitance. Figure 3.6(b) exhibits the specific capacitance of CNFs/MnO_2 at different scan rates, which shows that as the scan rates increase, the specific capacitance decreases.

This decrease is possibly due to the limited ions transfer to the interior pores of the electrode materials at high scan rates [27].

The sample S1 shows highest specific capacitance about 812 F/g higher than the corresponding values for S2 and S3 and retains its specific capacitance at larger value 203 F/g even at higher scan rate 100 mV/s. Retention of specific capacitance even at fast scan rate is desirable characteristics for high power supercapacitors. The higher specific capacitance of CNF/MnO_2 is due to combination of two charge storage mechanism, those are double layer capacitance and reversible redox reactions at the surface and in bulk of the active material [33]. The thickness of MnO_2 for S2 and S3 is higher, therefore the SC decreases as the film thickness increases due to the low conductivity of MnO_2 [34]. Figure 3.6(c) shows that with increase in scan rate the shape of CV deviates from rectangular shape due to the internal resistance of the electrode, which obstructs the diffusion of the ions.

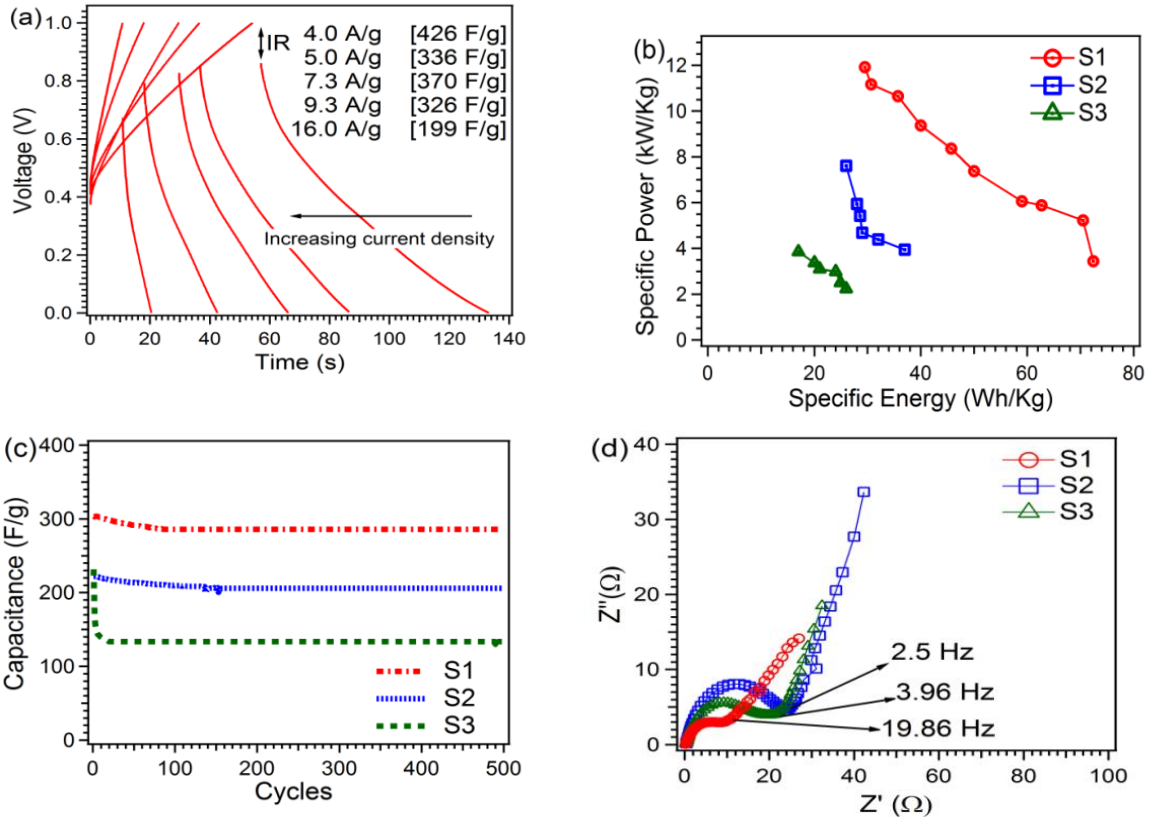

Figure 3.7. (a) Charge /discharge curves at different current for S1, (b) Ragone plot of specific power against specific energy for S1, S2 and S3, (c) Charge/discharge cyclic stability of supercapacitors with S1, S2 and S3, (d) Nyquist plot for S1, S2 and S3.

Galvanostatic charge/discharge curves were measured applying various current densities from 4 to 16 A/g. Figure 3.7(a) shows the charge/ discharge curves for S1 sample at different currents densities. The discharge capacitance (C) was estimated from the slope (*dV/dt*) of the linear portion of the discharge curve using equation 3.

$$C_s = \left(\frac{2I}{(dV/dt).m}\right) \tag{3.3}$$

Where C_s is the specific capacitance in F/g, *I*is the discharge current in A,*dV* is the voltage difference during the discharge curve in V, *dt* the discharge time in sand *m* is the mass of active material (MnO_2). As charge discharge current increases, the voltage drop (*IR*) goes larger, and the capacitance decreases. The calculated highest specific capacitance 426 F/g obtained at 4 A/g decrease to 199 F/g at current 16 A/g. It shows that nanocomposite retain the higher capacitance even at higher currents.

Specific energy and specific power are important parameters to analyse the electrochemical performance of energy storage devices. The specific power, P and specific energy, E, delivered upon discharge were estimated by equation (3.4) and (3.5) [35].

$$P = {}^{Vi}/_{m} \tag{3.4}$$

$$E = {}^{Vit}/_{m} \tag{3.5}$$

Where V is the voltage excluding *IR* drop, *i* is discharge current, and t is the discharge time in s and m is the mass of active material (MnO_2).

Figure 3.7(b) shows the Ragone plot for the S1, S2 and S3 at different current densities. The S1 shows highest energy 72.4 Wh/kg at 3.44 kW/kg at current density of (4 A/g) and decrease slowly to 29.5 Wh/kg at relatively very high power 11.91 KW/kg at a current density (18 A/g). The specific power and energy for S2 and S3 are much lower than S1. Cycling stability of the nanocomposite was investigated applying up to 500 galvanostatic charge/discharge cycles at different current densities 7.9, 5.7, and 3.8 A/g for S1, S2 and S3 respectively in the range of 0-1 V Figure 3.7(c). The discharge capacitance (C) is estimated from the slope (*dV/dt*) of the linear portion of the discharge curve using the

equation 3. It is evident that S1 exhibits higher capacitance 303 F/g and capacitance retention in comparison with S2 and S3. For S3 the capacitance fading from 231 to 138 F/g in the first 10 cycles was observed, which is due to the thicker and random structure of MnO_2 on the CNFs.

Electrochemical impedance spectroscopy was performed to investigate the kinetics behavior of hybrid electrodes. The solution resistance for all samples was almost similar ~ 0.3 Ω, whereas the Faradaic charge transfer resistance R_f varies. The R_f was ~ 9, 23 and 20 Ω for S1, S2 and S3 respectively see Figure 3.7(d). The R_f of S2 and S3 is higher possibly because of thicker and random structure of MnO_2. The Nyquist plot of the samples present an almost straight line parallel to the imaginary axis that describes exactly polarized systems. Deviation from this vertical line at low frequencies to smaller slopes corresponds to a higher contribution of the ionic diffusion resistance. The knee frequency of S1 was 19.86 Hz higher that of S2 and S3.

Table 3.1. Pore parameters for CNFs and CNFs/MnO_2

Sample	S_{BET} (m^2/g)	S_{micro} (m^2/g)	S_{mesoo} (m^2/g)	S_{macra} (m^2/g)	V_{total} (cm^3/g)	V_{micro} (cm^3/g)	V_{meso} (cm^3/g)	V_{macra} (cm^3/g)
CNFs	68	4.8	50.2	13	0.34	0.001	0.188	0.152
S1	240	59	153	28	1.63	0.13	0.85	0.65
S2	148	36	93	19	0.98	0.03	0.439	0.511
S3	133	27	87.5	18.5	0.7	0.001	0.38	0.32

S_{BET}= BET surface area, S_{micro}=Micropore surface area, S_{meso}=Mesopore surface area, S_{macra}=Macrapore surface area, V_{total}= Total volume, V_{micro}=Micropore volume, V_{meso}=Mesopore volume, V_{macra}=Macrapore volume.

To understand the influence of surface area and pore size distribution of CNFs, S1, S2 and S3 samples on the specific capacitance BET analysis were performed. The textural properties of all samples were evaluated by collecting the nitrogen sorption isotherms, as

shown in Figure 3.8(a). The isotherms present a small hysteresis loop from higher to middle pressure range, which is the indication of meso and macro porous structure. According to IUPAC classification the isotherm of sample can be classified as type II and type IV isotherm [36]. The total volume of pores (V_{total}, cm^3/g) was calculated by the number of adsorbed nitrogen at P/P0 ≈ 0.9932. The volume of micropores and the values of surface areas of micro (S_{micro}, m^2/g) were investigated by the use of t-Plot Harkins and Jura method. The total pore volume for S1 (1.63 cm^3/g) is about 4.8 times higher than CNFs, about 1.66 times higher than S2 and about 2.32 times higher than S3. The pore volume distribution is presented in table 1. The surface area (BET) was determined by multiple point Brunauer-Emmett-Teller (BET) method in the region of the isotherm, which is limited by the range of relative pressure P/P_0 = 0.02–0.2 as seen in Figure 3.8(b). The adsorption volume shows that BET surface areas for CNFs, S1, S2 and S3 are 68, 240, 148 and 133 m^2/g respectively.The pore size distribution of the materials is classified into three groups: micro pores (< 2nm), meso pores (2-50 nm) and macro pores (> 50 nm) [37]. The pore size distributions were calculated from adsorption isotherms by the Barrett−Joyner−Halenda (BJH) method. Figure 3.8(c) presents the pores of all sample are mainly distributed in between meso and macro pores. The dominant pores sizes for S1 and S2 are centered in the range of 20, 35 and 80 nm. While the main pore size distribution for S3 is (8 and 20 nm) and for CNFs (2.5, 20 and 80 nm) Figure 3.8(c). The correlation between BET results and specific capacitance can be understand by equation $C = \varepsilon A/d$ where ϵ is electrolyte dielectric constant, A is the surface area accessible to ions and d is the distance from ions to the pore surface of electrode on the order of angstrom. According to the above equation, two approaches can be taken to enhance the charge storage of supercapacitors effectively: increasing the specific surface area and reducing the distance between ions and the surface of the electrode. The BET results reveal that S1

have higher specific surface area and higher number of mesopores. The high surface area and large amount of mesopore structures provide the possibility of efficient transport of electrons and ions, which leads to the high electrochemical capacitance. Beside this the thickness of MnO_2 film plays an important role during charging and discharging supercapacitor. It is evident that the thickness of the electrode S1 is much thinner than that of the S2, S3 and CNFs Figures 3.4 Hence, it can be speculated that a longer distance of ionic motion in the electrodes of S2, S3 and CNFs is necessary from electrolyte to the inner MnO_2. The thinner film sample S1 delivers higher specific capacitance in comparison to S2 and S3.

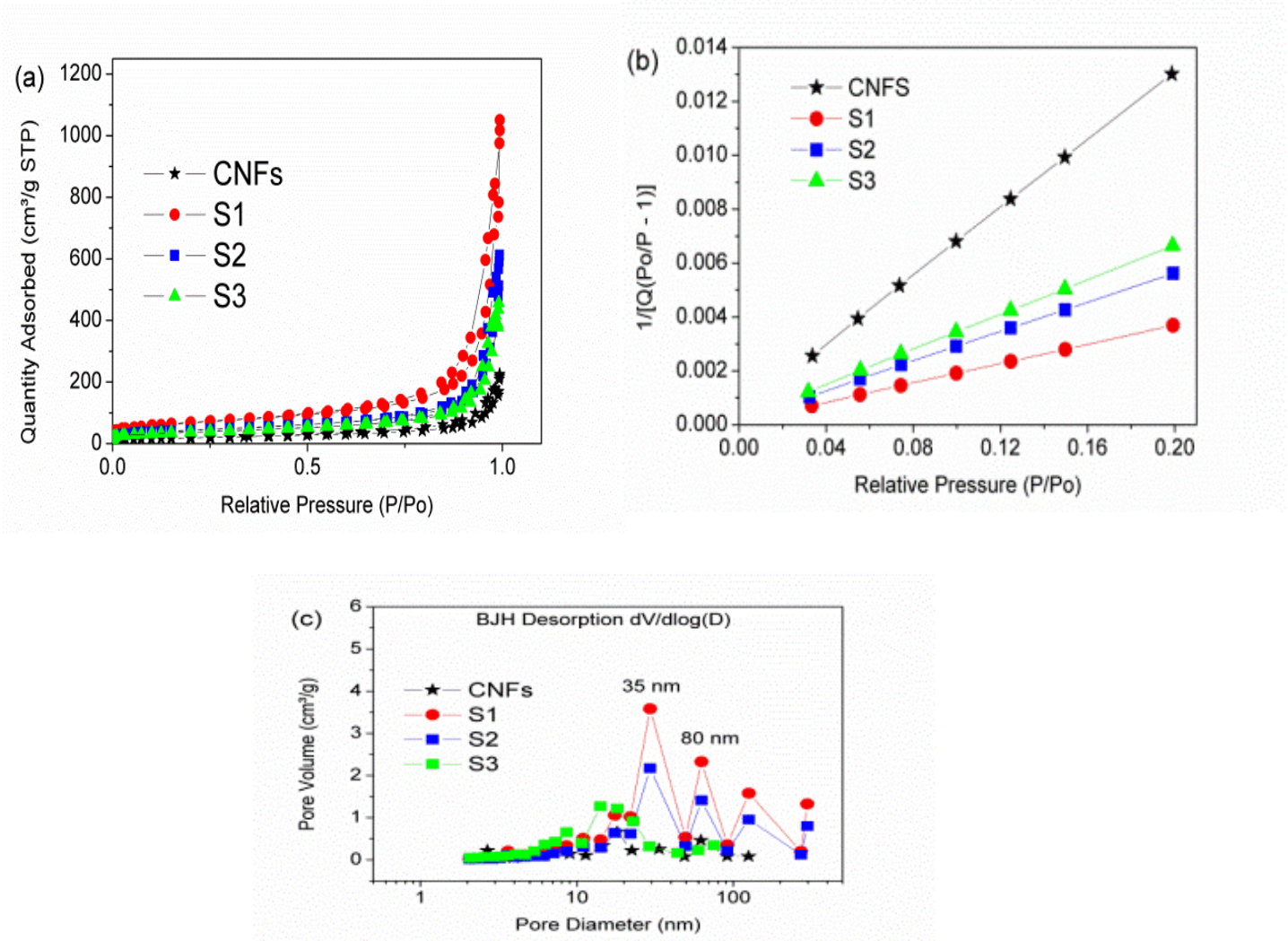

Figure 3.8. (a) Nitrogen adsorption/desorption isotherms, (b) BET surface area, (c) Pore size distribution

3.4. Conclusions

The supercapacitor performance of flexible Carbon nanofibers (CNFs) electrodes in different concentrations of KOH was investigated. It was found that the specific capacitance increased to 38 F/g with increasing concentration up to 9 M, beyond this value specific capacitance decreased due to undissolved salt and ion mobility. A fast and easy method to obtain a hybrid nanostructure having uniform distribution of MnO_2 on the CNFs has been introduced. The chemical treatment of CNFs with different concentration of $KMnO_4$ solution at moderate temperature for 10 min has been performed obtaining different structures of MnO_2. SEM images shows that the less concentrated (0.1g $KMnO_4$) favor the even thinner coating of MnO_2 on the surface of CNFs. Raman results tells us that the manganese is in MnO_2 oxidation state. The highest specific capacitance is 812 F/g, low Faradaic charge transfer resistance (~ 9 Ω), long cycling stability with higher capacitance (303 F/g) at current of 7.9 A/g was achieved when MnO_2 is uniformly in contact as a thin film with the surface of CNFs and containing high BET surface area. Moreover, the highest energy density of 72.4 Wh/kg at 3.44 kW/kg specific power was calculated.

References:

[1] ClaramuntS, MonereoO,BoixM, Leghrib R, PradesJ D, Cornet A, Merino C, Cirera. A. Flexible gas sensor array with an embedded heater based on metal decorated carbon nanofibers. 2013 Sensors and Actuators B: Chemical. 187 401–406.

[2] HuangY, Candelaria S L, Li Y, Li Z, TianJ, Zhang L, Cao G.Sulfurized activated carbon for high energy density supercapacitors.2014 Journal of Power Sources

[3] Amade R, Jover E, Caglar B, Mutlu T, Bertran E. Optimization of MnO_2/vertically aligned carbon nanotube composite for supercapacitor application. 2011Journal of Power Sources. 1965 779–5783

[4] Hussain S, Amade R, Jover E, Bertran E. Nitrogen plasma functionalization of carbon nanotubes for supercapacitor applications. 2013 Journal of Materials Science.18 7620–7628

[5] Hussain S, Amade R, Jover E, Bertran E. Functionalization of carbon nanotubes by water plasma. 2012 Nanotechnology. 23 385604 (1–8).

[6] Jung K H, Denga W, Smith Jr D W, Ferraris J P. Carbon nanofiber electrodes for supercapacitors derived from new precursor polymer: Poly (acrylonitrile-co-vinylimidazole). 2012 Electrochemistry Communications. 23 149–152.

[7] Wu Z S, Parvez K, Feng X, Mullen. K. Graphene-based in-plane micro-supercapacitors with high power and energy densities. 2013 Nature Communications. 4: Article number: 2487

[8] Yang X, Zhang G, Zhong M, Wu D, Fu R. Ammonia-Assisted Semicarbonization: A Simple Method toIntroduce Micropores without Damaging a 3D Mesoporous Carbon Nanonetwork Structure.2014 Langmuir. 30 9183–9189

[9]Li C, Yang X, Zhang G. Mesopore-dominant activated carbon aerogels with high surface area for electric double-layer capacitor application. 2015 Materials Letters. 161 538–541.

[10] Yang X, Li C, Fu R. Nitrogen-enriched carbon with extremely high mesoporosity and tunable mesopore size for high-performance supercapacitors. 2016 Journal of Power Sources. 319 66–72.

[11] Yang D. Application of Nanocomposites for Supercapacitors: Characteristics and Properties (2012) Chapter 12, DOI: 10.5772/50409

[12] Hussain S, Amade R, Jover E, Bertran E. Water Plasma Functionalized CNTs/MnO_2 Composites for Supercapacitors. 2013 The scientific world journal., 8, Volume 2013, Article ID 832581, 8 pages. http://dx.doi.org/10.1155/2013/832581

[13] Lang X, Hirata A, Fujita T, Chen. M. Nanoporous metal/oxide hybrid electrodes for electrochemical supercapacitors. 2011 Nature Nanotechnology. 6 232–236.

[14] Ma C, Li Y, Shi J, Song Y, Liu. L. High-performance supercapacitor electrodes based on porous flexible carbon nanofiber paper treated by surface chemical etching. 2014 Chemical Engineering Journal. 249 216–225.

[15] Liu Y, Zhou J, Chen L, Zhang P, Fu W, Zhao H, Ma Y, Pan X, Zhang Z, Han W, Xie E. Highly flexible freestanding porous Carbon nanofibers for electrodes materials of high-performance all-carbon supercapacitors. 2015 ACS Appl. Mater.Interfaces., 7, 23515–23520.

[16] Zhi M, Manivannan A, Meng F, Wu N. Highly conductive electrospun carbon nanofiber/MnO_2 coaxial nano-cables for high energy and power density supercapacitors. 2012 Journal of Power Sources. 208 345–353.

[17] Huang Y, Miao Y E, Tjiu W W, Liu T. High-performance flexible supercapacitors based on mesoporous carbon nanofibers/Co_3O_4/MnO_2 hybrid electrodes. 2015 RSC Adv. 5, 18952–18959.

[18] Zhou D, Lin H, Zhang F, NiuH, Cui L,Wang Q,QuF. Freestanding MnO_2nanoflakes/porous carbon nanofibers for high-performance flexible supercapacitor electrodes.2015 ElectrochimicaActa. 161, 427–435.

[19] Nataraj S K, Song Q, Al-Muhtaseb S A, Dutton S E, Zhang Q, Sivaniah E. Thin flexible supercapacitors made from carbon nanofiber electrodes decorated at room temperature with manganese oxide nanosheets. 2013 Journal of Nanomaterials, Volume 2013, ID 272093, 6 pages

[20] Liu Q, Nayfeh O, Nayfeh M H, Yau S T. Flexible supercapacitor sheets based on hybrid nano composite materials. 2013 Nano Energy 2 133–137.

[21] Vera-Agullo J, Varela-Rizo H, Conesa J A, Almansa C, Merino C, Martin-Gullon I. Evidence for growth mechanism and helix-spiral cone structure of stacked-cup carbon nanofibers. 2007 Carbon 45 2751–2758.

[22] Hu X B, Zhao B Y, Hu K A. A novel fabrication of doped C/C composite laminations by aqueous tape casting. 2004 ActaMaterialia 52 467–473.

[23] Korkut S, Roy-Mayhew J D, Dabbs D M, Milius D L, Aksay. I. A. High surface area tapes produced with functionalized graphene. 2011 ACSNano 5 5214–5222.

[24] Ramos F M. Integración de la tecnología cerámica multicapa, PhD thesis, University of Barcelona, 2014.

[25] Stoller M D, Ruoff R S. Best practice methods for determining an electrode material's performance for ultracapacitors. 2010 Energy Environ. Sci. 3 1294–1301.

[26] Azam M A, Fujiwara A, Shimoda T. Significant capacitance performance of vertically aligned single-walled carbon nanotube supercapacitor by varying potassium hydroxide concentration. 2013 Int. J. Electrochem. Sci. 8 3902–3911.

[27] Tsay K-C, Zhang L, Zhang. J. Effects of electrode layer composition/thickness and electrolyte concentration on both specific capacitance and energy density of supercapacitor. 2012 Electrochimica Acta. 60 428–436.

[28] Liu C G, Liu M, Li F, Cheng. H. M. Frequency response characteristic of single-walled carbon nanotubes as supercapacitor electrode material. 2008 Applied physics letters. 92 143108 (1–3).

[29] Hussain S, Amade R, Bertran. E. Study of CNTs structural evolution during water assisted growth and transfer methodology for electrochemical applications. 2014 Materials Chemistry and Physics. 148 914–922.

[30] Buciuman F, Patcas F, Craciun R, Zahn D R T. Vibrational spectroscopy of bulk and supported manganese oxides. 1999 Physical Chemistry Chemical Physics.1 185–190.

[31] Bernard M-C, Goff A H-L, Thi B V, Torresi S C De. Electrochromic reactions in manganese oxides.1993 Journal of the Electrochemical Society. 140 3065–3070.

[32] Yue H, Li F, Yang Z, Li X, Lin S, He. D. Facile preparation of Mn_3O_4-coated carbon nanofibers on copper foam as a high-capacity and long-life anode for lithium-ion batteries. 2014 J. Mater. Chem. A. 2 17352–17358

[33] Tran V M, Ha A T, Le M L P. Capacitance behavior of nanostructured ε-MnO_2/C composite electrode using different carbons matrix. 2014 Adv. Nat. Sci: Nanosci. Nanotechnol. 5 025005 (9pp)

[34] Nagarajan N, Cheong M, Zhitomirsky I. Electrochemical capacitance of MnO_x films. 2007 Materials Chemistry and Physics. 103 47–53.

[35] Farma R, Deraman M, Awitdrus, Talib I A, Omar R, Manjunatha J G, Ishak M M, Basri N H, Dolah B N M. Physical and electrochemical properties of supercapacitor electrodes derived from carbon nanotube and biomass carbon. 2013 Int. J. Electrochem. Sci. 8 257–273.

[36] Gregg S J, Sing K S W. Adsorption, Surface Area and Porosity, 2nd ed.; Academic Press: New York, 1982; pp 4, 287.

[37] Huang J, Sumpter B G, Meunier V. A Universal Model for Nanoporous Carbon Supercapacitors Applicable to Diverse Pore Regimes. 2008 Chemistry. 14 6614–6626.

Chapter 4 A study of Carbon nanofibers and Active carbon as symmetric supercapacitor in aqueous electrolyte

4.1 Introduction

Supercapacitors or electrochemical capacitors have attracted much interest due to their high power density and long cycling capabilities. They have found potential applications in electric vehicles, portable devices and power tools [1]. The electrical vehicles need high power at high current drain rate whereas memory backup systems require high energy density at low current drain rate. Consequently, the material should be chosen according to the desired applications [2]. The main components of a supercapacitor are the electrodes and the electrolyte. Since the charge storage takes place at the electrode/electrolyte interface, the surface area of the electrode and the electrolyte used will greatly influence the performance of the device. Supercapacitor performance is indeed influenced by the specific surface area, pore size distribution of electrode material [3]. Carbon materials are widely used as electrodes due to their low cost, available diversity of morphologies and, chemical and thermal stability [4-7]. CNFs nanoscale tubular morphology can offer a unique combination of low electrical resistivity and high porosity in a readily accessible structure [8]. An AC material is very attractive material for supercapacitors due to high porosity, low cost, abundance, high stability and charge discharge cycling [9]. The fabrication of electrodes (AC or CNFs) for supercapacitors requires the addition of binder -e.g. poly(tetrafluoroethylene) (PTFE), polyvynilidene chloride (PVDC) and polyvynilidene fluoride (PVDF)- in proportions that usually vary from 5 to 10 wt. % in order to maintain the integrity of electrodes [10, 11]. However, binder blocks part of porosity of carbon and additionally causes an increase in electrical resistivity [11-13].

The capacitance of supercapacitor is highly linked to the electrode material and the electrolyte. The electrode properties of like, material nature, electrode thickness, surface area, pore size distribution and surface groups highly influence the performance of supercapacitor. The electrolyte compatibility with the electrode material also plays a crucial role in development of supercapacitor because electric double layer is built at the electrode/electrolyte interface. The voltage of a supercapcitor depends on the stability potential window of the electrolyte. The aqueous electrolytes usually provide potential until 1.0 V and organic electrolyte until 2.7 V [14]. Aqueous electrolytes are

environmentally friendly, whereas organic electrolytes are not good environmentally. Aqueous electrolytes are mostly composed of small anions and simple hydrated cation (angstrom level). These ions can easily penetrate to the micropores, mesopores and macropores of the material under the applied electric field. The electric double layer (EDL) is built at the electrode/electrolyte interfacial region can be treated as a capacitor with and electric double layer capacitor (EDLC), which can be expresses as $C=\epsilon A/d$. Where ϵ is electrolyte dielectric constant, A is the surface area accessible to ions and d is the distance from ions to the pore surface of carbon electrode on the order of angstrom. According to the above equation, two approaches can be taken to enhance the charge storage of EDLC effectively: increasing the SSA and reducing distance between ions and the carbon surface by the development [15].

In this work the aim is to provide a comparative analysis of symmetric supercapacitor based on AC and CNFs by using similar amount of binder PVDF 7wt% for both materials.

4.2. Experimental procedure

4.2.1. Preparation of AC and CNFs electrodes

Symmetric supercapacitor based on AC and CNFs were prepared for comparison. AC reference Carbopal CCP80 from Donau Carbon supplied by Quimics Dalmau. CNFs were provided by Grupo Antolin. It has a helicoidally graphitic stacked cup structure, there is a presence of Ni (6%), diameter is 20-80 nm, length (MEB) >30um, electric resistivity $10^{-2}\Omega\cdot$cm. PVDF was used as a binder. In order to compare electrode preparation for supercapacitor analysis for both materials (AC, CNFs) was achieved in a similar way by following the below steps.

Step 1: Milling of (AC or CNFs) in a zirconia planetary ball mill (Pulverisette 7 from Fritch) employing a frequency 500 rpm for 30 minutes. Step 2: Mixing of (AC or CNFs) 93wt% with 7wt% PVDF polymer by using 15 ml acetone in an agate mortar. Step 3: The slurry was then mixed using a mechanical stirrer for 60 min followed by an ultrasonic for 30 minutes. Step 4: The slurry of the mixture dried in oven for 60 min at 70 °C. Step 5: In last step, the dried slurry was used to prepared electrodes in a way using hydraulic press with a die set (10 mm) at 10 tones force. The calculated mass of prepared electrode discs based on CNFs and AC were 0.018 g and 0.02 g respectively.

4.2.2. Surface characterization

The porous texture and specific surface area and pore size distribution of CNFs and AC electrodes were obtained by physical adsorption of gases N_2 at 77K using (Micromeritics TriStar 3000 V6.04 A). All samples were outgassed at $100C^0$ for 4h prior to the adsorption measurements. The specific surface area (S_{BET}, m^2/g) was determined by multipoint Brunauer-Emmett-Teller (BET) method in the region of the isotherm, which is limited by the range of relative pressure P/P_0 = 0.02–0.2. The total volume of pores (V_{total}, cm^3/g) was calculated by the number of adsorbed nitrogen at $P/P_0 \approx 0.9932$. The volume of micropores and the values of surface areas of micro (S_{micro}, m^2/g) were investigated by the use of t-Plot Harkins and Jura method , the pore size distribution for cnfs sample calculated from adsorption isotherms by the Barrett−Joyner−Halenda (BJH) method and using MP method for calculate the pore size distribution for AC .

4.2.3. Morphological characterization

The AC and CNFs sample were examined by scanning electron microscopy (SEM). TEM analyses were performed on a Philips Tecnai G2 F20 system operated at 300 kV. The samples were suspended into ethanol and dispersed ultrasonically for 15 min. A drop of the suspension was deposited on a copper grid coated with carbon.

4.2.4. Electrochemical characterization

The electrochemical performance comparison of AC and CNFs as symmetric capacitors were studied in two electrode Swagelok cell and using a Gamry 600 potentiostat using 6 M KOH solution as an electrolyte. The specific capacitance of electrode materials was investigated by: cyclic voltammetry (CV), galvanostatic charging/discharging (GCD) and electrochemical impedance spectroscopy (EIS).

4.3. Results and discussion

4.3.1. Morphological characterization

The surface morphology of prepared electrodes was investigated by SEM Figure 4.1 and TEM Figure 4.1 (inset). It can be seen clearly that PVDF binder effectively bond the

CNFs Figure 4.1(a) and AC Figure 4.1(b). The different structures for both electrodes of CNFs and AC are visible. The typical CNF structure, cylindrical shape, and crystals structure inset Figure 4.1(a). TEM image of AC demonstrate interconnected spheres with homogeneous size and smoother surface inset Figure 4.1(b).

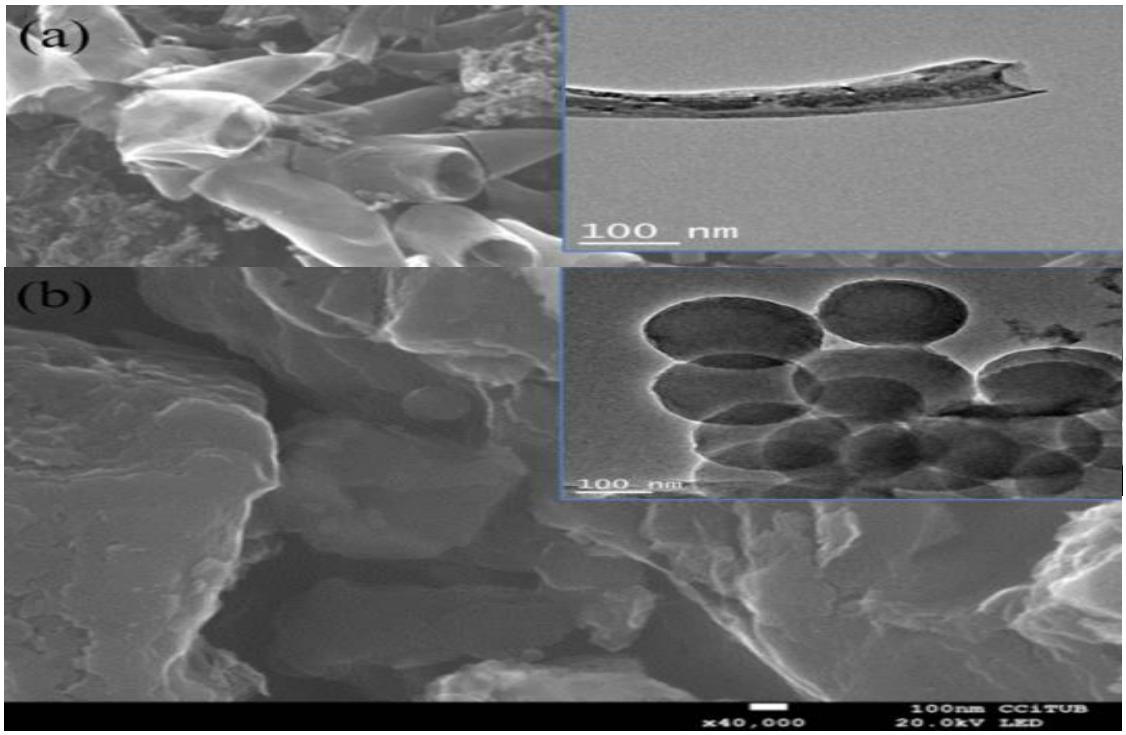

Figure 4.1 .SEM images and TEM images (inset) for (a) CNFs, (b) AC.

4.3.2. Pore texture of CNFs and AC

The N_2 adsorption/desorption isotherm of CNFs and AC are shown in Figure 4.2. Pore volume and pore size distribution was calculated by BJH method, t-plot method and MP method. Only MP method analysis can reveal the fine difference of micro pore size distribution of the sample [16]. The pore size distribution of the materials is classified into three groups: micro pores (< 2nm), meso pores (2-50 nm) and macro pores (> 50 nm) [17]. The isotherm of CNFs presents a small hysteresis loop from higher to middle pressure range, which indicates CNFs contains mesoporous structure figure 4.2(a). According to IUPAC classification the isotherm of CNFs can be classified as type II isotherm. The pore distribution of CNFs is as follows: 59 % mesopores (2-50 nm), 17.9

% micropores (0.5-2 nm) and 23 % macropore (> 50 nm). The details are presented in table 4.1.

Table 4.1. Physicochemical parameters of CNFS and AC.

Pore size distribution												
							P%					
sample	BET[a] m^2/g	V_t[b] cm^3/g	$V_{0.5-2}$[c] cm^3/g t-plot	$V0._{2-0.5}$[d] cm^3/g MP	V_{2-50}[e] cm^3/g BJH	$V_{>50}$[f]	0.5-2[g]	0.2-0.5[g]	2-50[g]	> 50[g]	APS nm	Ext m^2/g
CNFs	83	0.39	0.07	-	0.23	0.09	17.9	-	59	23	4- 7.5	157.4
AC	1040	0.582	0.19	0.32	0.072	-	33	55	12	-	0.47	21

[a]BET surface area, [b]Single point volume adsorption total volume of pores at p/p0=0.9932, [c]super micro volume from (0.5-2 nm) t-plot,y-intercept, [d]ultramicro volume-from MP method, [e]Meso volume from BJH method, [f]Volume greater than 50 nm by BJH method ,[g]the micro and meso percentage calculated by $V_{MICR}/V_{TOTAL}*100\%$, $V_{MESO}/V_{TOTAL}*100\%$, APS (average pore size), EXT (External area) area from the slope of t –plot.

AC adsorption/desorption isotherm presents that most of the adsorption quantity takes place at very low relative pressure ($P/P_0 \leq 0.02$) and a plateau from low to high relative pressure (0.6-0.8). The total pore volume is 0.582 cm^3/g at relative pressure (P/P_0 =0.9932). Fig 4.2 (b) presents that the curvature of isotherm from 0 to 0.4 relative pressure presents pore volume for less than 50 nm pores (micro+meso) and this pore volume is equal to 0.534 cm^3/g which is the indication of highly microporous structure. The system of AC sample isotherm classified as type I isotherm. The pore distribution of AC is as follows:

supermicropores (0.5-2 nm) occupied 33 %, ultramicro (0.2-0.5 nm) occupied 55% and mesopores occupied 12%. The details are presented in table 4.1.

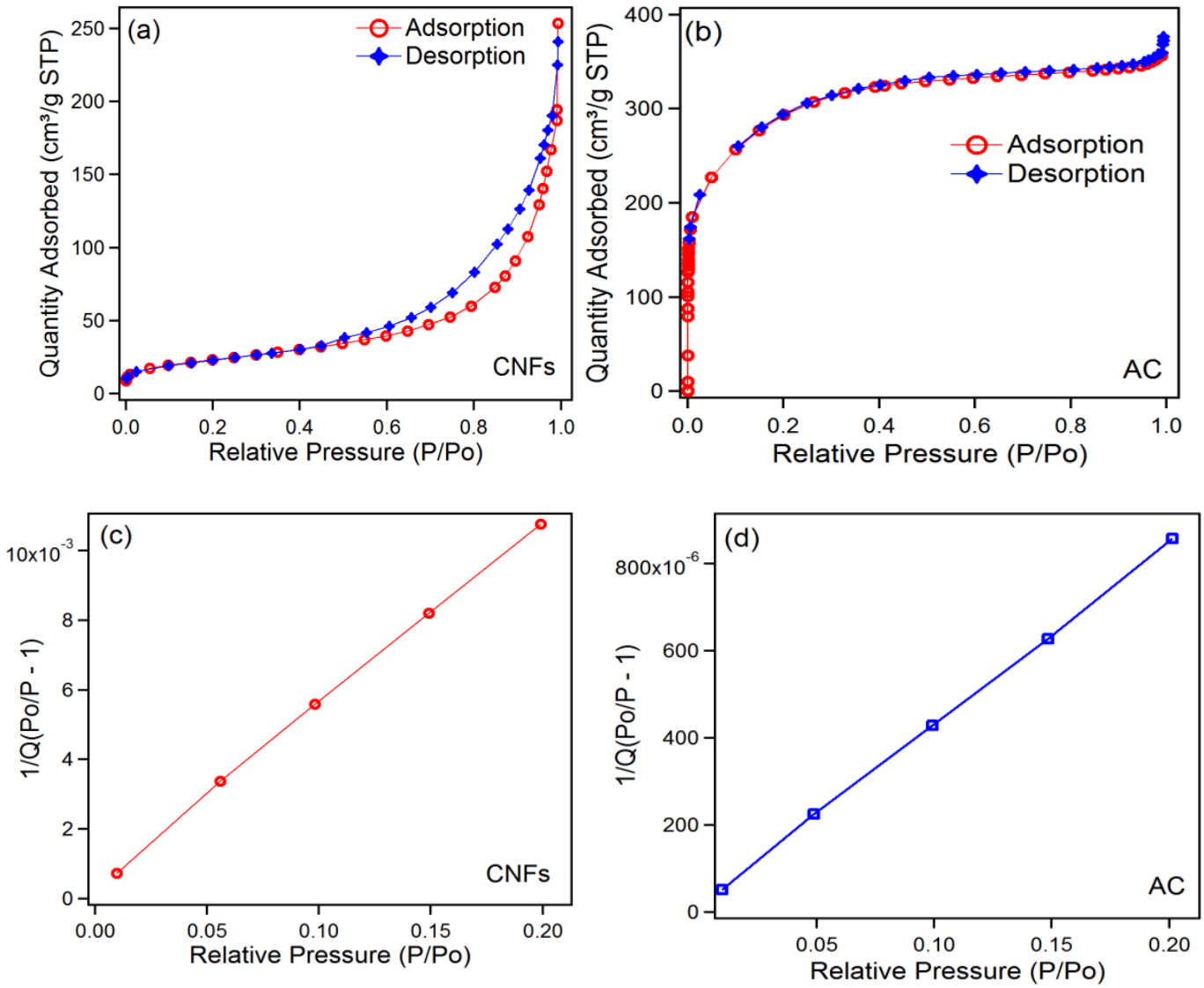

Figure 4.2.Nitrogen adsorption/desorption isotherms, (a) CNFs, (b) AC. BET surface area (c) CNFS, (d) AC.

The specific surface area (BET) was determined by multiple point Brunauer-Emmett-Teller (BET)method in the region of the isotherm, which is limited by the range of relative pressure P/P_0 = 0.02–0.2 as seen in Figure 4.2 (c, d). The total volume of pores (V_{total}, cm^2/g) was calculated by the number of adsorbed nitrogen at $P/P_0 \approx 0.9932$. The

adsorption volume shows that BET surface areas for CNFs and AC are 83 m^2/g and 1042 m^2/g respectively.

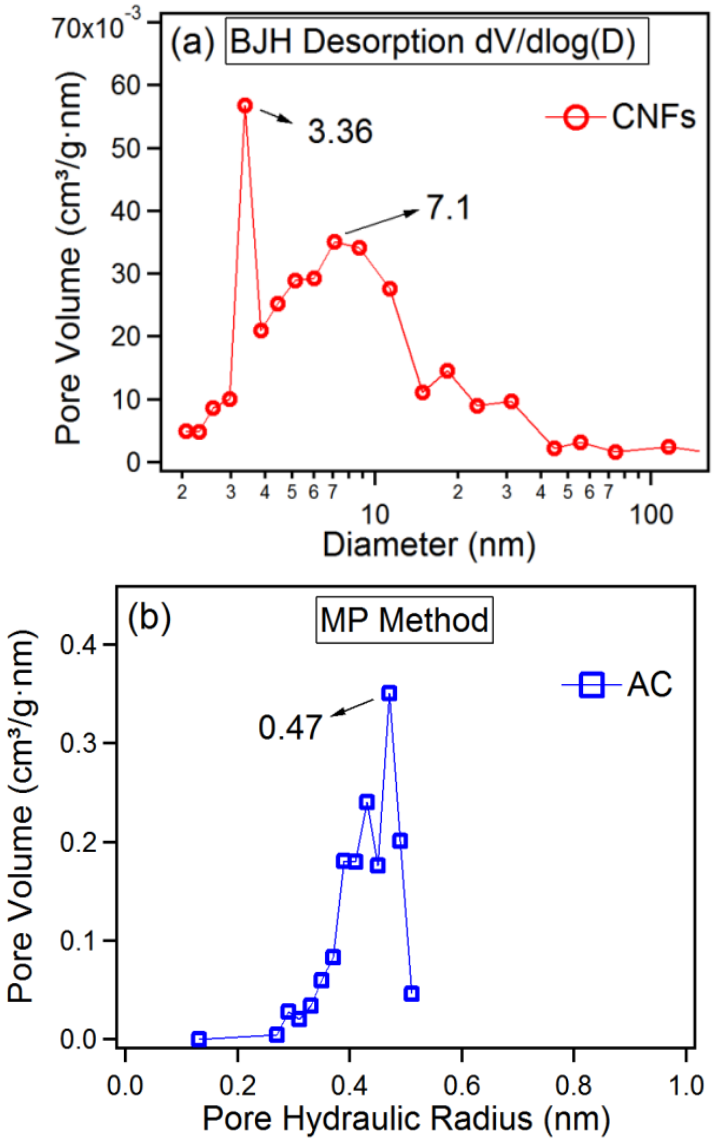

Figure 4.3. Pore size distribution (a) CNFs by BJH method, (b) AC by MP method.

The pore size distribution analysis are presented in Figure 4.3 (a, b) obtained via MP method for AC and using Barrett–Joiner–Halenda (BJH) method for CNFs. CNFs contains two type of dominant pores centered in the ranges of 3.36 nm and 7.1 nm, while AC is mainly comprises with pores of 0.47 nm. Microspores are beneficial for a charge

accumulation in aqueous electrolytes [18, 19]. It can be seen that for CNFs most dominant pores are mesopores while for AC ultra-micro pores.

4.3.3. Electrochemical behaviour of CNFs and AC

The main accepted approaches to evaluate the capacitance of supercapacitor are cyclic voltammetry, galvanostatic charge/discharge and impedance spectroscopy. The working principle of each technique varies from one to another. The electrochemical behaviour of AC and CNFs were first characterized by cyclic voltammetry in the range of 0 to 1 V. CV is a most convenient method to characterize the capacitive behaviour of electrode materials. The specific capacitance per unit mass for one electrode was calculated using equation (4.1, 4.2).

$$C_s = 4 * C/m \tag{4.1}$$

$$C = \frac{q_a + |q_c|}{\Delta V} \tag{4.2}$$

Where C_s is the specific capacitance in F/g, C is the measured capacitance for the two-electrode cell by equation4.2 and m is the total mass of the active material in both electrodes [20]. Figure 4.4 (a, b) shows CVs of CNFs and AC respectively from 5 to 500 mV/s scan rates. CVs of CNFs in wide range of scan rates are near box like shape without any hump or deviation indicates clear double layer characteristics and high reversibility. The CVs for AC shows much higher current than the CNFs. At low scan rates the CV shape is rectangular, presenting that the electrode response in charging and discharging is highly reversible. However at higher scan rates CV deviate from rectangular shape. There could be several possible reasons related to this deviation, (1) due to low electrical

conductivity of porous structure of AC of inner pores are not accessible to ions, (2) nonzero time constant and elevated transient current, resulting in a longer capacitor charging time and a collapse of the rectangular shape [21, 22].

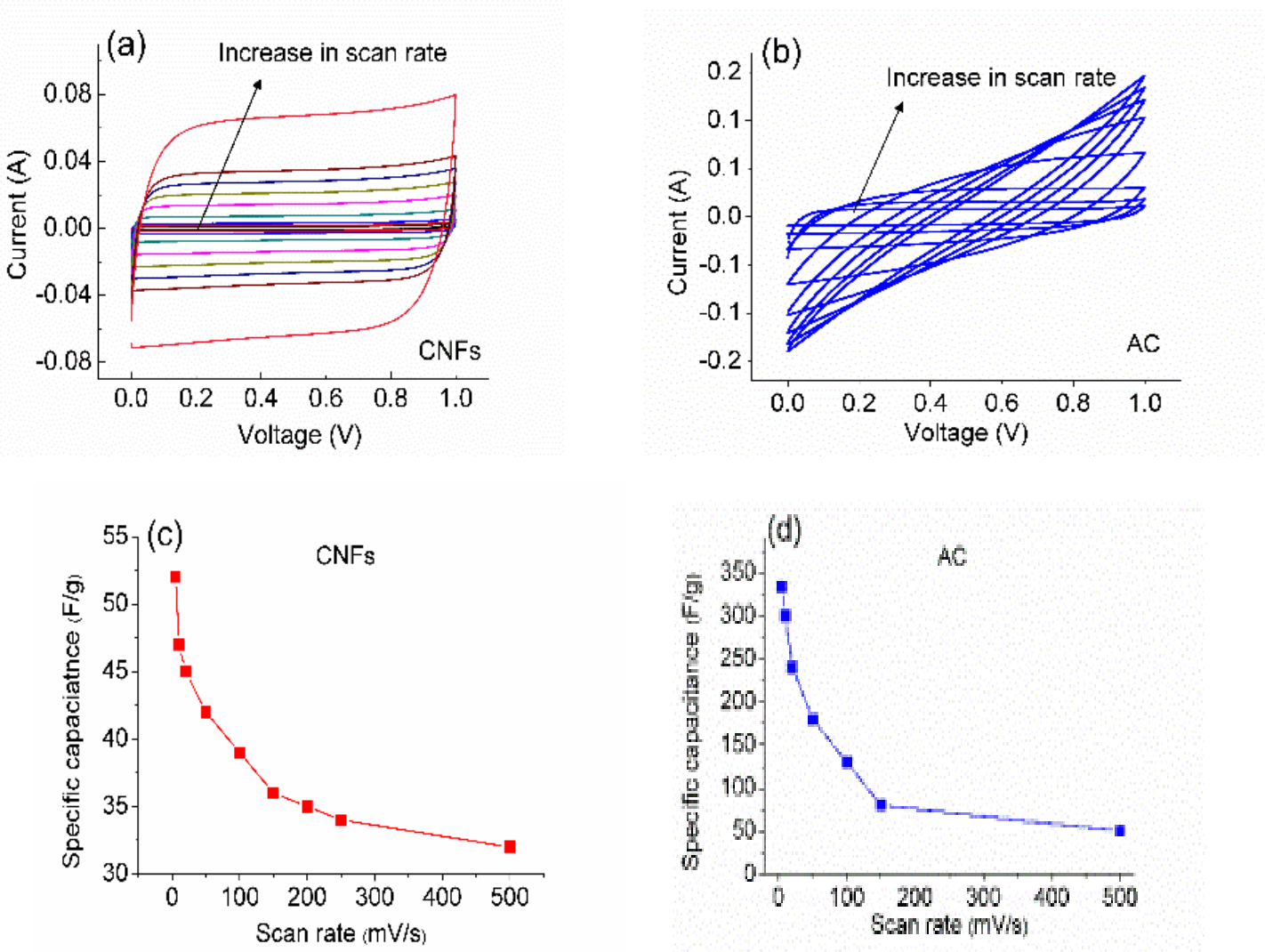

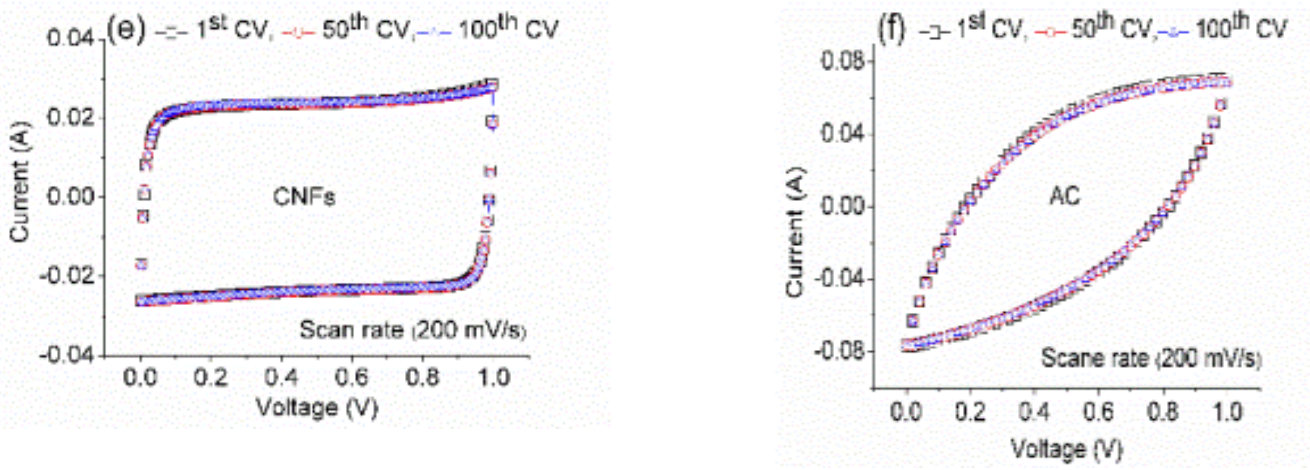

Figure 4.4. (a, b) CVs of CNFs and AC respectively at 5, 10, 20, 50, 100, 150, 500 mV/s scan rates, (c, d) specific capacitance comparison at different scan rates, (e, f) CVs of CNFs and AC respectively from 1st to 100th cycle.

Figure 4.4 (c, d) present the specific capacitance comparison of CNFs and AC from 5 to 500 mV/s scan rates. As it can be seen from Figure 4.4(c) CNFs shows highest specific capacitance 52 F/g at scan rate 5 mV/s. The specific capacitance decreased to 32 F/g at 500 mV/s scan rate. These results indicate moderate decrease in specific capacitance and at even higher scan rates most of the surface area and pores of CNFs are accessible to the ions. The capacitance of AC decreases from 334 to 50 F/g for 5 to 500 mV/s Figure 4(d). Very high specific capacitance at low scan rate is due to ions have enough time to go deep inside the microporus (less than 2 nm) structure of AC. It can be presumed that at higher scan rates mostly the larger pores mesopores (2-50 nm) are contributing to capacitance. This is mainly due to the difference in diffusion rate of electrolyte in the pores of different size and also due to network connection between large and small pores [23]. As discussed by A. G. Pandolofo et al, the measured surface area is contributed by the all the open pores, but all pores are not accessibly electrochemically [8]. The higher specific capacitance of AC in comparison to CNFs could be due to the higher surface area, which results in the increase in the accessible areas for electrolyte ions for charge storage within relatively small pores. The CV curves of the CNFs and AC Figure 4.4(e, f) indicates stable capacitance behaviour measured until 100th cycle at a scan rate of 200 mV/s. The 100th CV for both samples retain the shape as it for 1st one, suggests excellent stability and reversible electrode processes. The supercapacitive performance of CNFs and AC was further compared by GCD as shown in Figure 4.5 (a, b).The discharge capacitance

(C) is estimated from the slope (*dV/dt*) of the linear portion of the discharge curve using equation 4.3.

$$C_s = \left(\frac{2I}{(dV/dt).m}\right) \qquad (4.3)$$

Where *Cs* is the specific capacitance in F/g, ΔV is the voltage difference during the discharge curve in V, *I* is the current in A and Δt the discharge time in s.

It can be seen that the charging and discharging process are nearly symmetric, indicating excellent electrochemical reversibility of the electrodes. The discharging curves of CNFs show a small *IR* drop imply a small equivalent series resistance, which is essential to power characteristic of supercapacitors. The lower *IR* drop of CNFs to the AC is due to the fact that the high conductivity of CNFs. The *IR* drop is large for AC means higher ESR. The calculated specific capacitance for CNFs 23.8 F/g at 0.23 A/g decreases to 19 F/g at 2 A/g.

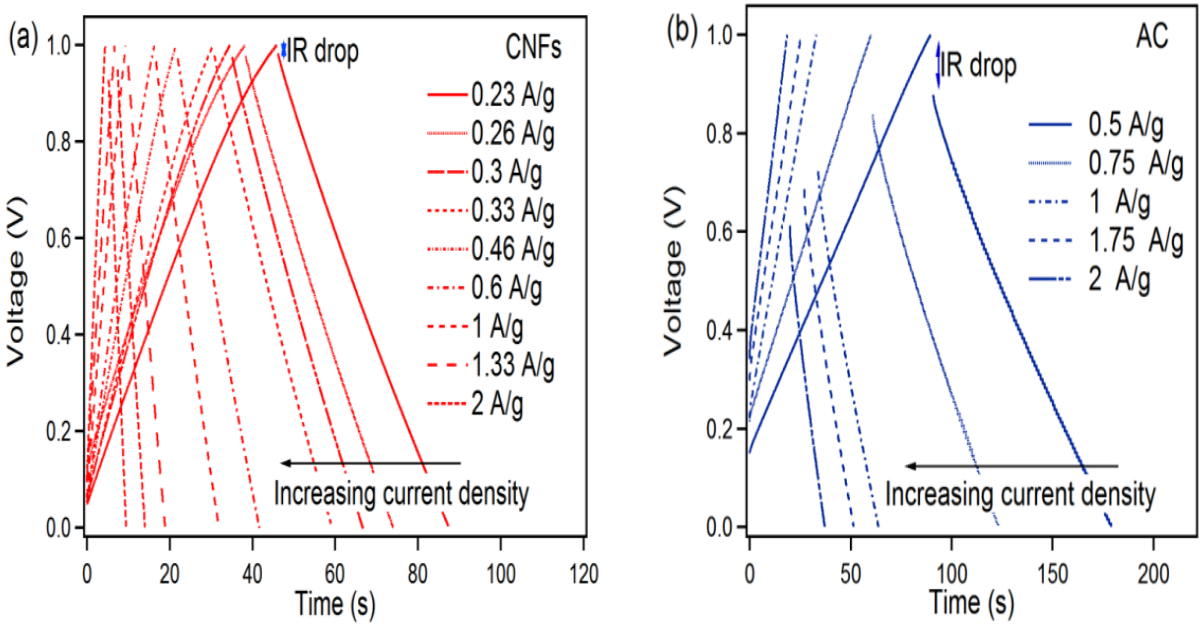

Figure 4.5. (a) GCD curves at different current densities of CNFs, (b) GCD curves at different current densities of AC.

The specific capacitance of AC decreases from 159 F/g at current density 0.5 A/g to 139 F/gat 2.5 A/g Figure 4.6(a).The specific capacitance of both symmetric capacitors of CNFs and AC decreases with the increase of current density, which is very common for supercapacitors and is mainly caused by the diffusion limitation of electrolyte ions in the microspores of the electrode.

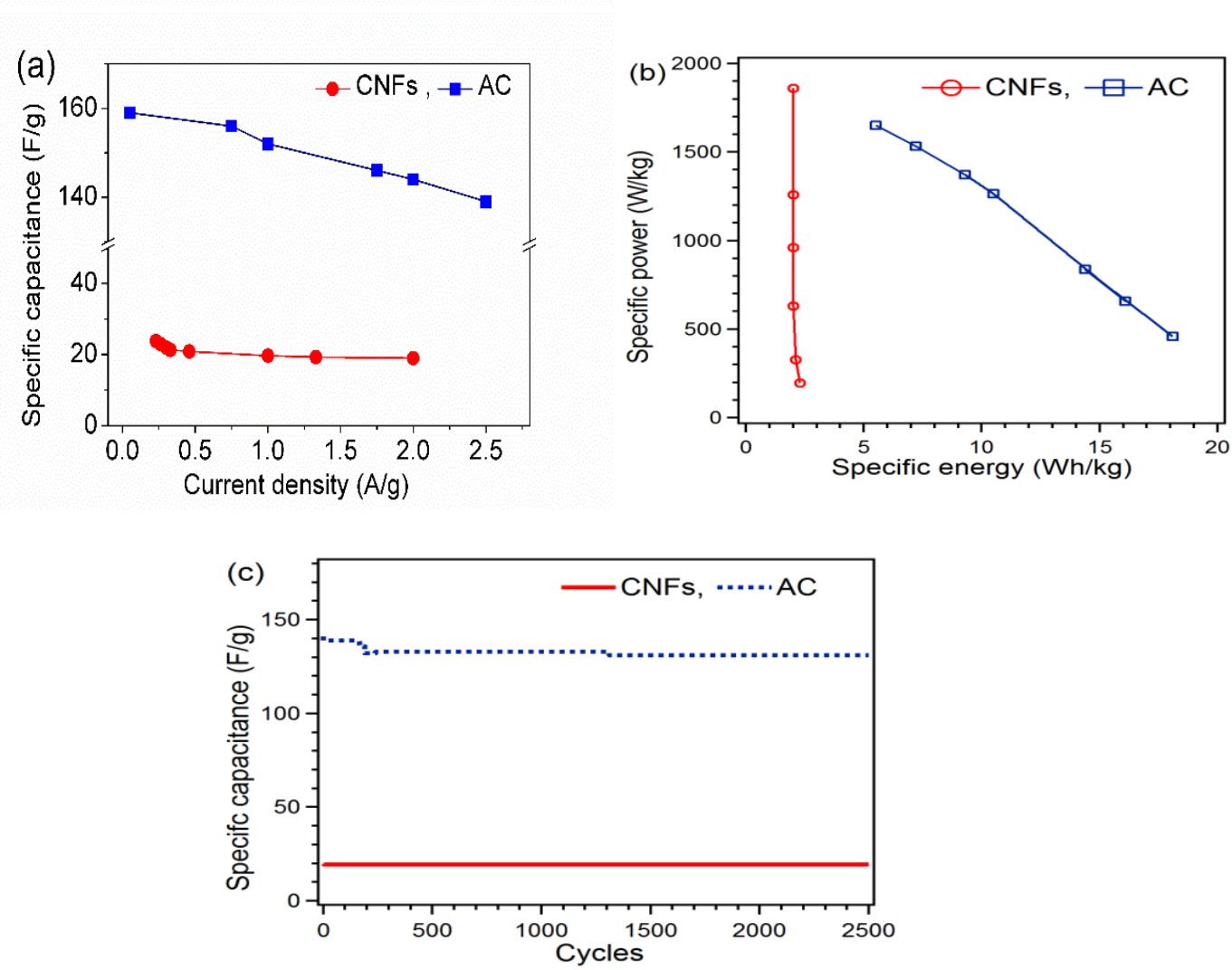

Figure 4.6. (a) Specific capacitance comparison from discharge curve of GCD, (b) Ragone plot of specific power against specific energy for CNFs and AC, (c) Cycling stability of CNFs and AC.

The specific power, P and specific energy, E, delivered upon discharge were estimated by equation (4.4) and (4.5).

$$P = {}^{Vi}/_{m} \tag{4.4}$$

$$E = {}^{Vit}/_{m} \tag{4.5}$$

Where V is the voltage excluding *IR* drop, *i* is discharge current, and t is the time [24].
As can be seen in the Ragone plot Figure 4.6 (b) the CNFs electrode shows maximum specific energy of 2.3 Wh/kg at a specific power of 197 W/kg and a maximum power density of 1860 W/kg at a specific energy of 2 Wh/kg indicating its good power characteristics. These results show an increase of specific power, the specific energy only decreases a little, which is a signature of excellent electrochemical properties of high energy density and power output, therefore very promising for application in the scenarios where high power output as well as high energy capacity is required [25]. For AC with the increase in specific power from 459 to1650 W/kg, the specific energy decreased from 18.1 to 5.5 Wh/kg.
The cycling stability is also a vital factor for practical applications. Galvanostatic charge discharge cycling measurement was performed at a constant current density 2 A/g for AC and for CNFs up to 2500 cycles Figure 4.6(c). The behaviour of AC during cycling stability shows small decrease in capacitance in from 141 to 131 F/g in 2500 cycles. This result express the capacitance fading is due to the irreversible reactions at the beginning of the cycling [10]. The CNFs cycling measurements reveal excellent capacitance retention 19 F/g in 2500 cycles.
The supercapacitor was further analysed by EIS. It depicts the Nyquist plot at in the frequency range 100 kHz–0.1Hzfor CNFs and AC Figure 4.7 (a).The Nyquist plots consist of (1) a high-frequency intercept on the real Z'axis, (2) a semicircle in the high-to-medium-frequency region, and (3) a straight line at the very low-frequency region [26]. The two Nyquist plots are similar in shape, namely, one semicircle at high frequency range, a straight line with a slope of close to 45° at high middle frequency region and a nearly vertical line at low frequency range. The phenomenon in the high-frequency region could be caused by the double-layer process as the response of this process is faster than

that of the faradaic process. In the high-frequency region, the intercept with Z' of CNFs and AC are 0.11 and 0.16 Ohm respectively. This value is considered as the total electrical resistance of the electrode material, electrolyte and electrical contacts [27]. The semicircle from high to medium frequency corresponds to parallel combination of $R_{ct}$and double layer capacitance [28]. It can be seen that semicircle (R_{ct}) is higher for AC (3.56) than CNFs (0.17). It can be speculate that higher conductivity of CNFs presents smaller semicircle loop while porous characteristic of AC shows larger loop of semicircle higher charge transfer resistance. The calculated ESR for CNFs is 0.28 ohm and for AC 3.72 ohm. The small value of CNFs indicates the facile electron and ion transport/diffusion in the device due to higher conductivity. Furthermore, the impedance curve intersected the real axis ($Re(Z)$) at a 45° angle, is consistent with the porous nature of the electrode when saturated with electrolyte [29]. CNFs exhibits a larger slope over AC means higher capacitive behaviour.

The specific capacitance of the CNFs and AC supercapacitor were calculated from the impedance analysis employing the imaginary component of impedance by following equation 4.6 [30].

$$C_s = 4\left(-(1/2\pi f z'' m)\right) \qquad (4.6)$$

Where *f* is frequency in Hz'' is the imaginary component of impedance and m, the mass of CNFs or AC calculated for one electrode. Figure 4.7(b) shows that the higher change in the specific capacitance of CNFs and AC below the frequency of 10Hz. The obtained specific capacitance for CNFs (36 F/g) and AC (284 F/g) at frequency of 0.1 Hz are pretty much comparable to capacitance calculated by CV.

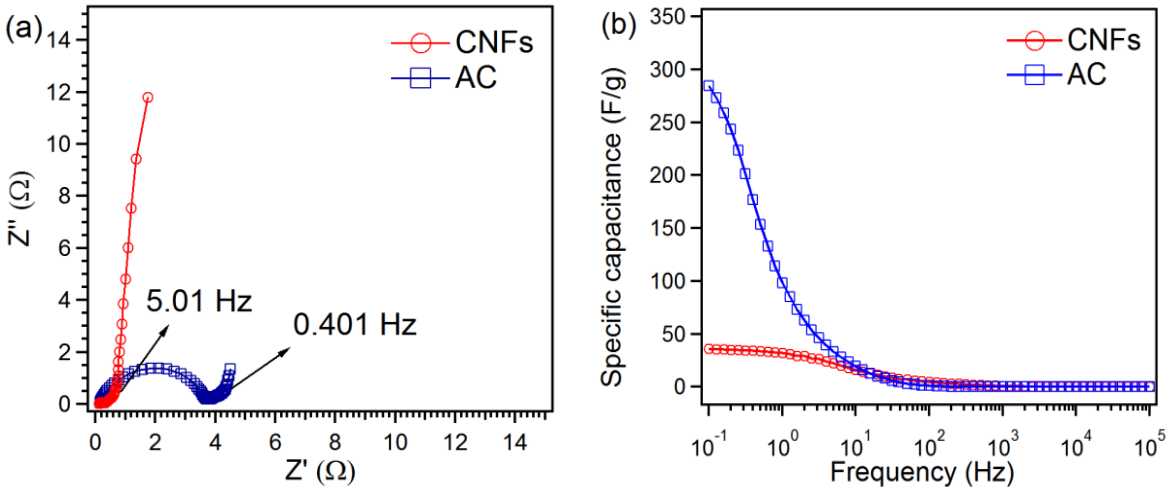

Figure 4.7. (a) Nyquist plot of CNFs and AC, (b) Csp comparison calculated from EIS.

Time constant τ is the property of the supercapacitor which reflects the response of the device. A small value of τ gives indication of better response. The time constant τ was calculated by using following equation.

$$2\tau = \frac{E_D}{P_D} \tag{4.7}$$

Where E_D is energy density and P_D is power density.E_D and $P_D$were calculated by using following equations.

$$E_D = 0.5C\,V^2/m \tag{4.8}$$

$$P_D = V^2/4(ESR)m \tag{4.9}$$

Where V is the voltage window during charge discharge curve, C is the capacitance from charge discharge and ESR calculated from Impedance spectroscopy and m is the mass of electrode. The calculated the time constant τ for AC was 3.1 s and for CNFs 0.08 at current

density 2 A/g, by using equations (7, 8, 9). The relationship between Z_{real} and frequency gives us information about the electrolyte and charge transfer resistance in electrolyte Figure 4.8(a). The resistance behaviour of electrode is greatly influenced by the nature of carbon electrode. For AC at high frequency 100 KHz, ESR is at lowest value of 0.16 Ω, which presents the electrolyte resistance Rs. With lowering down the frequency until 506 Hz, there is a sharp increase in resistance to 3.19 Ω. At the lowest frequency 0.1 Hz the ESR values is 4.5 Ω. In comparison CNFs sample display almost similar ESR 0.115 Ω at 100 KHz to AC. However, it show very small increase in ESR (0.34 Ω) at 506 Hz. At the lowest frequency 0.1 Hz the obtained ESR for CNFs was 1.87 Ω, much lower the AC. The increase in ESR with decreasing frequency could be due to the difficulty of penetration of the electric signal into the deeper pores (filled with electrolyte) and/or in the smaller particles [31].This variation can be justified by the fact that as the frequency decreases, ions can easily reach the deeper zones of the activated carbon pores, and consequently, their longer displacement within the electrolyte results in higher electrolyte resistance [32].

The relationship between Z_{Img} and frequency gives us information about relaxation time at the boundary region, where supercapacitor transfer from resistor to capacitor Figure 4.8(b). The time constant τ_0 corresponds to phase angle 45° represents the transition of electrochemical capacitor from a purely resistive to purely capacitive behaviour. It is well known that higher power delivery corresponds to lower τ_0 values. For a frequency, $f > 1/\tau_0$, it acts as a pure resistor and for $f < 1/\tau_0$, it behaves as a pure capacitor. The phase angle 45 ° was found for AC at frequency 5020 Hz and for CNFs at 1.99 Hz. This shows that translation frequency from resistive behavior to capacitive behavior for AC is much higher than CNFs.

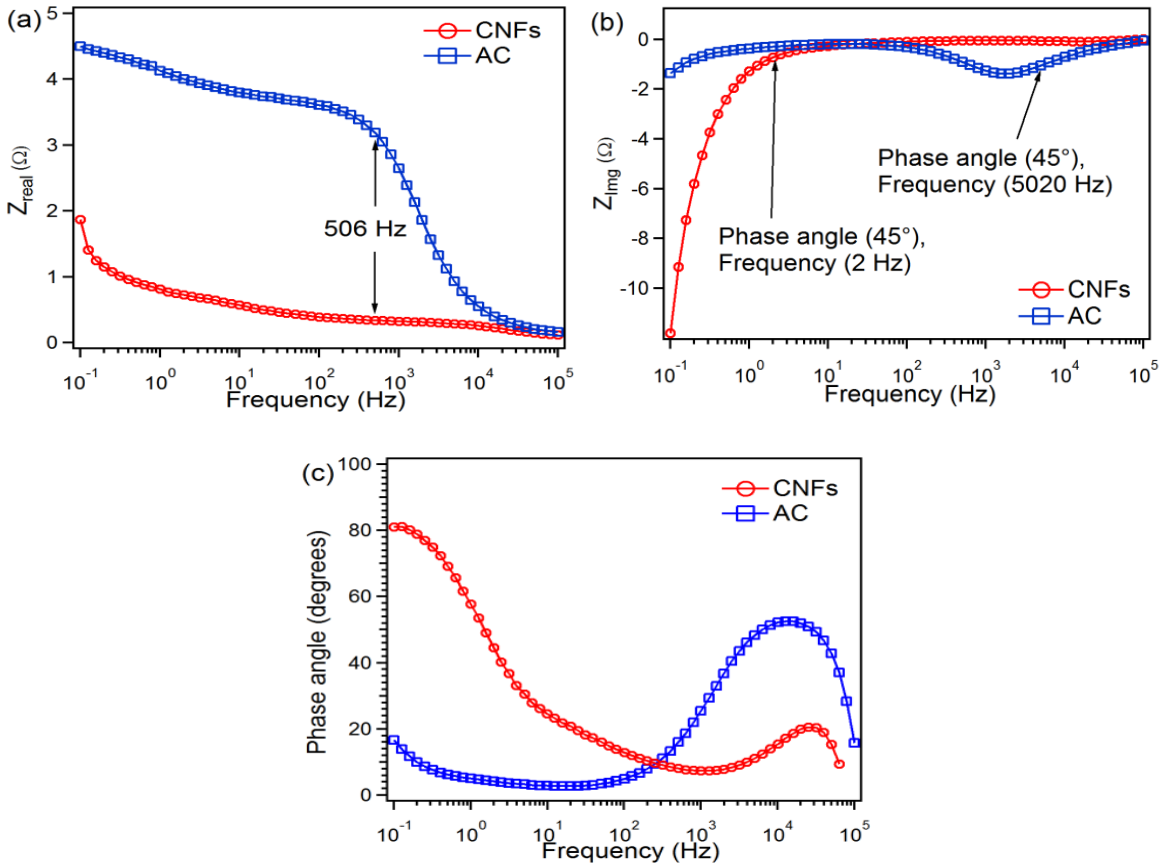

Figure 4.8. (a) The real and (b) imaginary parts are plotted as a function of log of frequency, (c) phase shift as function of frequency for AC and CNFs.

Figure 4.8(c) represents the variation of phase angle as a function of frequency, which is known as Bode plot. The phase angles are found to be -20°, -88° at low frequency 0.1 Hz in the AC and CNFssystems, respectively (Figure 4.8(c)). In general, phase angle approach to -90° confirms better capacitive performance and rapid charge discharge process. The relaxation time constant, τ0, defines the time required to deliver the stored charge effectively as seen from Figure 4.8(b) [33].

4.4. Effect of carbon structure and porous texture on EDLC performance

From electrochemical characterization it is evident that supercapcitor based on AC electrodes gives higher specific capacitance than CNFs in 6 M KOH electrolyte. According to the equation, $C = \in A/d$, d distance is very small when the electrode contains micropores. The higher capacitance of AC is due some important properties, those are higher BET surface area and existence of higher 88 % of ultramicropores and micropores. Whereas, the CNFs sample have low BET surface area and 17.9 % of micropores. Another important factor influence the capacitance is related to the following equation, $\tau = L^2/D$. Where L refers to the ion transport length and D refers to the ion transport coefficient. According to this equation, the ions enter fast inside the micropores, but as the size of pores increase the external area also increase. Due to this fact the ions accumulate outside of the pores, hence results in the decrease in the capacitance. According to E. Raymundo-Pinero et al. in aqueous solution the double layer formation is much favorable when the pore size is around 0.7 nm [19]. Our results reveals that pore size of AC (0.47 nm) is in the optimal range to build the double layer, hence presents higher specific capacitance over CNFs.

4.5. Conclusions

CNFs and AC electrodes have been prepared in a similar technique and compared as symmetric supercapacitor using aqueous solution. BET results reveal that CNFs electrode contains dominant mesosporous structure and surface area 83 m^2/g, whereas AC has high number of micropores, ultramicropores structure and a surface area of 1042 m^2/g. The key factors which help to achieve higher specific capacitance are surface area and existence of higher number of micropores of electrodes. AC material delivers a specific capacitance of 334 F/g, much higher than CNFs (52 F/g) at scan rate of 5 mV/s due to existence of microporous structure.

References

[1] J R Miller, A F Burke, Electrochemical Capacitors: Challenges and Opportunities for Real-World Applications. *The Electrochemical Society Interface*, 2008, Spring, 53–57.

[2] D Qu, H Shi, Studies of AC used in double layer supercapaciors. *Journal of Power Sources*, 1998, 74 99–107.

[3] Shao-yun ZHOU, Xin-hai LI, Zhi-xing WANG, Hua-jun GUO, Wen-jie PENG. Effect of activated carbon and electrolyte on properties of supercapacitor, *Trans. Nonferrous Met. Soc. China*, 2007, 17, 1328–1333.

[4] E Frackowiak, Carbon materials for supercapacitor application, *Phys. Chem. Chem. Phys*, 2007, 9, 1774-1785.

[5] R Amade, E Jover, B Caglar, T Mutlu, E Bertran, Optimization of MnO_2/vertically aligned carbon nanotube composite for supercapacitor application, *J. Power Sources*, 2011, 196, 5779–5783.

[6] S Hussain, R Amade, E Jover, E Bertran, Functionalization of carbon nanotubes by water plasma, *Nanotechnology*, 2012, 23, 385604.

[7] S Hussain, R Amade, E Jover, E Bertran, Nitrogen plasma functionalization of carbon nanotubes for supercapacitor applications, *J. Mater. Sci*, 2013, 48, 7620–7628.

[8] A G Pandolfo , A F Hollenkamp. Carbon properties and their role in supercapacitors. *Journal of Power Sources*, 2006, 157, 11–27.

[9] X Sun, X Zhang, H Zhang, D Zhang, Y Ma. A comparative study of activated carbon-based symmetric supercapacitors in Li_2SO_4 and KOH aqueous electrolytes. *J Solid State Electrochem*, 2012, 16, 2597–2603.

[10] V Ruiza, C Blanco, R Santamaría, J M Ramos-Fernández, M Martínez-Escandell, A Sepúlveda-Escribano, F Rodríguez-Reinoso. An activated carbon monolith as an electrode material for supercapacitors. *Carbon*, 2009, 47, 195–200.

[11] Q Abbas, D Pajak, E Frackowiak, F Béguin, Effect of binder on the performance of carbon/carbon symmetriccapacitors in salt aqueous electrolyte. *Electrochimica Acta*, 2014, 140, 132–138

[12] V Ruiz, C Blanco, M Granda, R Menéndez, R Santamaría, Influence of electrode preparation on the electrochemical behaviour of carbon-based supercapacitors. *J Applied Electrochem*, 2007, 37, 717–721.

[13] To-Chi Weng and HsishengTeng, Characterization of High Porosity Carbon Electrodes Derived from Mesophase Pitch for Electric Double-Layer Capacitors, *Journal of the Electrochemical Society*, 2001, 148, A368–A373.

[14] Q Gao, L Demarconnay, E Raymundo-Pinero, F Beguin, Exploring the large voltage range of carbon/carbon supercapacitors in aqueous lithium sulfate electrolyte, *Energy Environ. Sci*., 2012, 5, 9611.

[15] O Barbieri, M Hahn, A Herzog, R. Kotz, Capacitance Limits of High Surface Area Activated Carbons for Double Layer Capacitors, Carbon, 2005, 43,1303–1310.

[16] X Wei, X Jiang, J Wei, S Gao. Functional Groups and Pore Size Distribution Do Matter to Hierarchically Porous Carbons as High-Rate-Performance Supercapacitors. *Chem. Mater*. 2016, 28, 445−458.

[17] J Huang, B G. Sumpter, V Meunier. A Universal Model for Nanoporous Carbon Supercapacitors Applicable to Diverse Pore Regimes. *Chemistry*, 2008, 14, 6614 – 6626.

[18] C Ma, Y Li, J Shi , Y Song, L Liu, High-performance supercapacitor electrodes based on porous flexible carbon nanofiber paper treated by surface chemical etching. Chemical Engineering Journal, 2014, 249, 216–225.

[19] E Raymundo-Pinero, K Kierzek, J Machnikowski, F Beguin, Relationship between the nanoporous texture of activated carbons and their capacitance properties in different electrolytes, *Carbon*, 2006, 44, 2498–2507.

[20] M D Stoller, R S Ruoff, Best practice methods for determining an electrode material's performance for ultracapacitors, *Energy Environ. Sci*., 2010, 3, 1294–1301.

[21] S R S Prabaharan, R Vimala, Z Zainal, Nanostructured mesoporous carbon as electrodes for supercapacitors. *Journal of Power Sources*, 2006, 161, 730–736.

[22] D Saha, Y Li, Z Bi, J Chen, Jong K. Keum, Dale K. Hensley, Hippolyte A. Grappe, Harry M. Meyer, Sheng Dai, M. ParansParanthaman, and A. K. Naskar.Studies on Supercapacitor Electrode Material from Activated Lignin- Derived Mesoporous Carbon. *Langmuir*, 2014, 30, 900−910.

[23] E Frackowiak, F Beguin, Carbon materials for the electrochemical storage of energy in capacitors, *Carbon*, 2001, 39, 937–950.

[24] R Farma, M Deraman, Awitdrus, I A Talib, R Omar, J G Manjunatha, M M Ishak, N H Basri, B N M Dolah. Physical and Electrochemical Properties of Supercapacitor Electrodes Derived from Carbon Nanotube and Biomass Carbon. *Int. J. Electrochem. Sci*., 2013, 8, 257 – 273.

[25] W Xing, S Z Qiao, R G Ding, F Li, G Q Lu, Z F Yan, H M Cheng. Superior electric double layer capacitors using ordered mesoporous carbons. *Carbon*, 2006, 44, 216–224.

[26] H Xia, Y Wang, J Lin, L Lu. Hydrothermal synthesis of MnO_2/CNT nanocomposite with a CNT core/porous MnO_2 sheath hierarchy architecture for supercapacitors. Nanoscale Research Letters, 2012, 7, 33.

[27] C Y Lee, H M Tsai, H J Chuang, S Y Li, P Lin, T Y Tseng. Characteristics and Electrochemical Performance of Supercapacitors with Manganese Oxide-Carbon NanotubeNanocomposite Electrodes. *Journal of The Electrochemical Society*., 2005, 152, A716-A720.

[28] W Wei, X Cui, W Chen, D G. Ivey, Phase-Controlled Synthesis of MnO_2 Nanocrystals by Anodic Electrodeposition: Implications for High-Rate Capability Electrochemical Supercapacitors. *J. Phys. Chem. C*, 2008, 112, 15075–15083

[29] C Du, N Pan. High power density supercapacitor electrodes of carbon nanotube films by electrophoretic deposition, *Nanotechnology*, 17 (2006) 5314–5318.

[30] E G Calvo, F Lufrano, P Staiti, A Brigandì, A Arenillas, J A Menéndez. Optimizing the electrochemical performance of aqueous symmetric supercapacitors based on an activated carbon xerogel, *Journal of Power Sources*, 2013, 241, 776-782.

[31] F Lufrano, P Staiti, M Minutoli. Influence of Nafion Content in Electrodes on Performanceof Carbon Supercapacitors. *Journal of The Electrochemical Society*, 2004, 151, A64-A68.

[32] B E Conway, Electrochemical Supercapacitors, 1nd Ed.New York, Springer, 1999 36.

[33] A Ghosh, Y H Lee, Carbon-Based Electrochemical Capacitors, ChemSusChem, 2012 5 480-99.

Chapter 5: Impact of PVDF concentration and pressing force on performance of symmetric CNFs based supercapacitors

5.1. Introduction

The current research and development efforts on electrochemical power sources are mainly focused on fuel cell, electrochemical capacitors and are directed towards achievement of high specific energy, high specific power, long cycle life, at relative low cost [1, 2, 3]. Most of supercapacitor electrodes include carbon material like Activated Carbon (AC), Carbon nanofibers (CNFs), Carbon nanotubes (CNTs) or graphene because of good electric conductivity, high surface area and large specific capacitance [4-10]. The charge stored for carbon material at electrode/electrolyte interface produce high capacitance because of high surface area [10, 11].

CNFs have been receiving higher attention for use it as electrodes in supercapacitors because of their high length to diameter ratio, high surface area and excellent electric conductivity. CNFs could be defined as sp2-based linear filaments with diameter of 100 nm that are characterized by flexibility and their aspect ratio (above 100) [12, 13]. Since CNFs could be considered as the 1-D form of carbon, their structure and properties are closely related to those of other forms of carbon, especially to crystalline three-dimensional graphite, turbostratic carbons, and to their constituent 2-D layers [3, 14]. The fabrication of CNFs based electrodes for supercapacitors requires a binder to join them together forming a compact layer and adhere homogeneously onto the current collector [15]. Various types of polymers such as polyvynilidene fluoride (PVDF), polyvynilidene chloride (PVDC) and Teflon [10], are commonly used in proportions that usually vary from 5 to 10 wt. % [16-18]. The main role of binder is to provide enough strength during the electrode formation and appropriate pore sizes. The amount of binder therefore should be kept as low as possible, in order not to reduce surface area or conductivity in the electrode. At the same time, enough polymer should be added to ensure that CNFs are compact and so that the electrode is manageable [19]. The porous carbon material having dominant pores in the range 0.7-1 nm size exhibits excellent performance of forming double layer in aqueous electrolyte [16, 17]. However, binders inevitably cover some surface areas or pores of active materials, which block the paths for ions to move inside the pores. It is important to find a relationship between the amounts of binder usage for

the preparation and pore size distribution as well as its impact on the electrochemical properties of electrode. PVDF is a semi-crystalline fluoropolymer that presents high mechanical stability, proper swelling properties and extraordinary performance due to high integration within electrodes. PVDF combines the active materials to each other to form the electrode material [20]. Recently the optimal content of PVDF for the preparation of AC electrodes was found 5 wt% [21]. In fact, Zhu and coworkers found the highest capacitance in AC electrodes blended with PVDF at 5% among diferent concentrations of PTFE and Nafion [21]. As far as we know there is no systematic study concerning the testing of various PVDF % weight and hydro pressure force to fabricate electrodes based on CNFs.

The PVDF polymer has a typical stability of fluoropolymers but interactive groups will produce a unique polarity, thus results in its good chemical and oxidative resistances, poor hydrophilicity and significant swelling property in the electrolyte. Compared to other fluoropolymers, like polytetrafluoroethylene (Teflon), PVDF has a low density (1.78 g/cm^3). Besides PVDF does not dissolve in the aqueous electrolyte like PVA [21]. For all these reasons PVDF could be a suitable polymer for carbonaceous electrodes in supercapacitors.

In our work the two objectives were chosen to study the electrochemical properties of CNFs, first the effect polymer concentration with 5, 10 and 20 wt% PVDF, and second the influence of various pressure forces to manufacture the pellets (3, 7, 10 and 14 ton).

5.2. Experimental procedure:

5.2.1. Electrode Preparation

Symmetric supercapacitor based CNFs were fabricated with different concentration of PVDF for comparison. CNFs were provided by Grupo Antolin (GANF). It has a helicoidally graphitic stacked cup structure, there is a presence of Ni (6%), diameter is 20-80 nm, length >30um, electric resistivity 10^{-2} Ωcm. The electrode preparation for supercapacitor was achieved by milling of CNFs in an agate ball mill employing a frequency 500 rpm for 30 minutes. PVDF was used as a binder. Mixed CNFs were joint together using different concentration of PVDF in solution of 15 ml of acetone in agate mortar. The slurry was then mixed using a mechanical stirrer for 1 hour, and this was followed by an ultrasonic for 30 minutes. The slurry was dried in vacuum oven at 70 °C.

The dried sample was then used to assemble the supercapacitores electrode. The samples of CNFs/PVDF were pressed using hydraulic press with a die set (10 mm) at different pressing forces to form the disc electrodes.

The prepared samples with PVDF concentration of (5, 10 and 20 wt% with 7 ton pressing force) are designated as wt-5, wt-10 and wt-20. The influence of pressing force to prepare the electrode disc was investigated in the range from 3 to 14 ton. At lower pressing force (3 ton) it was difficult to fabricate the disc due to lack of powder adhesion and at higher pressing force (20 ton) the electrode disc was broken. We were able to prepare the electrode discs at 7 and 14 ton. These samples were prepared using concentrations 10 wt% of PVDF. The sample manufactured with 7 ton force is designated as wt-10 and with 14 ton force, as wt-10-1. It was noticed that thickness of discs decreases from 0.55 mm to 0.33 mm for 7 ton to 14 ton. The mass of all the prepared electrode discs was ~ 20 mg. Figure 1 (a) shows a prepared disc of CNFs electrode.

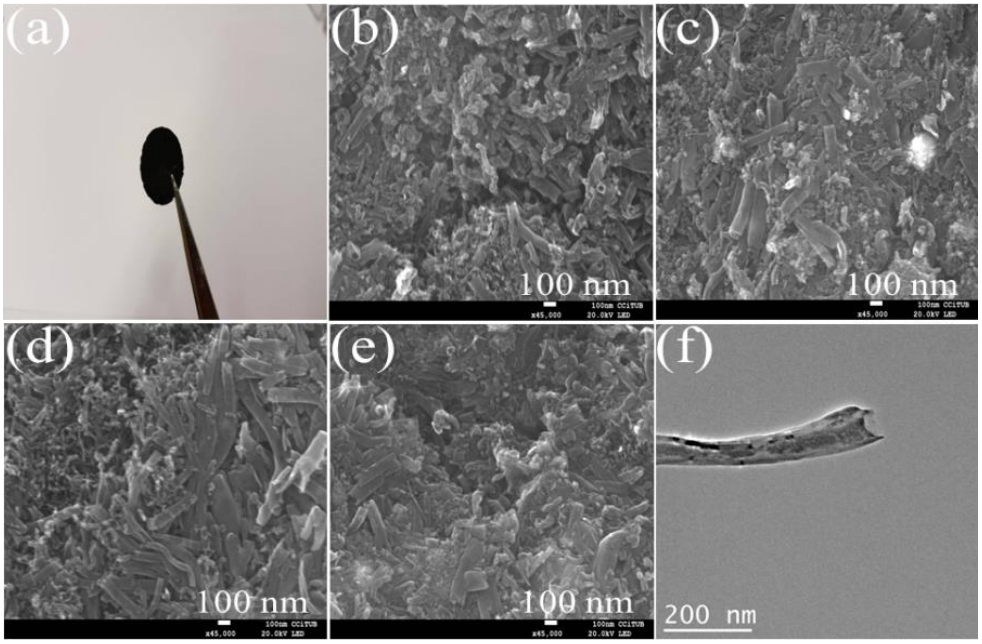

Figure 5.1. Photograph of prepared electrode disc (a), SEM images of CNFs electrodes prepared with different concentration of PVDF with 7 ton force: wt-5 (b), wt-10 (c), wt-20(d), with 14 ton force wt-10-1 (e), TEM image of CNF (f).

5.2.2. Morphological characterization

The samples were examined by scanning electron microscopy (SEM) (Jeol J-7100). Transmission electron microscopy (TEM) was performed on a Philips Tecnai G2 F20

system operated at 300 kV. The samples were suspended into ethanol and dispersed ultrasonically for 15 min. A drop of the suspension was deposited on a copper grid coated with carbon.

5.2.3. Surface characterization

The porous texture, specific surface area and pore size distribution (BET) of CNFs with different concentration of binder PVDF were obtained by physical adsorption of N_2 at 77 K using an automated gas adsorption analyzer (Micromeritics TriStar 3000 V6.04 A). All samples were outgassed at 100 °C for 4 h prior to the adsorption measurements.

5.2.4. Electrochemical characterization

The electrochemical performance comparison of AC and CNFs as symmetric capacitors were studied in two electrode Swagelok cell and using a Gamry 600 potentiostat in a 6 M KOH solution as an electrolyte. The specific capacitance of electrode materials was investigated by: cyclic voltammetry (CV), galvanostatic charging/discharging (GCD) and electrochemical impedance spectroscopy (EIS).

5.3. Results and discussion

5.3.1. Morphological characterization

The surface morphology of prepared electrodes was examined by SEM and TEM, see figure (5.1). It can be seen that PVDF binder effectively bonds the CNFs figure 5.1(b, c, d, e). The different structures for the electrodes of CNFs with different concentration of PVDF are visible. It was observed that increasing pressure force from 7 to 14 ton, the CNFs become more compact figure 5.1(c, e). The typical cylindrical CNF structure is distinguished from TEM image (figure 5.1(e)).

5.3.2. Surface area and Pore texture of CNFs

The specific surface area and pore size distribution of CNFs electrodes prepared with different concentration of polymer PVDF were obtained from the N_2 adsorption/desorption. The N_2 adsorption/desorption isotherm of CNFs different concentration of PVDF are shown in Figure 5.2(a). The isotherms of CNFs for all samples present a small hysteresis loop in middle pressure range from 0 to 0.45, which indicates CNFs contain mesoporous and macro pores structure. According to IUPAC classification

the isotherm of all samples can be classified as type II isotherm [22]. The pore distribution of CNFs for all sample are listed in table 5.1.

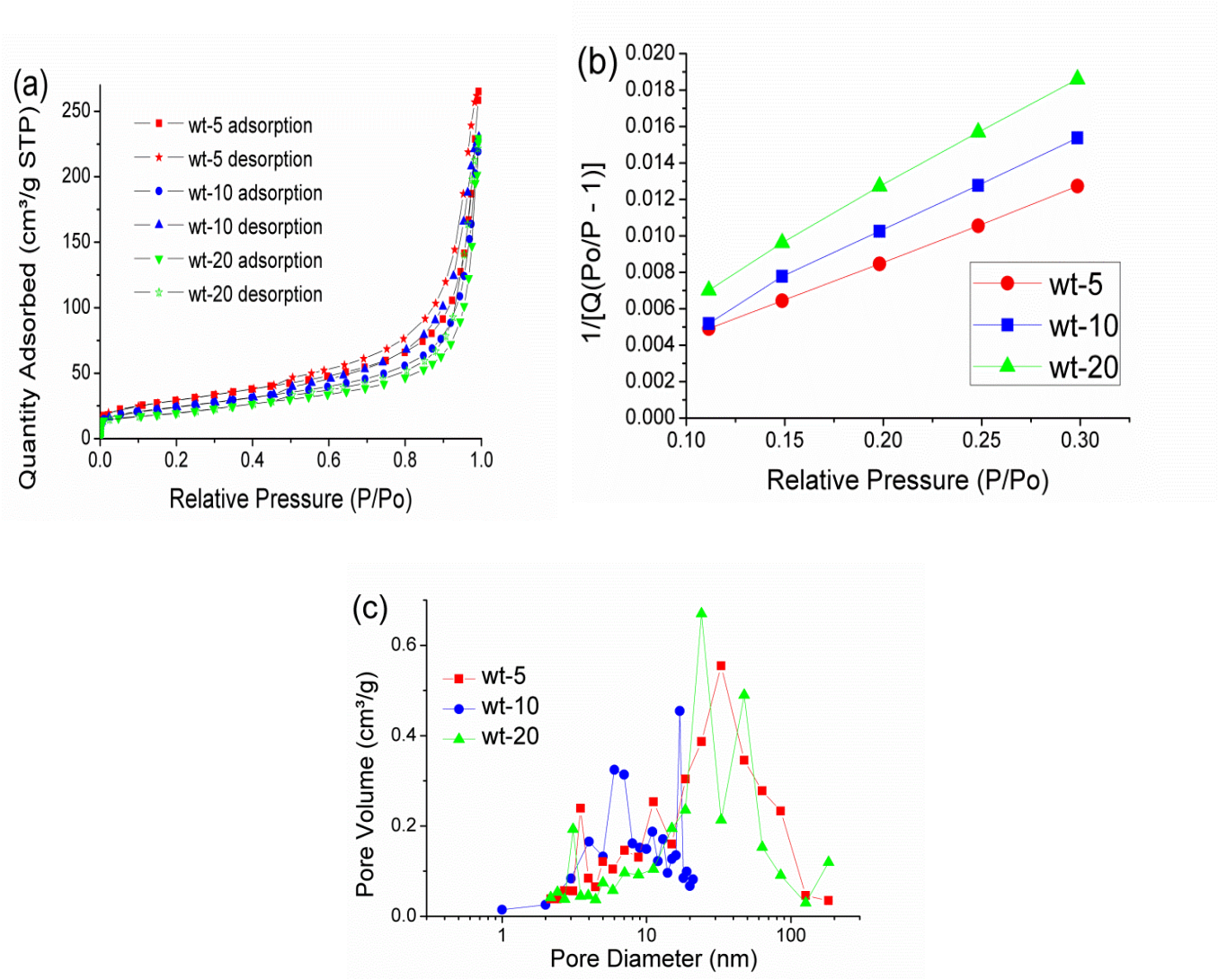

Figure 5.2. (a) Nitrogen adsorption/desorption isotherms, (b) BET surface area, (c) Pore size distribution calculated by BJH Desorption dV/dlog(D) Pore Volume.

The BET specific surface area is extracted from the linear region of $1/[Q_m(p_0/p - 1)]$ versus p/p_0 in the classical BET range of 0.1-0.3 Figure 5.2(b). The sample wt-5 contains surface area of 103 m^2/g while wt-10 and wt-20 have surface areas of 86 m^2/g ad 71 m^2/g respectively. The total volume of pores (V_t, cm^3/g) was calculated by the number of adsorbed nitrogen at $P/P_0 \approx 0.9932$. The volume of micropores and the values of surface areas of micro (S_{micro}, m^2/g) were investigated by the use of t-Plot Harkins and Jura

method, the pore size distribution of CNFs with different concentration of PVDF sample calculated from adsorption isotherms by the Barrett−Joyner−Halenda (BJH) method. The total pore volume are 0.41, 0.356 and 0.35 cm^3/g for wt-5, wt-10 and wt-20 respectively at relative pressure (P/P_0=0.9932). These results indicate that with increase in PVDF concentration most of the pores get blocked which do not contribute during the measurements of surface area.

Table 5.1. Physicochemical parameters of CNFs electrode prepared with different concentration of PVDF

Sample	SSA[a] (m^2/g)	V_t[b] (cm^3/g)	V_{Micro}[c] (cm^3/g)	V_{Meso}[d] (cm^3/g)	V_{Macro}[e] (cm^3/g)	P_{Micro}[f] (%)	P_{Meso}[g] (%)	P_{Macro}[h] (%)	Ext_{area}[i] (m^2g)
wt-5	103	0.4	0.00288	0.285	0.109	0.72%	72%	27.3%	97
wt-10	86	0.356	0.00233	0.244	0.11	0.65%	68.4%	30.8%	80
wt-20	71	0.35	0.00042	0.184	0.166	0.12%	52.4%	47.4%	68

[a]specific surface area, [b]Single point volume adsorption total volume of pores at p/p0=0.9932, [c]micro volume from t-plot (y-intercept), [d]Meso volume from BJH method, [e]Macro Volume by BJH method ,[(f, g, h)]the micro, meso and macro percentage calculated by V_{MICR}/V_{TOTAL}*100%, V_{MESO}/V_{TOTAL}*100%, , [i]EXT (External area) area from the slope of t –plot.

The pore size distribution of the materials is classified into three groups: micro pores (< 2nm), meso pores (2-50 nm) and macro pores (> 50 nm) [23]. Figure 5.2(c) exhibits pore size distribution of CNF mixtures. CNFs electrode manufactured with 5 wt% (wt-5) contains 0.72 % (micropores), 72 % (mesopores) and 27.3 % (macropores). It was observed with increase in PVDF concentrations for samples wt-10 and wt-20, micro and mesopores contribution decreases and the external surface area increases, as shown table 5.1. These finding tells that higher PVDF concentration blocks small sizes of pores which are also the result of decrease in surface area. It was observed that there was no difference in the surface area or pore size distribution for wt-10 and wt-10-1 even when the electrode were prepared with different pressure forces. This is because for BET analysis it was needed to break the electrode to make in powder form.

5.3.3. Electrochemical measurement

The electrochemical properties of supercapacitor were tested based on two electrode cell systems, which can measure their performance more accurately [24]. The cyclic voltammetry analysis of supercapacitor is a basic technique to understand the electrochemical performance of the electrode material. The specific capacitance per unit mass for one electrode was calculated using equation (1).

$$C_s = 4 * C/m \tag{5.1}$$

$$C = \frac{q_a + |q_c|}{\Delta V} \tag{5.2}$$

Where C_s is the specific capacitance in F/g, C is the measured capacitance for the two-electrode cell by equation 2 and m is the total mass of the active material in both electrodes [25]. Figure 5.3(a) presents the comparison of cyclic voltammograms (CVs) for the samples at a scan rate 5 mV/s. The CVs display rectangular shape without any redox active peaks which is a signature of excellent double layer behavior. Figure 5.3(b) shows the specific capacitance comparison for different scan rates. It can be seen that sample wt-10-1 gives higher specific capacitance 96 F/g at scan rate 5 mV/s. It was found a 64 % specific capacitance retention at high scan rate (500 mV/s).

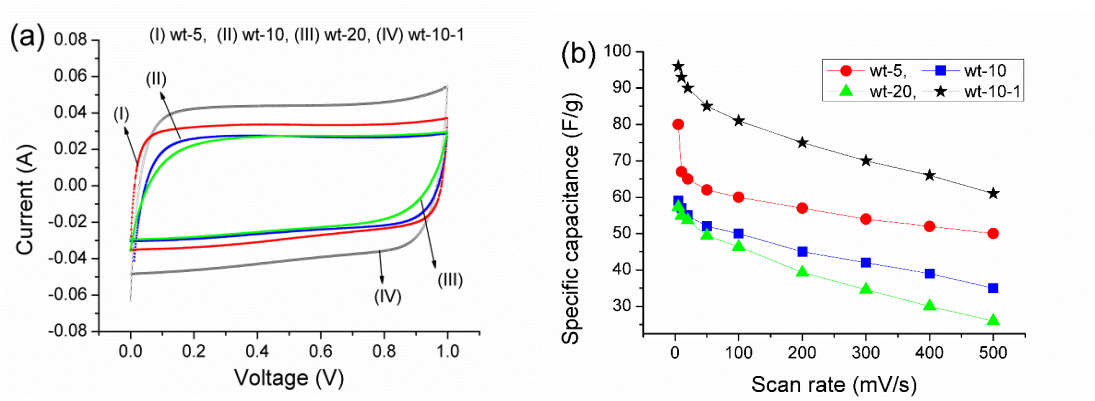

Figure 5.3. (a) CV comparison at scan rate of 5 mV/s, (b) Evolution of the specific capacitance at different scan rates.

For the sample wt-5 the specific capacitance decreases from 80 to 50 F/g for scan rate 5 to 500 mV/s respectively. The other two sample wt-10 and wt-20 delivers the specific capacitance of 59 and 57 F/g respectively at scan rate 5 mV/s, which is much lower than others. Comparing only PVDF concentration, the sample prepared with lowest concentration (5 wt%) shows higher capacitance over the others at scan rate, but it was observed that pressure force also make a significant effect on the properties of supercapacitor. The sample wt-10-1 prepared with 10 wt% and 14 ton pressing force shows highest specific capacitance and retention at all scan rate. This could mean that even at higher scan rate the interior micropores are accessible to the ions.

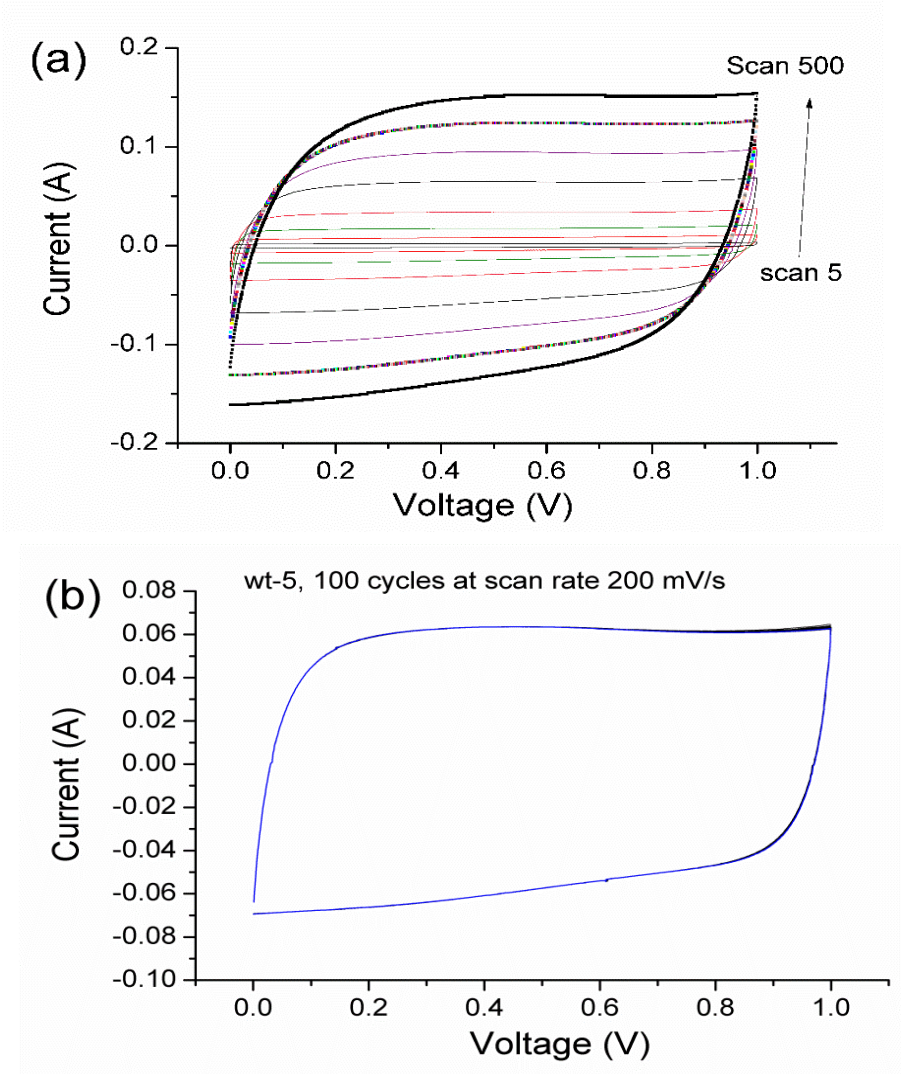

Figure 5.4. (a) CVs of wt-5 at different scan rates (5, 10, 20, 50, 100, 200, 300, 400 and 500 mV/s), (b) CVs of wt-5 from 1st to 100th cycle at a constant scan rate of 200 mV/s.

Once studied the Faradic behavior of the supercapacitors we wonder about the stability. Figure 5.4(a) shows cyclic voltammograms of the sample wt-5 measured at different scan rates from 5 mV/s to 500 mV/s. The rectangular shapes of CV curves at all scan rates tell about the excellent conductivity and low mass transport resistance [26]. The cycling stability test for up to 100 cycles at a high scan rate 200 mV/s is presented in figure 5.4(b). The 100 CVs are overlapping each other, which mean stable capacitance behavior.
The dynamics of the charge and discharge where investigated through GCD. Figure 5.5(a) shows a comparison of the GCD curves at a constant current density of 0.45 A/g

in the potential range of 0-1 V. As can be seen all samples show a similar symmetrical triangular curve with a nearly linear variation of voltage as a function of time during charge and discharge but different IR drop values. This type of curve is typical for CNFs based supercapacitors [5]. The data shows that all three concentrations of PVDF and different pressing force based supercapacitors present good performance. However, despite having similar shape the curve for the sample wt-10-1 tooks significantly longer charge and discharge times, which indicates that higher number of electrons and electrolytes ions are participating in charge and discharge process.
Figure 5.5(b) shows GCD curves recorded at different current densities for sample wt-5. The nearly symmetric rectangular shapes of charge/discharge curves indicate the high and reversible charge storage capacity of CNFs. It has been reported that appearance of the IR drop is the consequence of combined resistance of solution, electrode and ion migration in the electrode [27, 28]. IR drop was enhanced with increase in the current density. Figure 5.5(c) shows the plotted graph between discharge currents and IR drops. The slope of the diagram could be used to estimate the overall resistance of the capacitor: the higher the slope, the greater the overall resistance of the capacitor [28]. The slopes have a trend like wt-10-1 < wt-5 < wt-10 < wt-20. It can be suggested that higher pressure force can significantly reduce the resistance of the capacitor, which is a worth to increase supercapacitor performances.

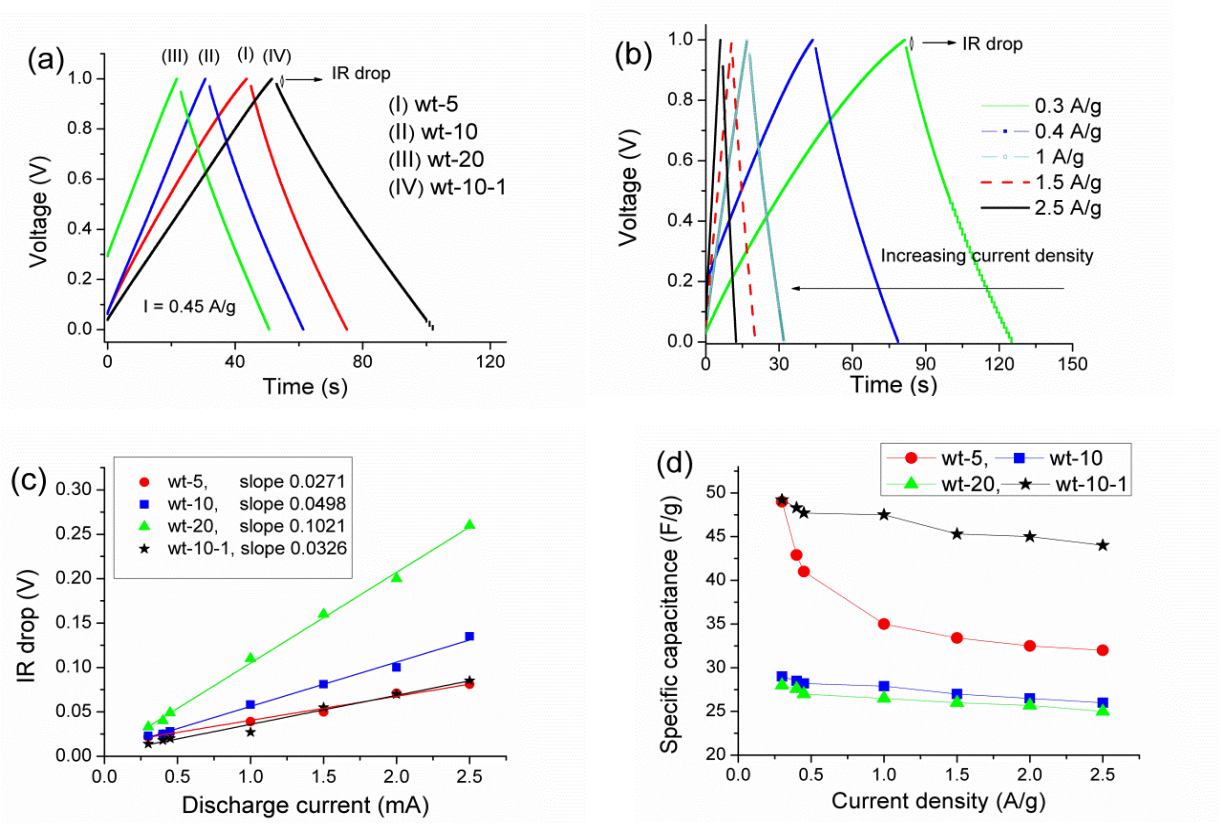

Figure 5.5. (a) Charge/discharge comparison at a constant current density of 0.45 A/g, (b) charge/discharge curves for wt-5 at different current densities, (c) Variation of IR drop with discharge currents, (d) specific capacitance comparison at different current densities.

The discharge capacitance (C) is estimated from the slope (*dV/dt*) of the linear portion of the discharge curve using equation 5.3.

$$C_s = \left(\frac{2I}{(dV/dt).m}\right) \tag{5.3}$$

Where C_s is the specific capacitance in F/g, ΔV is the voltage difference during the discharge curve in V, I is the current in A and Δt the discharge time in s, m is the mass of electrode.

Figure 5.5(d) shows the variation of the specific capacitance with current density. The specific capacitance of wt-10-1 decrease from 49.2 to 44 F/g for current densities 0.3 to 2.5 A/g respectively, indicates small decrease in capacitance even at higher current densities. Whereas a big drop in specific capacitance was observed for wt 5 from 49 to 32 F/g with increase in current density. The other two samples also present decrease in specific capacitance with increase in current density.

The charge discharge cycling stability up to 2000 cycles was tested at affixed current density 1.5 A/g Figure 5.6(a). The capacitance was calculated by using equation 5.3. All samples show almost constant capacitance from the first to the last cycle. The specific capacitance follow the trend like wt-10-1<wt-5<wt-10<wt-20. The specific energy density is defined as the amount of energy stored per unit weight in a particular device, while specific power density is directly related to the rate at which energy can be transferred from the device [29].

The specific power, *P* and specific energy, *E*, delivered upon discharge were estimated by equation (5.4) and (5.5).

$$P = {}^{Vi}/_{m} \tag{5.4}$$

$$E = {}^{Vit}/_{m} \tag{5.5}$$

Where *V* is the voltage excluding *IR* drop, *i* is discharge current, and t is the time [30].

As can be seen in the Ragone plot figure 6 (b), the wt-10-1 electrode shows maximum specific energy of 6.2 Wh/kg at a specific power of 296 W/kg and a maximum power

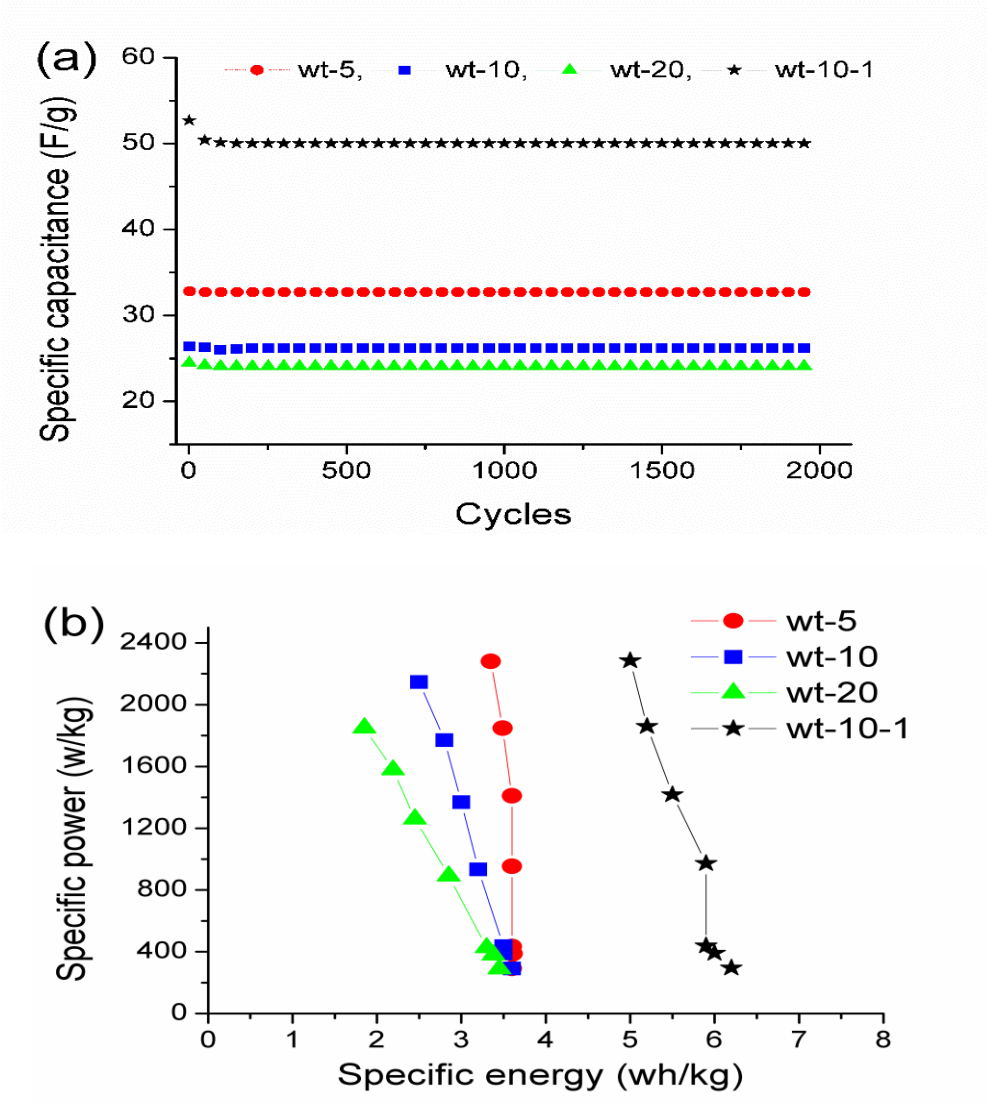

Figure 5.6. (a) Charge/discharge cycling stability at constant current density 1.5 A/g, (b) Ragone plot of specific power against specific energy.

density of 2285 W/ kg at a specific energy of 5 Wh/kg for current density of 1 A/g to 4.5 A/g. These results show, with increase of specific power, the specific energy only decreases a little, which is a signature of excellent electrochemical properties of high energy density and power output, therefore very promising for application in the scenarios where high power output as well as high energy capacity is required [31]. The other samples present smaller power and energy then the wt-10-1.

AC impedance spectroscopic measurements were performed to investigate the electrochemical characteristics of the symmetric supercapacitors. Figure 7(a) shows the Nyquist plot for all the samples. The impedance measurements were carried out at AC

with 10 mV amplitude over a frequency range between 100 kHz to 0.1 Hz. Generally the complex plane of impedance (Nyquist) plot of porous electrode consists on a high frequency semicircle, a 45° region (Warburg region) of transition between high and low frequencies, and almost a vertical line at low frequencies [3].The equivalent series resistance (ESR) comprises on contact resistance, solution resistance, and charge transfer resistance of the electrode material. The appearance of Warburg region is the consequence of the combination of resistive and capacitive behaviors of the ions penetrating into the electrode pores [30]. It can be seen from the figure 5.7(a) that all the samples show a semicircle in the high frequency region and a straight line in the lower frequency region. This indicates that the supercapacitors have a blocking behavior at high frequencies and a capacitive behavior at low frequencies. A very big semicircle from high to mid frequency is observed for the sample wt-20, which indicates high intrinsic resistance (charge transfer resistance) of porous structure [32]. It can be seen that for the four samples intrinsic resistance of electrodes are in the order of wt% that is wt-5<wt-10-1<wt-10<wt-20. The reason might be that higher polymer concentration would block the conductive paths of the pores. However, with high pressing force 14 ton intrinsic resistance values decreases. The possible reason behind this could be a decrease in the thickness of electrode means reduce in the space between the pores which effectively reduced the internal resistance. The equivalent series resistance (ESR) values of the electrode material are (0.3, 0.6, 1.9 and 0.5 (Ω)) for wt-5, wt-10, wt-20 and wt-10-1 respectively. These results tell that electrical conductivity decrease with increase in the PVDF concentration, whereas pressing force reduces it.

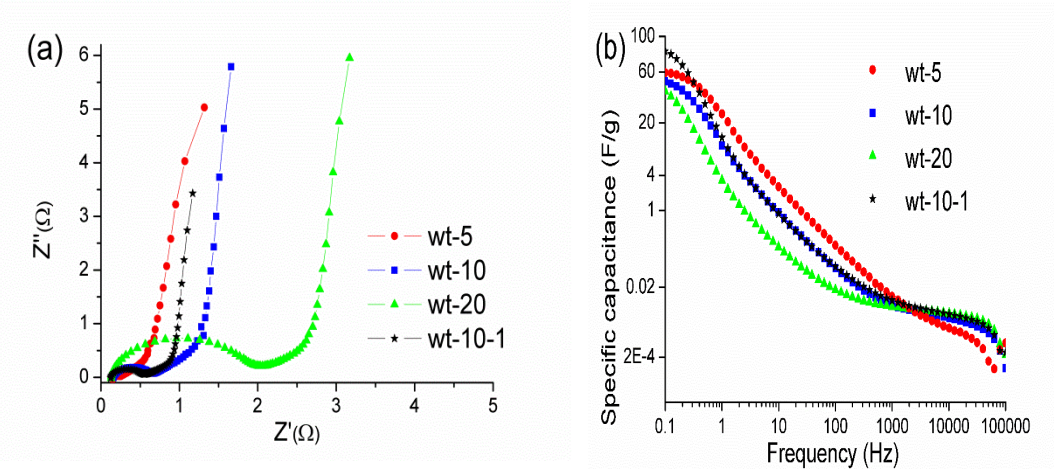

Figure 5.7. (a) Nyquist plot for all samples, (b) Specific capacitance comparison calculated from EIS.

The specific capacitance of the samples were calculated from the impedance analysis employing the imaginary component of impedance by following equation 5.6 [33].

$$C_s = 4\left(-(1/2\pi f z'' m)\right) \quad (5.6)$$

where *f* is frequency in Hz. z'' is the imaginary component of impedance and *m*, the mass of CNFs or AC calculated for one electrode. Figure 5.7(b) shows that the change in the specific capacitance of electrodes mainly below the frequency of 1500 Hz. The obtained specific capacitances at low frequency 0.1 Hz for wt-5, wt-10, wt-20 and wt-10-1 are 59.2, 50.8, 41.6, 83 F/g respectively.

The relaxation time constant represents the transition of electrochemical capacitor from purely resistive to purely capacitive and can be calculated by using $\tau_0 = {}^{1}/_{f_k}$, where f_k is the knee frequency at phase shift 45° [34]. The relaxation time constant were 1, 2, 5 and 2.5 s for wt-5, wt-10, wt-20 and wt-10-1 respectively. It shows that relaxation time constant increased with increase in PVDF concentration but decreased again with increase in pressing force.

Our results show much lower values of time constant in comparing other reports [30, 35]. R Farma et al. obtained τ_0 values 25.12 and 50.13 s for carbon electrode based on carbon nanotubes and biomass carbon [30]. T Thomberg et al. results show the τ_0 values in the range of 3 to 68 s for carbon electrodes manufactured from micro/mesoporous carbon [35]. Figure 5.8(b) represents the variation of phase angle as a function of frequency, which is known as Bode plot. The phase angles at low frequency 0.1 Hz are found -75°, -74°,-60° and 75.3 for wt10-1 respectively. These values are close to -90° which means better capacitive performance and rapid charge discharge process.

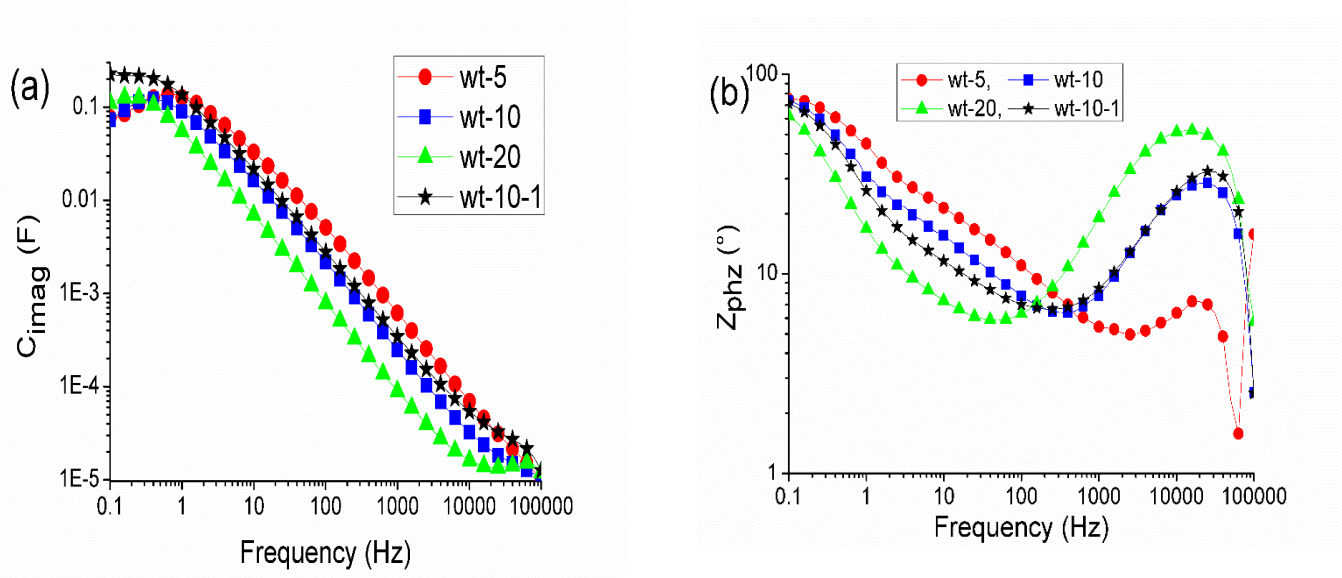

Figure 5.8. (a) Imaginary capacitance as function of frequency, (b) the relation of phz angle vs frequency.

5.4. Correlation between BET surface area and Porous Texture on EDLC Performance

Supercapacitor performance can be evaluated by correlating the surface texture, pore size distribution and thickness of electrodes with the electrochemical analysis. The BET specific surface area drops down with increase in PVDF binder concentration. PVDF is a hydrophobic agent, this nature of binder makes the carbon electrode more hydrophobic which makes it difficult for ions to penetrated deep inside the pores of electrode when using aqueous electrolyte. As a result decrease in the ion mobility, the electrode performance will be reduced. In addition from BET results it was found with increase in PVDF concentration the (micro, mesopore %) and surface area decreases. The increase in the pressure force from 7 to 14 ton decrease the thickness of electrode from 0.55 mm to 0.33 mm. This lessening of thickness diminishes the space between the pores and outer area. All of above mentioned properties make a significant influence on the specific capacitance of electrode according to the equation.

$C = \in A/d$. Where A is the specific surface area of the electrode accessible to the electrolyte ions, and d is the effective thickness of the EDL (the Debye length) [36].

5.5. Conclusions.

CNFs based symmetric supercapacitors have been prepared and test with different concentration of PVDF and pressure forces. The highest surface area 103 m^2/g was obtained for lowest concentration of PVDF (5 wt%). The percentage of (micro, meso) pores decreased with increase in PVDF concentration from (5 to 20 wt%). Cyclic voltammetry, constant current charge/discharge and electrochemical impedance spectroscopy methods have been used to evaluate the electrochemical characteristics. Highest specific capacitance (96 F/g) was achieved with 10 wt% of PVDF,and a force of 14 ton. The comparison with lower pressing force indicates the important role this parameter plays. The specific power increased to 2285 W/kg from 296 W/kg with a very little decrease in specific energy from 6.2 Wh/kg to 5Wh/kg.

References.

[1] B E Conway, V Birss, J Wojtowicz. The role and utilization of pseudocapacitance for energy storage by supercapacitors. *Journal of Power Sources*, 66 (1997) 1.

[2] J P Zheng, T R Jow. A New Charge Storage Mechanism for Electrochemical Capacitors. J. Electrochem. Soc. 142 (1995), L6-L8.

[3] R Kotz, M. Carlen. Principles and applications of electrochemical capacitors. *Electrochimica Acta*, 45 (2000) 2483-2498.

[4] H Shen, E Liu, X Xiang, Z Huang, Y Tian, Y Wu, Z Wu, H Xie. A novel activated carbon for supercapacitors. *Materials Research Bulletin*. 47, (2012), 662–666.

[5] A Daraghmeh, S Hussain, L Servera, E Xuriguera, M Blanes, F Ramos, A Cornet, A Cirera. Flexible supercapacitors based on low-cost tape casting of high dense carbon nanofibers. *Mater. Res. Express* 4 (2017) 025007

[6] S Hussain, R Amade, E Jover, E Bertran. Nitrogen plasma functionalization of carbon nanotubes for supercapacitor applications. J. Mater. Sci. 18, (2013), 7620–8.

[7] C M Ghimbeu, E Raymundo-Piñero, P Fioux, F Béguin, C Vix-Guterl. Vanadium nitride/carbon nanotube nanocomposites as electrodes for supercapacitors. *J. Mater. Chem.* 21 (2011) 13268-13275.

[8] C Zhu, T Liu, F Qian, T Yong-Jin Han, E B. Duoss, J D. Kuntz, C M. Spadaccini, M A. Worsley, Y Li. Supercapacitors Based on Three-Dimensional Hierarchical Graphene Aerogels with Periodic Macropores. *Nano Lett.*, 16 (**2016),** 3448–3456.

[9] Zhong–Shuai Wu, K Parvez, X Feng, K Mullen. Graphene-based in-plane micro-supercapacitors with high power and energy densities. Nature Communications 4, Article number: 2487 (2013). DOI: 10.1038/ncomms3487

[10] Q Y Li, Z S Li, L Lin, X Y Wang, Y F Wang, C H Zhang, H Q Wang. Facile synthesis of activated carbon/carbon nanotubes compound for supercapacitor application. Chem. Eng. J., 156 (2010) 500-504.

[11] J M Ko, K M Kim. lectrochemical properties of MnO_2/activated carbon nanotube composite as an electrode material for supercapacitor. Mater. Chem. Phys., 114 (2009) 837-841.

[12] O Monereo, S Illera, A Varea, M Schimidt, T Sauerwald, A Schütze, A Cirera, J D Prades. Localized self-heating in large arrays of 1D nanostructures. Nanoscale, 8 (**2016**) 5082-5088.

[13] S Claramunt, O Monereo, M Boix, R Leghrib, J D Prades, A Cornet, P Merino, C Merino and A Cirera, Flexible gas sensor array with an embedded heater based on metal decorated carbon nanofibres, Sens. Actuator B, 187 **(2013)** 401-406.

[14] J.B. Donnet, R.C. Bansal: Carbon Fibers (MarcelDekker, New York 1984)

[15] Keh-Chyun Tsay, L Zhang, J Zhang. Effects of electrode layer composition/thickness and electrolyte concentration on both specific capacitance and energy density of supercapacitor. Electrochimica Acta. 60 (2012) 428– 436.

[16] E Frackowiak, F Béguin, Carbon materials for the electrochemical storage of energy in capacitors. Carbon 39 (2001) 937-950.

[17] K H An, W S Kim, Y S Park,Y C Choi, S M Lee, D C Chung, D J Bae, S C Lim, Y H Lee. Supercapacitors Using Single-Walled Carbon Nanotube Electrodes. Advanced Materials 13 (2001) 497-500.

[18] S Shiraishi, H Kuriharea, A Oya. Preparation and Electric Double Layer Capacitance of Mesoporous Carbon. Carbon Sicence 1 (2001) 133-137.

[19] V Ruiz, C. Blanco, M Granda, R. Menéndez, R. Santamaría. Influence of electrode preparation on the electrochemical behaviour of carbon-based supercapacitors. Appl Electrochem 37, (2007), 717-721.

[20] Q Abbas, D Pajak, E Frąckowiak, F Béguin. Effect of binder on the performance of carbon/carbon symmetric capacitors in salt aqueous electrolyte. Electrochimica Acta, 140 (2014), 132-138.

[21] Z Zhu, S Tang, J Yuan, X Qin, Y Deng, R Qu, G M Haarberg. Effects of Various Binders on Supercapacitor Performances. Int. J. Electrochem. Sci., 11 (2016) 8270 – 8279.

[22] Li-Feng Chen, Xu-Dong Zhang, Hai-Wei Liang, Mingguang Kong, Qing-Fang Guan, Ping Chen, Zhen-Yu Wu, Shu-Hong Yu. Synthesis of Nitrogen-Doped Porous Carbon Nanofibers as an Efficient Electrode Material for Supercapacitors. ACS Nano, 8 (2016) 7092– 7102.

[23] J Huang, B G. Sumpter, V Meunier. A Universal Model for Nanoporous Carbon Supercapacitors Applicable to Diverse Pore Regimes. *Chemistry*, 14 (2008), 6614 – 6626.

[24] Qiong Wu, Yuxi Xu, Zhiyi Yao, Anran Liu, and Gaoquan Shi. Supercapacitors Based on Flexible Graphene/Polyaniline Nanofiber Composite Films. ACNANO, 4 (2010), 1963–1970

[25] M D Stoller, R S Ruoff. Best practice methods for determining an electrode material's performance for ultracapacitors. Energy Environ. Sci. 3 (2010)1294–1301.

[26] Y Liu, J Zhou, L Chen, P Zhang, W Fu, H Zhao, Y Ma, X Pan, Z Zhang, W Han, E Xie. Highly Flexible Freestanding Porous Carbon Nanofibers for Electrodes Materials of High-Performance All-Carbon Supercapacitors. ACS Appl. Mater. Interfaces. 7 (2015) 23515−23520.

[27] M Endo, T Maeda, T Takeda, Y J. Kim, K. Koshiba, H. Hara and M. S. Dresselhaus, J. Electrochem. Soc., 2001, 148, 910.

[28] Q Guo, X Zhou, X Li, S Chen, A Seema, A Greiner, H Hou. Supercapacitors based on hybrid carbon nanofibers containing multiwalled carbon nanotubes. J. Mater. Chem., 19 (2009), 2810–2816.

[29] W K Chee, H N Lim, I Harrison, K F Chong, Z Zainal, C H Ng , N.M. Huang, Performance of Flexible and Binderless Polypyrrole/Graphene Oxide Zinc Oxide Supercapacitor Electrode in a Symmetrical Two-Electrode Configuration. Electrochimica Acta 157 (2015) 88–94.

[30] R Farma, M Deraman, Awitdrus, I A Talib, R Omar, J G Manjunatha, M M Ishak, N H Basri, B N M Dolah. Physical and Electrochemical Properties of Supercapacitor Electrodes Derived from Carbon Nanotube and Biomass Carbon. *Int. J. Electrochem. Sci*., 8 (2013), 257 – 273.

[31] W Xing, S Z Qiao, R G Ding, F Li, G Q Lu, Z F Yan, H M Cheng. Superior electric double layer capacitors using ordered mesoporous carbons. *Carbon*, 44, (2006), 216–224.

[32] L Li, E Liu, H Shen, Y Yang, Z Huang, X Xiang, Y Tian. Charge storage performance of doped carbons prepare from polyaniline for supercapacitors. J Solid State Electrochem. 15, (2011), 175–182

[33] E G Calvo, F Lufrano, P Staiti, A Brigandì, A Arenillas, J A Menéndez. Optimizing the electrochemical performance of aqueous symmetric supercapacitors based on an activated carbon xerogel, *Journal of Power Sources*, 241 (2013) 776-782.

[34] V Ganesh, S. Pitchumanib, V. Lakshminarayanan. New symmetric and asymmetric supercapacitors based on high surface area porous nickel and activated carbon. Journal of Power Sources. 158 (2006), 1523-1532.
[35] T Thomberg, A Jänes, E Lust. Energy and power performance of electrochemical double-layer capacitors based on molybdenum carbide derived carbon. Electrochimica Acta, 55 (2010), 3138–3143
[36] Li Li Zhang, X S Zhao. Carbon-based materials as supercapacitor electrodes. Chem.

Chapter 6: Carbon nanofibers/Activated carbon composite for supercapacitor applications

6.1. Introduction.

Supercapacitors could be used in conjunction with batteries to satisfy the power requirements in electric vehicle systems by combining the high energy density of batteries with the high power density of supercapacitors. The battery could power the vehicle and electrically charge the supercapacitors during normal operation, while the capacitors could deliver large amounts of power when needed, such as during rapid acceleration. Requirements for such capacitors would include a high energy density, very high recyclability, sustained power densities greater than those of batteries at the same operating voltage, and reliable discharge characteristics. [1] Supercapacitors have been evaluated using three principal types of electrode materials which are high-surface-area activated carbons .[2-4], electroactive polymers [5], and transition metal oxides. [6] The basic structure of a supercapacitor depends on high surface area and porous carbon electrodes. For example, charge separation in the double layer capacitor technology stores energy in the interface between the solid electrode surface and the liquid electrolyte. The ions which moved to form the double-layers are transferred between the electrodes by diffusion through the electrolyte .[7-11] The application of transition metal oxides and electroactive polymers are providing higher energy densities for capacitors but each type has limitations. For the first one, the problem is high cost; and for the second, the problem is stability. [12,13] However, high surface area activated carbons are still the predominant electrode material for supercapacitor applications in the world market. Supercapacitors (i.e., electrochemical capacitors) constitute a class of capacitors that contain an electrolyte solution in place of a dielectric layer. Recently there has been growing interest in the development of robust supercapacitor devices for energy storage and harvesting mainly because of their high capacitance, long cycle life, and superior power and energy density .[2] The Supercapacitor electrode materials should be designed with an appropriate physical structure to have larger surface area for electrolyte wetting and ion

accessibilities. In the case of carbon material electrode, although the pore size is good enough for electrolyte wetting and rapid ionic motion .[1,14], consideration on other factors is also extremely critical. Another important factor in obtaining better electrochemical performance is the electrolyte or solvent .[14] Carbon materials are widely used for supercapacitors electrode because of their low cost ,versatile existing forms, large specific surface area ,good electric conductivity and excellent chemical stability . Supercapacitors use nanoporous electrodes based on carbon materials like AC, CNFS, graphene and CNTs to store large amounts of charge on their high surface areas, and use the ions in electrolytes to carry charge into the pores. Polymers have also been widely studied as electrode materials for supercapacitors because of their high capacitance, easy production, and low cost. However, poor conductivity and weak flexibility of conducting polymers limit them from usage in high performance flexible supercapacitors. [15-19] CNFs have been receiving increasing attention for use it as electrode in supercapacitors because of their high length to diameter ratio and high surface area and excellent electric conductivity . CNFs could be defined as sp2-based linear filaments with diameter of ca. 100 nm that are characterized by flexibility and their aspect ratio (above100) The combination of high specific area, flexibility, and high mechanical strength allow nanofibers to be used in our daily life as well as in fabricating tough composites for vehicles and aerospace. [19-23] Since carbon nanofibers could be considered as the 1-D form of carbon, their structure and properties are closely related to those of other forms of carbon, especially to crystalline three-dimensional graphite, turbostratic carbons, and to their constituent 2-D layers The specific strength (strength/weight) and specific modulus (stiffness/weight) of carbon fiber-reinforced composites demonstrate their importance as engineering materials, due to the high performance of their carbon fiber constituents. The fabrication of CNFs based electrodes for supercapacitors requires a binder to join them together forming a compact layer and adhere homogeneously onto the current collector. CNFs nanoscale tubular morphology can offer a unique combination of low electrical resistivity and high porosity in a readily accessible structure. [19 -21] An AC material is very attractive material for supercapacitors due to high porosity, low cost, abundance, high stability and charge discharge cycling The fabrication of electrodes mixture Of CNFS and AC for supercapacitors requires the addition of binder polyvynilidene fluoride (PVDF)) in propotions that usually vary from 5 to 10 wt. % in order to maintain the integrity of

electrodes. However, binder blocks part of porosity of carbon and additionally causes an increase in electrical resistivity .[24-27] AC electrode produce high specific capacitance because of high specific surface area of the AC electrode . However , a relatively low electronic conductivity of AC. This impact in increase in internal resistance, decrease in energy and power. In previous chapter we found the specific capacitance of AC electrode 334 F/g and CNFS as electrode 52 F/g by using 7 % PVDF as binders. In the other hands the internal resistance for AC electrode 3.7 ohms was higher than CNFs 0.2 ohms.

The question must answer it if we mix AC with CNFs having same concentrations of binder study 7% PVDF can we resolve this problem to increase specific power and specific energy by decreasing internal resistance?

6.2. Experimental procedure.

6.1.1. Electrode preparation and cell fabrication

AC reference 7780 from QimicsDalmau was bought by company, CNFs were provided by GrupoAntolin (GANF). It has a helicoidally graphitic stacked cup structure, there is a presence of Ni (6%), diameter is 20-80 nm, length (MEB) >30um, electric resistivity 10^{-2} Ω·cm. Mixing AC with CNFS which have higher electronic conductivity because Cnfs have lower specisific capacitance than AC in our study mix different concentration of AC with different concentration of CNFs using same concentration of PVDF 7% to find at which concentration of mixture AC and CNFS gives high capacitance and small internal resistance.

Table 6.1. Description of samples at different concentraions.

Activecarbon concentration %	Carbonano fibers%	Binders 7% PVDF	NAME of sample
90	10	7	M1
70	30	7	M2
50	50	7	M3
30	70	7	M4
10	90	7	M5

The mixture prepared from AC and CNFs by using 7% concenteation PVDF was used as binder milling all different samples of AC and CNFS in agate mill resch at fruequncy 500 rmp for1 hours after this mixing AC , CNFS concentration with PVDF polymer by using 15ml acetone in gate mortar, after this sonication all samples for 1 hours then put the samples in oven for 1 hours at 70 C^0 to dry the mixture after this pressing all sample by using 10 ton force all sample . 10 mm area discs were cut, removed the aluminium foil and measured the mass of obtained electrodes and the thickness 0.4 mm, the mass 0.02 g ,as shown in table 6.1.

6.2.1. Surface characterization

The specific surface area and pore size distribution of all sample electrodes were obtained by physical adsorption of gases N_2 at 77K using (Micromeritics TriStar 3000 V6.04 A). All samples were outgassed at 100 °C for 4h prior to the adsorption measurements. The specific surface area (S_{BET}, m^2/g) was determined by multipoint Brunauer-Emmett-Teller (BET) method in the region of the isotherm, which is limited by the range of relative pressure P/P_0 = 0.02–0.2. The total volume of pores (V_{total}, cm^3/g) was calculated by the number of adsorbed nitrogen at $P/P_0 \approx 0.9932$. The volume of micropores and the values of surface areas of micro (S_{micro}, m^2/g) were investigated by the use of t-Plot Harkins and Jura method , the pore size distribution for all sample calculated from adsorption isotherms by the Barrett−Joyner−Halenda (BJH) method and MP method for calculate the pore size distribution .[28]

6.2.2. Morphological characterization

The samples were examined by scanning electron microscopy (SEM). TEM analyses were performed on a Philips JEOL 2011system operated at 300 kV. The samples were suspended into ethanol and dispersed ultrasonically for 15 min. A drop of the suspension was deposited on a copper grid coated with carbon.

6.2.3. Electrochemical characterization

The electrochemical performance of all sample M1, M2, M3, M4 and M5 as symmetric supercapacitor were studied in two electrode Swagelok cell and using a Gamry 600 potentiostat using 6 M KOH solution as an electrolyte.

The electrochemical properties and capacitive behaviour of the supercapacitor electrodes were studied by cyclicvoltammetry (CV), galvanostatic charge–discharge and impedance spectroscopy measurements, using an electrochemical instrument-interface (GAMRY reference 600). All of the measurements were carried out at room temperature.

6.3. Results and discussion

6.3.1. Morphological characterization.

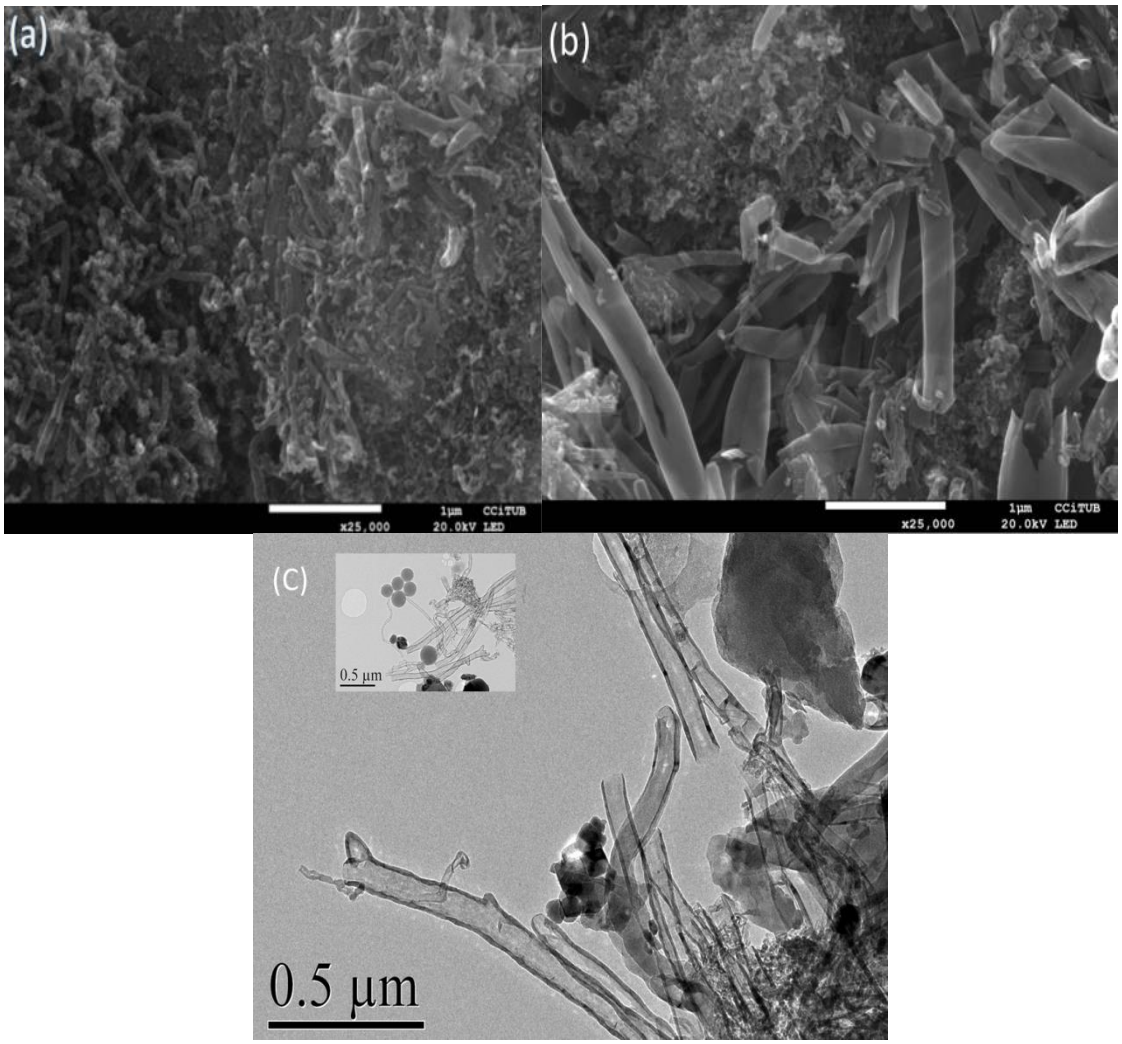

Figure 6.1. (a) SEM image of sample M1 (90% AC / 10 % CNFs). (b) M5 (10 % AC / 90 % CNFs).(C) TEM image of sample M1

The surface morphology of prepared electrodes was investigated by SEM as clear Figure 6.1(a,b) for sample M1 and M5. TEM Figure 6.1(C) for sample M1.

by SEM the cnfs and active carbone are clear can be seen clearly The different structures for both sample M1 and M5 are visible. The typical cnfs structure, cylindrical shape, and crystals structureas , and AC interconnected spheres with homogeneous size and smoother surface as shown in figure 6.1(c)

6.3.2. Pore size distribution of carbon material samples.

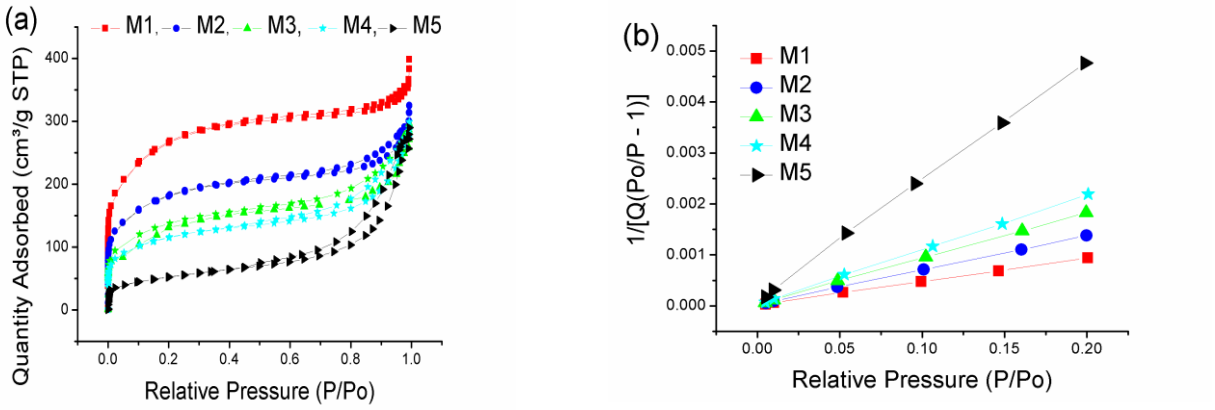

Figure 6.2.(a) Nitrogen adsorption/desorption isotherms for all sample (b) BET surface area(c) pore size

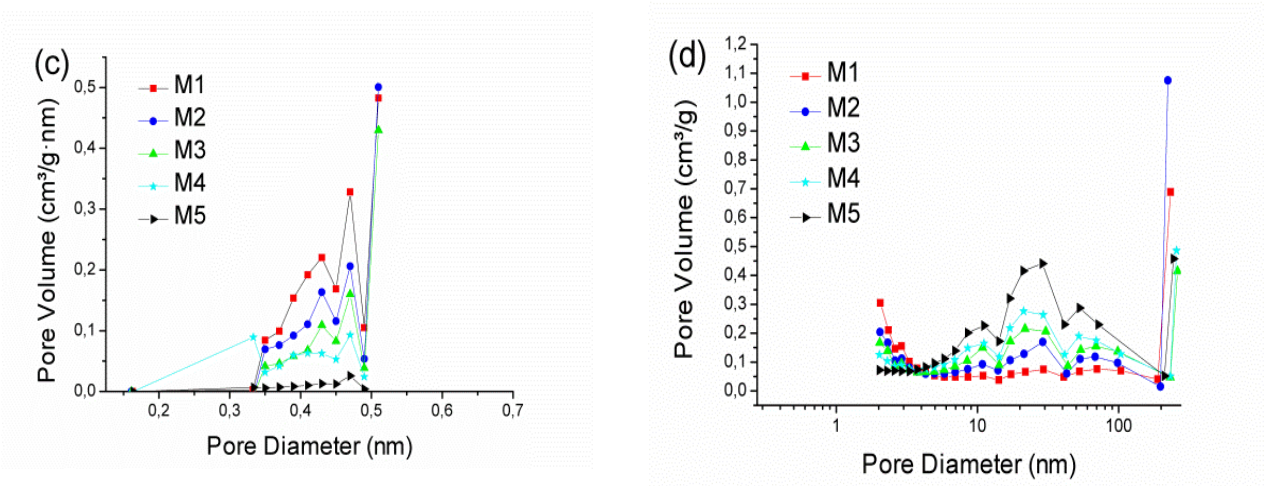

by MP method for all sample (d) pore size by BJH method for all sample .

Considering the strong relationship between the porosity development of active electrode material and the amount of charge accumulated in the electric-double layer, the porous texture of samples was determined by N_2 sorption at 77 K. Figure 6.2(a) shows the nitrogen adsorption–desorption isotherms for mixture AC/CNFS for all sample . The calculated textural parameters are given in Table 6.2. Most of the

adsorption quantity takes place at very low relative pressure (P/P0 < 0.02) and the plateau ranges from low relative pressure to high relative pressure (P/P0 = 0.45), indicating highly microporous carbon. It seems sample M1 have high microporous comparing with other sample as increasing the concentration of CNFs and decreasing concentration of AC the micro volume decreased .

Table 6.2. Physicochemical parameters of AC/CNFS sample

sample	V_{TOTAL} $\frac{cm^3}{g}$	V_{MICRO} $\frac{cm^3}{g}$	V_{MESO} $\frac{cm^3}{g}$	V_{MACRA} $\frac{cm^3}{g}$	$P_{MIC\%}$	$P_{MESO}\%$	$P_{MACRA}\%$	BET_{AREA} $\frac{m^2}{g}$	$Micro_{area}$ $\frac{m^2}{g}$	$Meso_{area}$ $\frac{m^2}{g}$	$macra_{area}$ $\frac{m^2}{g}$	ext_{area} $\frac{m^2}{g}$
M1	0.615	0.414	0.11	0.064	71.8	17.8	10.4	939	894	111	1.74	45
M2	0.502	0.26	0.136	0.106	51.8	27	21.2	640	560	95	2.2	80
M3	0.457	0.16	0.159	0.138	35	34.8	30.2	482	366	96	3.1	116
M4	0.45	0.09	0.2	0.16	20	44.5	35.5	404	257	98	3.87	147
M5	0.44	-	0.28	0.16	-	63.6	36.4	184	-	103.5	4.5	207

Table 6.3. pore size distribution of the active material sample

Sample	Micro pore size nm	Meso pore size nm	Macra pore size nm
M1	**0.5- 0, 45**	**2**	**-**
M2	**0.5-0.45**	**2, 30**	**-**
M3	**0.5-0.45**	**10, 30**	**80**
M4	**-**	**10, 30**	**80**
M5	**-**	**10, 30**	**80**

The total volume of pores (V_{total}, cm^3/g) was calculated by the number of adsorbed nitrogen at P/P0 ≈ 0.9932 for all sample. The volume of micropores, the values of surface

areas of micro (Smicro, m^2/g)and external area were investigated by the use of t-Plot Harkins and Jura method. Meso and macra volume for all sample were investigated by the using BJH Adsorption Cumulative Pore Volume. The pore size distribution for all sample calculated from adsorption isotherms by the Barrett−Joyner−Halenda (BJH) method for meso and macra pore size and MP method for micro pore size .The pore size distribution of the materials is classified into three groups: micro pores (< 2nm), meso pores (2-50 nm) and macro pores (> 50 nm) .[28, 29] According to IUPAC classification the isotherm for sample M1 can be classified as type I isotherm indicate this sample high micropores ,sample M2, M3 M4 presents a small hysteresis loop in middle pressure at point 0.45, which indicates these sample contains mesoporous and macra pores. According to IUPAC classification the isotherm for these sample can be classified as type I due to micro pores ,type II and typte IV indicate to meso and macra pores .

The M5 is the combination of type II and type IV due to meso and macra pores. The total pore volume of all sample are 0.65, 0.502, 0.457 ,0.45 and 0.44 cm^3/g for M1, M2, M3, M4 and M5, respectively at relative pressure (P/P0=0.9932). [28-30] The comparison between the micro, meso, macra volume for all sample table 1 shows the micro volume occupiced 71.8% from total volume for sample M1 and 51.8% , 35% , 20 % for sample M2, M3, M4 respectivily . No micropores appear in sample M5. Meso volume occupied 17.8 %, 27 %, 34.8 %, 44.5 %, 63 % for M1, M2, M3, M4 and M5 and the macra volume occupied 10.4%, 21.2% , 30.2% ,35.5%,36.4% for sample M1, M2, M3, M4 and M5 . The specific surface area were calculated using Brunauer, Emmett and Teller (BET) equation are 939, 640,482, 404, 184 m^2/g for sample M1, M2, M3, M4 and M5. , the micro , meso and macra area represent in table 6.2 in figure 6.2 (c) and (d) the avarge micro pore size for sample M1 ,M2 and M3 in the dominate 0,5 and 0.4 nm with in ultramicropore size and avarge pore size in meso 2 nm for sample M1, 2 and 30 nm for sample M2, 10 and 30 nm for sample M3, M4 and M5. The macra pore size of 80 nm for sample M3, M4 and M5 were obtained.

6.3.2. Electrochemical characterization.

6.3.2.1. Cyclic Voltammetry.

The electrochemical properties and capacitive behavior of the supercapacitor electrodes were studied by cyclicvoltammetry (CV), galvanostatic charge–discharge and impedance spectroscopy measurements, using an electrochemical instrument-interface (GAMRY REFRENCE 600). All of the measurements were carried out at room temperature.

The specific capacitance of the sample M1,M2,M3, M4and M5, cells were determined using cyclic voltammetry because this method provides valuable information on the charge-discharge behaviour of the cells. The specific capacitance per unit mass for one electrode was calculated using equation (1) and equation (2)

$$C_s = 4 * C/m \qquad (6.1)$$

$$C = \frac{q_a + |q_c|}{\Delta V} \qquad (6.2)$$

Where C_s is the specific capacitance in F/g, C is the measured capacitance for the two-electrode cell by equation 2 and m is the total mass of the active material in both electrodes .[31]

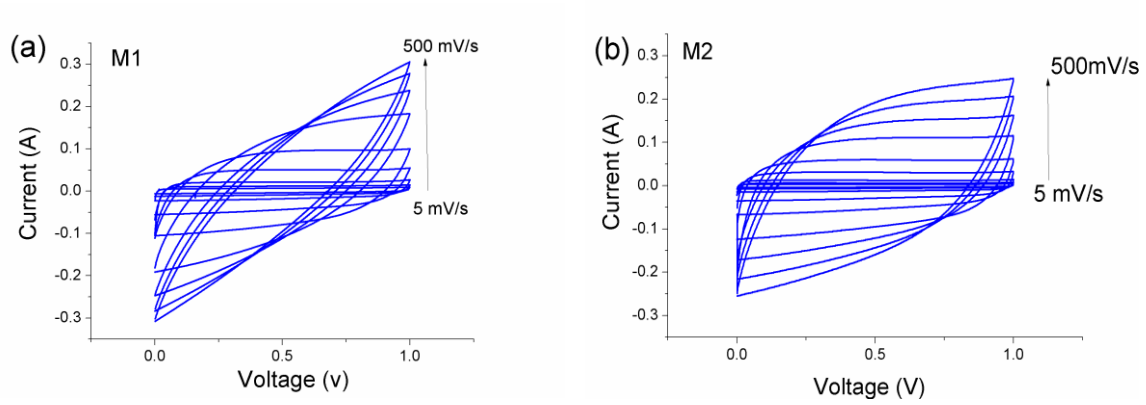

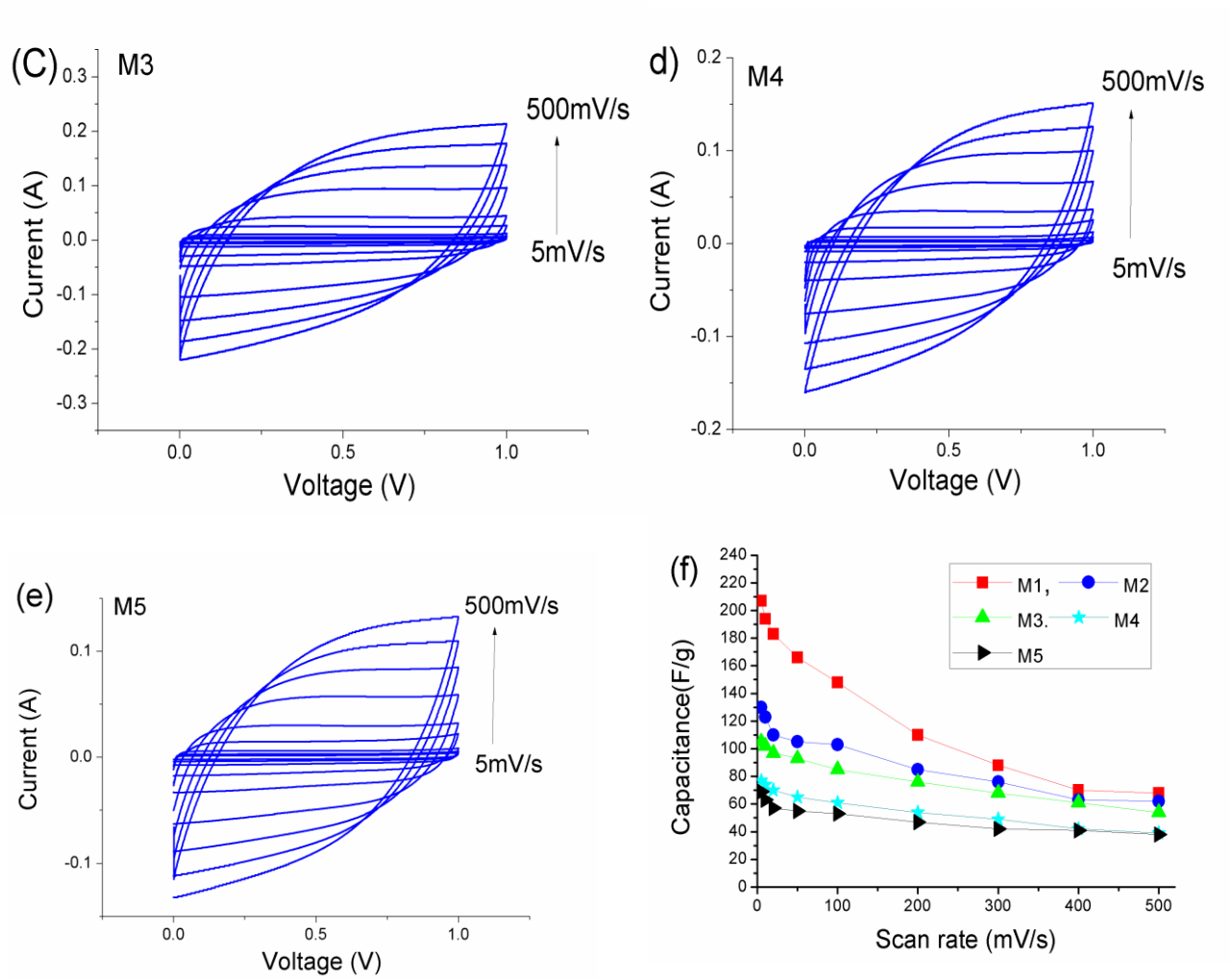

Figure 6.3. (a) M1, (b) M2, (c) M3, (d) M4 and (e) M5, Cyclic voltammograms of at different scan rates, (f) specific capacitance comparison at different scan rates.

Voltammetry testing was carried out at potentials between 0-1 V using 6 M KOH aqueous electrolyte solution , glass fibre used as a separator .The cyclic voltammetry (CV) response of the electrodes were measured at different scan rates varying from 5-500 mV/s are shown in figure 6.3 (a, b, c, d, e).The shape of the voltammograms for all the cells sample is rectangular, without deviation and do not have peak which indicates that the supercapacitive behavior is free from redox reactions or is purely based on the electrostatic mechanism. It also indicate low internal resistance representing a typical voltammogram for electric double-layer capacitance because all curve seem complete box. [31,32] Comparing the voltammograms of the all sample cells, it can be observed that the sample M1 cell has a broader voltammogram area. Furthermore, as the scan rate increased >100 mV/s for M1 and M2, the CV window tended to tilt toward the vertical axis, thereby becoming a quasi-rectangle. This result indicates the dominance of the

double layer formation in the energy storage process at lower scan rates. It is also observed that the CVs for all scan rates in fig 6.3 do not have any redox peaks, indicating that the supercapacitor is free from chemical reactions and/or is purely based on the electrostatic (physical separation) mechanism. These results indicate that the M1 cell has a better cycle reversibility and higher electric double-layer capacitance stability during the charge and discharge processes compared with the other cells. All CVs in Fig 6.3 present complete box this also indicate low ESR is mainly due to the lower contact resistance between the current collector and the electrode, since ESR arises from the resistance of the electrode, electrolyte and the contact resistance between the electrodes and current collectors.Fig 6.4 (a)shows CV curves comparison at scan rate 20 mV/s and scan rate 500mV/s. It can be seen M1 broader area than the other samples. The Csp of all sample electrodes were calculated using the equation (1) from the voltammograms recorded at scan rate range from 5 – 500 mV/s . in Fig 6.4 (b) shows CV curves comparision at scan rate 500mV/s . all samples M1, M2, M3, M4, M5 have the specific capacitance of 207, 130, 105, 77and 66 F/g respectively at scan 5mV/s and at scan 500 mv/s the specific capacitance 65, 62, 54, 39 and 33 F/g. Figure 3(f) shows the Csp values with different scan rates for all the sample cells. All cells show a common trend of decreasing Csp values against an increasing scan rate as shown in Table 6.4

Table 6.4. Specific capacitance of different sample from 5 mv/s to 500 mv/s with decrease rate from 5 mv/s to 500mv/s

	Scan rate mv/s									
Sample	5	10	20	50	100	200	300	400	500	Decrease Rate of Csp f/g
M1	207	194	183	166	148	110	88	70	68	68.6%
M2	130	123	115	105	103	85	76	63	62	52%
M3	105	102	97	93	85	76	68	61	54	48%
M4	77	74	70	65	61	54	49	42	39	49%

M5	69	63	57	55	53	47	42	41	38	52%

It is well known that for very low scan rates, the Csp values are higher because the ions have a much longer time to penetrate and reside in all the available electrode pores and form electric double layers, which are needed to generate higher capacitance. [33] Despite this common trend, the M1 cell displays higher Csp values throughout the whole scan region, clearly indicating its superiority over the other sample cell. These results indicate at sample M1 have high specific capacitance due to high surface area. Sample M1, the specific capacitance is high 207 F/g because the quantity of AC in mixture is high comparing with other sample and these gave high capacitance 207 F/g. On the other hand in previous chapter,AC alone gives 334 F/g is related to the BET for active carbon 1040 m^2/g and for sample M1 939 m^2/g but the internal resistance for sample one much too smaller than active carbon which related to CNFS which owns high conductivity and could be the pores size of mixture M1 is less than the pores size of AC alone. This decreasing the internal resistance this make pores size of mixture accessible ions and increasing the speed and mobility of ions from logic comparing specific capacitance of sample M5 (10% AC 90% CNFs) is 69 F/g. Its means that when the quantity of active carbon decrease the specific capacitance decrease from 207 F/g for sample M1 to 69 F/g for M5 at scan rate 5mV/s.

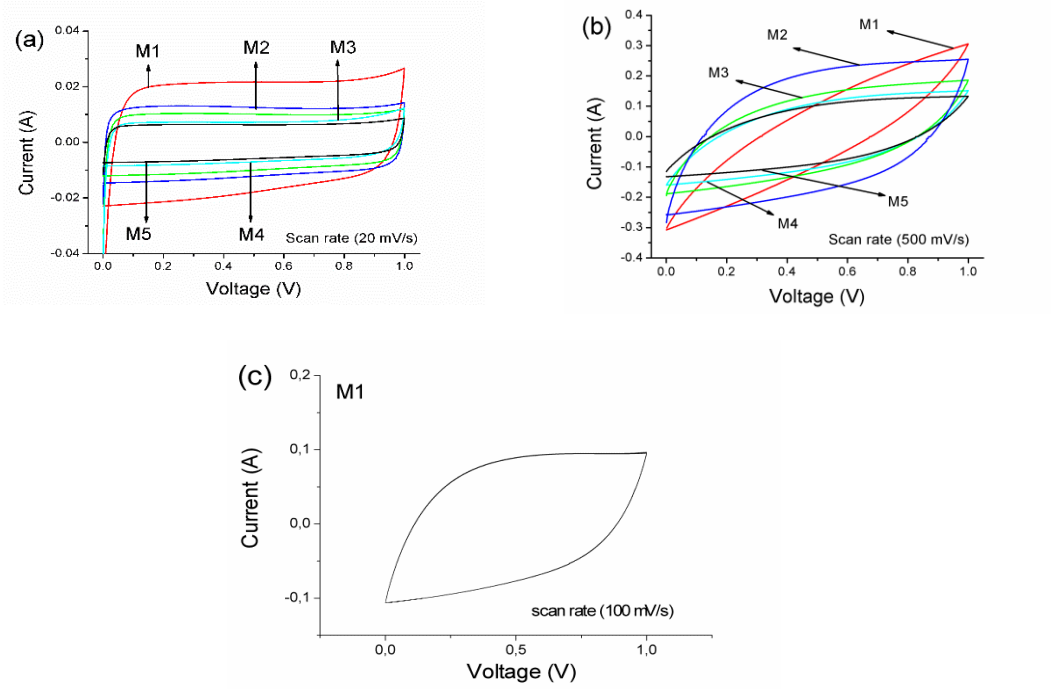

Figure 6.4. Cyclic voltammogram comparison at scan rates (a) 20 mV/s, (b) 500 mV/s. (c) 100 CV cycles for M1 at scan rate 100 mV/s.

For sample M5 this indicates surface area for this sample decrease from 939 m^2/g to184 m^2/g for sample M1 to sample M5. At all sample it was found that the capacitances decreased rate about 68.6 %, 52 %, 48 %, 49 % and 52 % for M1, M2, M3 M4 and M5 respectively from scan rate 5 mV/s to 500 mV/s as shown in table 6.4. Excellent charge propagation in an electrical double layer was observed for all samples. [33] This result confirms that how the effect of CNFs in mixture CNFs exhibit very good electrical conductivity properties. The cycling stability test for up to 100 cycles at a high scan rate 100 mV/s for sample M1. The 100 CVs are overlapping each other, which mean stable capacitance behaviour as shown in figure 6.4 (c).

6.3.2.2. Galvanostatic charge discharge (GCD)

The GCD curves for all the samples recorded at potential range from 0-1 V at a constant current density of 1 A/g as shown Fig 6.5 (a), All samples show a similar symmetrical triangular curve with a nearly linear variation of voltage as a function of time during charge and discharge. [41,42] This type of curve is typical for carbon based supercapacitors, and the data shows that all the 5 samples have a good supercapacitive

performance. The curves of M1 shows higher charge and discharge time this indicates that higher number of electrons and electrolyte ions are sharing in charge discharge processes compared with other sample. Fig 6.5(b) shows GCD curves as a function of current density for sample M1. It can be seen that the charging and discharging process are nearly symmetric at all currents which indicate excellent electrochemical reversibility of the electrode. The ESR value is calculated from this voltage drop using the equation ESR = iRdrop/2i . [34-36] The ESR values for the M1, M2, M3, M4 and M5 samples are 1.1, 0.95, 0.92, 0.98 and 0.75 ohm, respectively this indicate that ESR of all samples are approximation with small differences. The higher ESR related to the sample M1 is due to high quantity of AC is this sample comparing with other samples. This confirms as increase in the CNFs concentration in mixture of these sample ESR decrease due to effectivity of CNFs in sample. Fig 6.5(c) presents comparison of specific capacitance at different current densities for all samples. The discharge capacitance (C) is estimated from the slope (*dV/dt*) of the linear portion of the discharge curve using equation 6.3.

$$C_s = \left(\frac{2I}{(dV/dt).m}\right) \qquad (6.3)$$

Where C_s is the specific capacitance in F/g, ΔV is the voltage difference during the discharge curve in V, I is the current in A and Δt the discharge time in s, m is the mass of electrode.

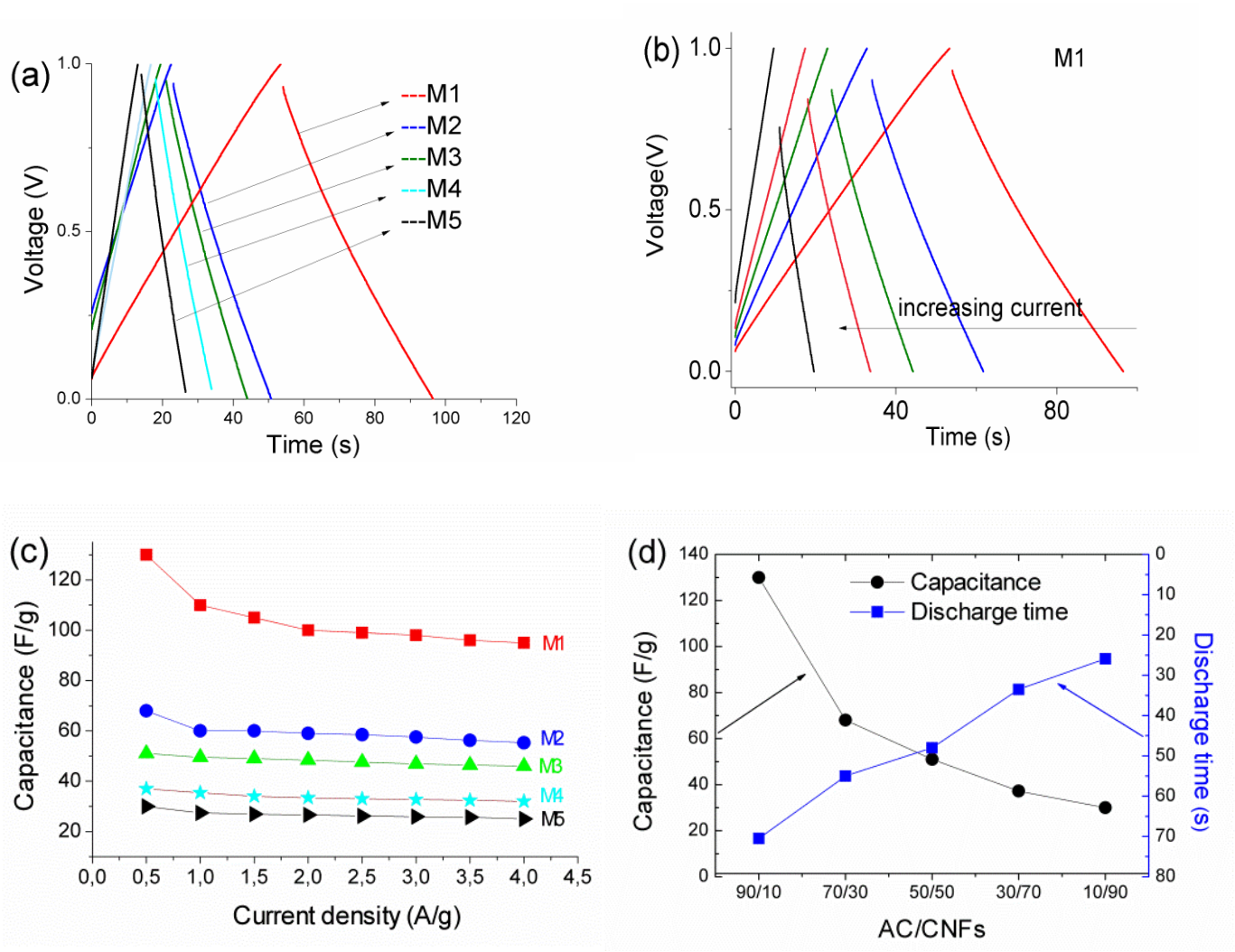

Figure 6.5. (a) Charge discharge comparison at current density 1 A/g, (b) Charge discharge comparison for M1 at current densities (1, 1.5, 2, 2.5 and 4 A/g), (c) Specific capacitance comparison at different current densities, (d) relationship between specific capacitance, discharge time at different concentration of AC/CNFs.

The specific capacitance for Sample M1 130 F/g at current density 0.5 A/g decreases to 95 F/g at current density 4 A/g. As expected, the specific capacitance decrease from 68 to 55 F for sample M2 electrodes, from 51 to 46 F/g for sample M3, M4 from 37.2 to 32 F/g and sample M5 from 30 to 25,6. However, the most interesting feature of these results concerns the high energy storage capacitance achieved in sample M1. The decreases in specific capacitance with the increase of current density is very common for supercapacitors and is mainly caused by the diffusion limitation of electrolyte ions in the

microspores of the electrode. [37,38] The similar trend of decrease in capacitance with increase in current was observed for all samples. Fig 6.5 (d) shows the relation between specific capacitance, AC %/CNFs % concentration with discharge time for all sample at current density 0.5 A/g. As seen for sample M1 the discharge time 70.3 s at the value the specific capacitance 130 F/g on the other hand when the decrease the AC in mixture as see in sample M5 the discharge time decrease to 25.9 s and specific capacitance become 30 F/g. this indicate that at sample M1 high surface area and high microporsity comparing with other sample as shown in adesorpistion /desorption of BET, its increase the number of ions enter to the pores structure and the ions free to enter deep inside pores this take more time than with surface area become small as sample M5. This indicate the ions didn't enter deep inside pores and this mean the path of ions travel is small .

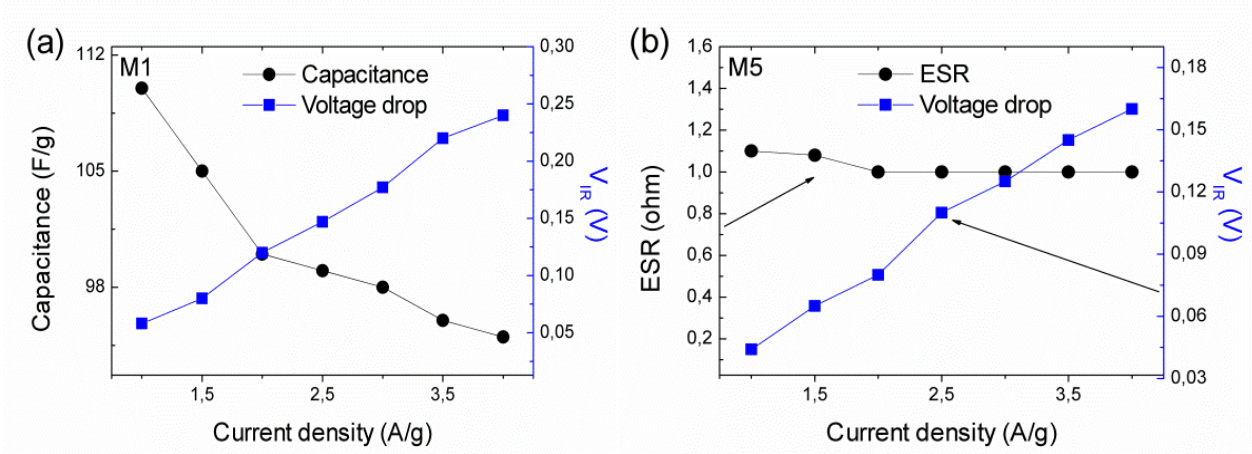

Figure 6.6 (a) The relationship between specific capacitance, voltage drop at different current densities for M1, (b) the relationship between ESR, voltage drop and different current densities for M5.

Fig 6.6 (a) shows the relation between specific capacitance and voltage drop for M1 at current densities from 1 to 4 A/g. When the current density is 1A/g the voltage drop is 0.058 V and the specific capacitace is 110 F/g. As the current density increase to 4 A/g the drop voltage increase to 0.24 V and the capacitance decreased to 95 F/g. This indicate as current increase the ions enter from electrolyte to pores size travel shorter distance in side, the conclusion is decrease the specific capacitance. Fig 6.6(b) confirm this result for sample M5 when the current density 1A/g the voltage drop 0.044 V, ESR 1.1 OHM. AS current density increase to 4 A/g the voltage drop increasing to 0.16 V and ESR to 1

OHMs. This indicates due to the higher concentration of CNFs in M5 provides higher conductivity.

Specific energy and specific power are important parameters to analyse the electrochemical performance of energy storage devices. The specific power, P and specific energy, E, delivered upon discharge were estimated by equation (6.4) and (6.5) .[39]

$$P = {}^{Vi}/_{m} \qquad (6.4)$$

$$E = {}^{Vit}/_{m} \qquad (6.5)$$

The Ragone plot Figure 6.7(a) The sample M1 shows the specific energy of 7.1 Wh/kg and specific power of 3040 W/kg at current density 4 A/g. When the current decrease to 1 A/g the specific energy increase 10.8 Wh/kg and specific power decrease to 925 W/kg and for sample M5 at current density 1 A/g the specific energy 3.2 Wh/kg and decrease to 2.3Wh/kg ,at current density 4 A/g specific power 960 W/kg increase to 3320W/kg. The higher specific power of M5 in comparison to M1 is due to it lower ESR values.

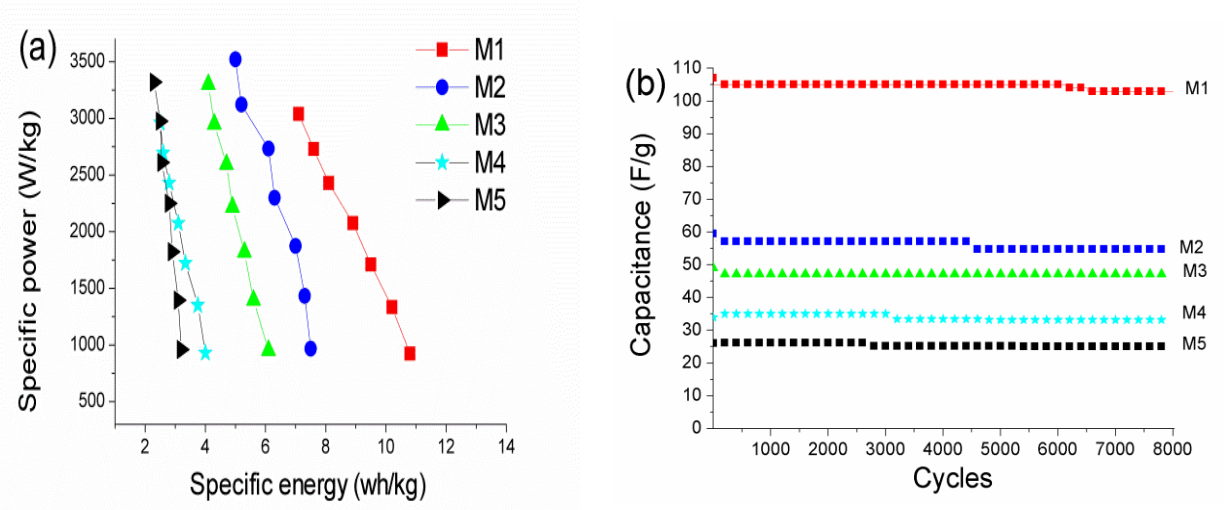

These results show excellent electrochemical properties of high energy density and power output, therefore very promising for application in the scenarios where high power output as well as high energy capacity is required. [35]

Figure 6.7. (a) Ragone plot, (b) long term cycling stability at current density (1.5 A/g).

6.3.2.3. Electrochemical Impedance Spectroscopy

To study the resistance of the electrochemical sample prepared, impedance spectroscopy measurements were carried out at sinusoidal signal of 100 mV over frequency range from 100 kHz and 0.1 Hz. Figure aa shows the Nyquist plot of all the sample , The Nyquist plots consist of a high-frequency intercept on the real Z_{Re} axis, a semicircle in the high-to-medium-frequency region, and a straight line at the very low-frequency region. In the mid-frequency range, the cell behaves as a combination of resistor and capacitor, where the electrode porosity and thickness play a vital role in the determination of capacitance values. This is also reflected in the low ESR values obtained for all the samples, low ESR values make these mixture materials very attractive for the application under study .[40] The impedance of a supercapacitor is associated with a double-layer capacitance C_{dl}, pseudo capacitance C_p, Faradaic charge-transfer resistance R_f, the sum of the electrolyte resistance, the electrode resistance, the contact resistance between the electrode and the current collector Rs .[40,41] in the middle of frequency at combination region between capacitors and resistors the (straight line with a slope of approximately 45°) this indicate the capacitive behaviors of the ions penetrating into the electrode pores. [2,40]

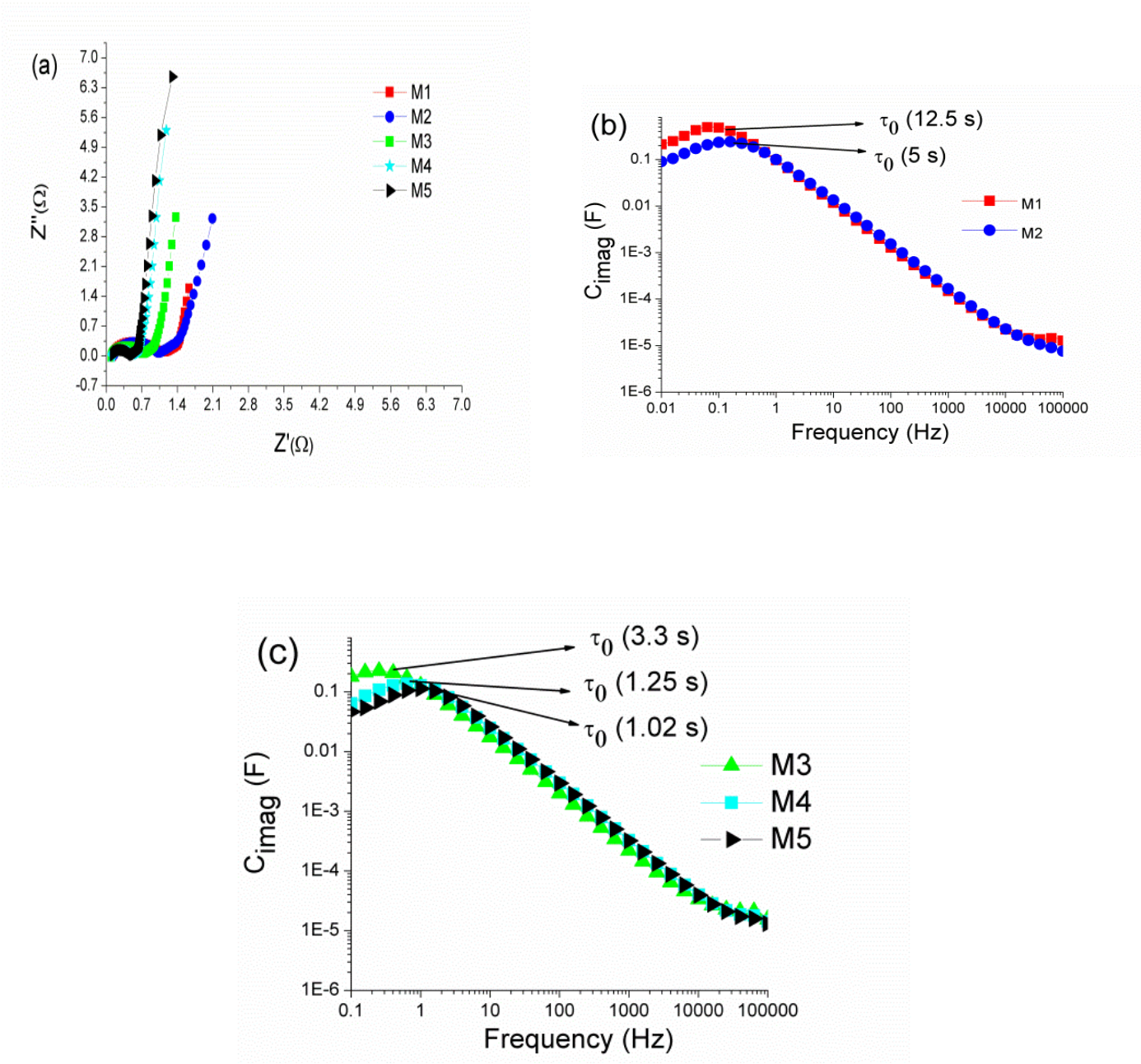

Figure 6.8. (a) Nyquist plot, (b, c) Imaginary part of capacitance as a function of frequency.

The length, slope and position of this segment appear to be affected by changes the quantity of CNFS concentration in mixture as seen from fig 6.8a as concentration of CNFs increase in sample the length of line increase and the semicircle become small this indicates CNFs excellent and high conductivity. A steep slope corresponding to electrodes that efficiently allow ions to penetrate pores. [40]. As seen from fig 6.8a the straight line increasing sharply at low frequency region is due to dominance of capacitive behavior this indicate from the formation of ionic and electronic charges of the double

layer system at micropore surfaces at this frequency the ions are easy to diffuse inside the porosity structure of electrode.[2,42]

In the range of medium-high frequencies is small semicircle can be observed for all samples which indicates that the materials have a really low intrinsic resistance. Additionally, the Warburg-like behaviour of the spectra indicates that there is a good electrolyte penetration in the porous structure of the bulk electrode .[2,42] The solution resistance R_s for all the samples was about 0.16 ohm. The charge transfer resistance R_f are (0.93, 0.84, 0.61, 0.43 and 0.37 ohms) for a samples M1, M2, M3, M4 and M5 respectively. The change R_f tells with the increase in CNFs concentration the charge transfer resistance of the electrodes decreased because of high conductivity of CNFs. The equivalent series resistance (ESR) contacts resistance are (1.09, 1, 0.7, 0.54 and 0.53 ohms) for samples M1, M2, M3, M4 and M5 respectively. The ESR values decreased as well with increase in CNFs concentrations.

The relaxation time constant, τ_0, defines the time required to deliver the stored charge effectively as seen from Figure 3(d) .[43,44] Fig 6.8(b, c) show the relation of imaginary part of capacitance as a function of frequncey. This gives information about knee frequncey and relaxation time constant τ_0. The knee frequency appears at 0.08, 0.2, 0.3, 0.8 and 0.98 HZ for sample M1, M2, M3, M4 and M5 respectivly. The knee frequency separates the capacitive behavior of the capacitor from the resistive one.[28] The time constant τ_0 corresponds to phase angle 45° represents the transition of electrochemical capacitor from a purely resistive to purely capacitive behaviour. It is well known that higher power delivery corresponds to lower τ_0 values. For a frequency, $f > 1/\tau_0$, it acts as a pure resistor and for $f < 1/\tau_0$, it behaves as a pure capacitor. [43,44] The phase angle 45 ° was found for M1, M2, M3, M4 and M5 at frequency 0.08, 0.2, 0.3, 0.8 and 0.98 Hz respectively. This gives relaxation time12.5, 5, 3.3, 1.2 and 1 for M1, M2, M3, M4 and M5 respectively. As the relaxation time becomes smaller the response of the electrode improves as a supercapcitor. [43,44]

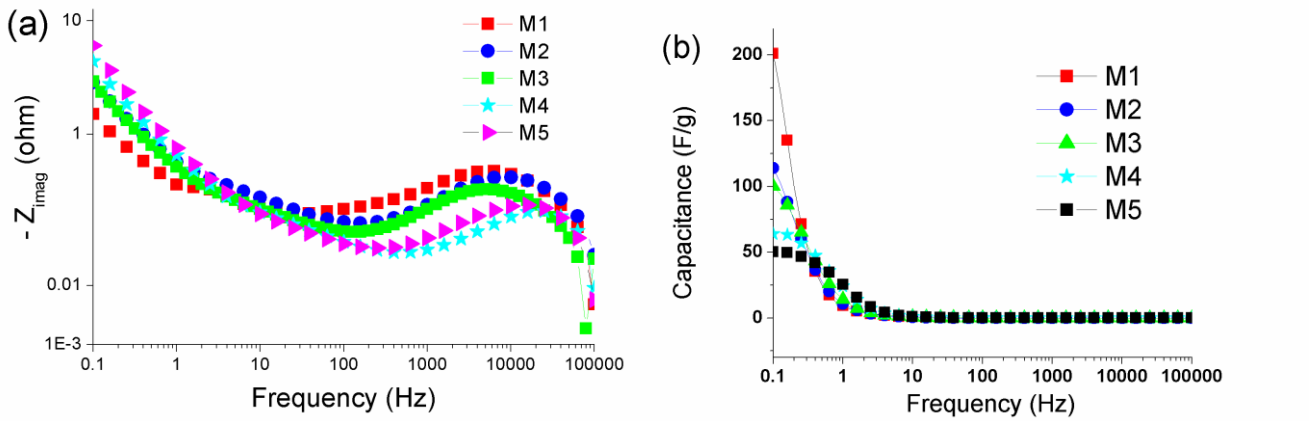

Figure 6.9. (a) Imaginary part of impedance as a function of frequency, (b) Specific capacitance as a function of frequency.

Specific capacitance of supercapacitor was calculated by the imaginary component of impedance by and following equation 6. [45]

$$C_s = 4\left(-(1/2\pi f z'' m)\right) \qquad (6.4)$$

Where f is lower frequency 0.1 Hz''and z'' is the imaginary component of impedance and m, the mass of each sample calculated for one electrode. The specific capacitances according to equation 6.4 are 201, 114, 100, 64 and 50 F/g for sample M1, M2, M3, M4 and M5 respectively. It seems is that almost similar result obtained by CV method. Figure 6.9(b) shows the relation between specific capacitance and frequency at frequency 0.1 Hz specific capacitance is 201,114,100, 64 and 50 F/g for all sample respectively. When the frequency increase the specific capacitance decrease because as frequency in increase the supercapacitors starts works as resistors at high frequency.

Fig 6.10 (a) shows the relation between specific capacitance, (AC (%) / CNFS (%)) and ESR for all samples. Sample M1 record 207 F/g capacitance at ESR 1.09 ohm. From figure can be seen when increase the CNFs % in mixture the surface area decrease and micro porosity decrease and conductivity increasing during the effect of CNFs

concentration in mixture which decrease the ESR value for to 0.37 ohm for sample M5

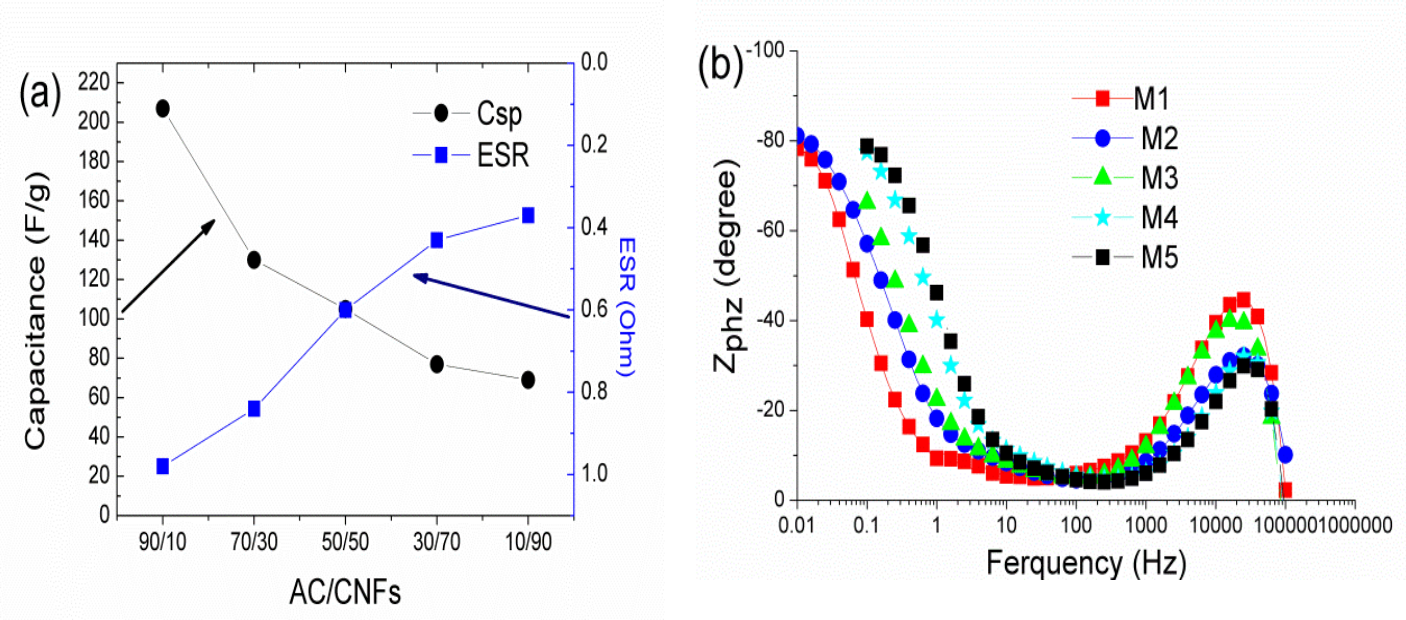

with decrease in the specific capacitance 69 F/g as well.

Figure 6.10. (a) Relation between concentrations, capacitance with ESR, (b) Bode plot.

Fig 6.10(b) represents the variation of phase angle as a function of frequency, which is known as Bode plot. The phase angles are found to be -78°, -81,-66°,-77° and 78° at low frequency 0.01Hz for sample (M1, M2) and at 0.1 Hz for (M3, M4 and M5). In general, phase angle approach to -90° confirms better capacitive performance and rapid charge discharge process. [46]

6.4. Correlation between BET, porosity sample and specific capacitance

From the results, it was found that the specific capacitance of the Sample M1 is 207 F/g and ESR 0.95 ohms higher than the other samples due to higher percentage of AC. High capacitance of carbon materials is related to several important factors such as high BET surface area and micro porous structure. M1 samples contain highest specific surface area (939 m^2/g) and M5 lowest specific surface area (184 m^2/g). According to the following equation (6.5). [47]

$$C = (\epsilon A)/d \qquad (6.5\ )$$

Specific capacitance is increased with increase in surface area. From BET analysis, it was found sample M1 has high micro pores comparing with other samples. The micro volume occupied 71.8 %. As increase the CNFs concentration and decrease in AC concentration from sample M1 to M5 the microporesity decrease and micro volume goes down to 0%. The decrease in micro pores volume means the presence of meso % and macra % volume increase. BET results tells sample M1 has narrow pore size of around 0.45 nm, but from sample M2 to M5 the pores size become broader (meso and macra) around 10, 30 and 80 nm. According to the following equation 6.6. [47]

$$\tau = L^2/D \qquad (6.6)$$

Where L refers to the ion transport length and D refers to the ion transport coefficient. The ions enter fast inside the micropores, but as the size of pores increase the external area also increase. Due to this fact the ions accumulate outside of the pores, hence results in the decrease in the capacitance. From BET results, it was found the external area increase from (45 to 207 m^2/g) for sample M1 to M5. After previous analysis, the important question arise why internal resistance decrease with increase in CNFs concentration from sample M1 to M5. As we Know CNFs lone have very high conductivity and it found in previous study. For CNFs the ESR value was around 0.28 ohms and for AC 3.7 ohms. For sample M1 the ESR is 0.95 ohms very small in comparing with AC alone because the low mixing if low number of CNFs in AC.

References

[1] Obreja V, on the performance of supercapacitors with electrodes based on carbon nanotubes and carbon activated material-A review. Physica E. 40, 2596-2605 (2008).

[2] Conway BE. Electrochemical Supercapacitors, Scientific Fundamentals and Technological Applications. New York: Kluwer Academic/Plenum Publishers; 1999:11-31.

[3] E. Raymundo-Piñero, K. Kierzek, J. Machnikowski, F. Béguin, Carbon 44 (2006) 2498e2507.

[4] M. Inagaki, H. Konno, O. Tanaike, J. Power Sources 195 (2010) 7880e7903

[5] M.Wu, Q. Zha, J. Qiu, Y. Guo, H. Shang, A. Yuan, Preparation and characterization of porous carbons from PAN-based preoxidized cloth by KOH activation Carbon 42 (2004) 205.

[6] M.S.A. Rahaman, A.F. Ismail, A. Mustafa, Polyacrylonitrile/acrylamidebased carbon fibers prepared using solvent-free coagulationPolym. Degrad. Stab. 92 (2007) 1421.

[7] A.G. Pandolfo, A.F. Hollenkamp, J. Power Sources 157 (2006) 11e27.

[8] R. Kötz, M. Carlen, Electrochim. Acta 45 (2000) 2483e2498.

[9] E. Raymundo-Piñero, F. Leroux, F. Béguin, Adv. Mater. 18 (2006) 1877e1882

[10].Lokhande,C.D., Dubal,D.P., Joo,O.-S., *J. Current Applied Physics* Vol. 11 (2011) pp. 255-70.

[11].Zhang,Y., Feng,H., Wu,X., Wang,L., Zhang,A., Xia,T., Dong,H., Li,X., Zhang,L.,*Int. J. Hydrogen Energy* Vol.34 (2009) pp. 4889-99.

[12] L. G. Gouy , *J. Phys. Theor. Appl.* 1910 , *9* , 457 .

[13] O. Stern , *Zeitschrift für Elektrochemie and Angewandte Physikalische Chemie* 1924 , *30* , 508

[14] F.C.Wu, R.L. Tseng, C.C. Hu, C.C.Wang, the capacitive characteristics of activated carbons—comparisons of the activation methods on the pore structure and effects of the pore structure and electrolyte on the capacitive performance, J. Power Sources 159 (2006) 1532.

[15] E Frackowiak, Carbon materials for supercapacitor application, *Phys. Chem. Chem. Phys*, 2007, 9, 1774-1785.

[16] R Amade, E Jover, B Caglar, T Mutlu, E Bertran, Optimization of MnO_2/vertically aligned carbon nanotube composite for supercapacitor application, *J. Power Sources*, 2011, 196, 5779–5783.

[17] S Hussain, R Amade, E Jover, E Bertran, Functionalization of carbon nanotubes by water plasma, *Nanotechnology*, 2012, 23, 385604.

[18] S Hussain, R Amade, E Jover, E Bertran, Nitrogen plasma functionalization of carbon nanotubes for supercapacitor applications, *J. Mater. Sci*, 2013, 48, 7620–7628.

[19] A G Pandolfo , A F Hollenkamp. Carbon properties and their role in supercapacitors. *Journal of Power Sources*, 2006, 157, 11–27.

[20] J.B. Donnet, R.C. Bansal: *Carbon Fibers* (Marcel Dekker, New York 1984)

[21] L.H. Peebles: *Carbon Fibers* (CRC, Boca Raton 1994)

[22] D.D.L. Chung: *Carbon Fiber Composites* (Butterworth Heinemann, Boston 1994)

[23] M.S. Dresselhaus, G. Dresselhaus, K. Sugihara,I.L. Spain, H.A. Goldberg: *Graphite Fiber and Filaments* (Springer, Berlin Heidelberg 1988)

[24] V Ruiza, C Blanco, R Santamaría, J M Ramos-Fernández, M Martínez-Escandell, A Sepúlveda-Escribano, F Rodríguez-Reinoso. An activated carbon monolith as an electrode material for supercapacitors. *Carbon*, 2009, 47, 195–200.

[25] Q Abbas, D Pajak, E Frackowiak, F Béguin, Effect of binder on the performance of carbon/carbon symmetriccapacitors in salt aqueous electrolyte. *Electrochimica Acta*, 2014, 140, 132–138

[26] V Ruiz, C Blanco, M Granda, R Menéndez, R Santamaría, Influence of electrode preparation on the electrochemical behaviour of carbon-based supercapacitors. *J Applied Electrochem*, 2007, 37, 717–721.

[27] To-Chi Weng and HsishengTeng, Characterization of High Porosity Carbon Electrodes Derived from Mesophase Pitch for Electric Double-Layer Capacitors, *Journal of the Electrochemical Society*, 2001, 148, A368–A373.

[28] Gregg S J, Sing K S W. Adsorption, Surface Area and Porosity, 2nd ed.; Academic Press: New York, 1982; pp 4, 287.

[29] Huang J, Sumpter B G, Meunier V. A Universal Model for Nanoporous Carbon Supercapacitors Applicable to Diverse Pore Regimes. 2008 Chemistry. 14 6614–6626.

[30] John Chmiola, Pore-size ion-size correlations for carbon supercapacitors, Doctor of Philosophy February 2009, Drexel University

[31]. A.I. Inamdar, Y.S. Kim, S.M. Pawar, J.H. Kim, H. Im, H. Kim, J. Power Sources, 196 (2011) 2393.

[32] Y Liu, J Zhou, L Chen, P Zhang, W Fu, H Zhao, Y Ma, X Pan, Z Zhang, W Han, E Xie. Highly Flexible Freestanding Porous Carbon Nanofibers for Electrodes Materials of High-Performance All-Carbon Supercapacitors.

[33]. J. Yan, T. Wei, B. Shao, Z. Fan, W. Qian, M. Zhang, F. Wei, Carbon, 48 (2010) 487.

[34] Farma R, Physical and Electrochemical Properties of Supercapacitor Electrodes Derived from Carbon Nanotube and Biomass Carbon, Int. J. Electrochem. Sci., 8 (2013) 257 - 273

[35] M Endo, T Maeda, T Takeda, Y J. Kim, K. Koshiba, H. Hara and M. S. Dresselhaus, J. Electrochem. Soc., 2001, 148, 910.

[36] Q Guo, X Zhou, X Li, S Chen, A Seema, A Greiner, H Hou. Supercapacitors based on hybrid carbon nanofibers containing multiwalled carbon nanotubes. J. Mater. Chem., 19 (2009), 2810–2816.

[37]. W.C. Chen, T.C. Wen and H. Teng, *Electrochim. Acta*, 48 (2003) 641.

[38] J. Gamby, P.L. Taberna, P. Simon, J.F. Fauvarque and M. Chesneau, *J. Power Sources*, 101 (2001) 109

[39] Farma R, Deraman M, Awitdrus, Talib I A, Omar R, Manjunatha J G, Ishak M M, Basri N H, Dolah B N M. Physical and electrochemical properties of supercapacitor electrodes derived from carbon nanotube and biomass carbon. 2013 Int. J. Electrochem. Sci. 8 257–273

[40] H Xia, Y Wang, J Lin, L Lu. Hydrothermal synthesis of MnO_2/CNT nanocomposite with a CNT core/porous MnO_2 sheath hierarchy architecture for supercapacitors. Nanoscale Research Letters, 2012, 7, 33.

[41] C Y Lee, H M Tsai, H J Chuang, S Y Li, P Lin, T Y Tseng. Characteristics and Electrochemical Performance of Supercapacitors with Manganese Oxide-Carbon NanotubeNanocomposite Electrodes. *Journal of The Electrochemical Society*., 2005, 152, A716-A720.

[42] F Lufrano, P Staiti, M Minutoli. Influence of Nafion Content in Electrodes on Performanceof Carbon Supercapacitors. *Journal of The Electrochemical Society*, 2004, 151, A64-A68.
[43] V Ganesh, S. Pitchumanib, V. Lakshminarayanan. New symmetric and asymmetric supercapacitors based on high surface area porous nickel and activated carbon. Journal of Power Sources. 158 (2006), 1523-1532.
[44] T Thomberg, A Jänes, E Lust. Energy and power performance of electrochemical double-layer capacitors based on molybdenum carbide derived carbon. Electrochimica Acta, 55 (2010), 3138–3143
[45] E G Calvo, F Lufrano, P Staiti, A Brigandì, A Arenillas, J A Menéndez. Optimizing the electrochemical performance of aqueous symmetric supercapacitors based on an activated carbon xerogel, *Journal of Power Sources*, 2013, 241, 776-782.

[46] A Ghosh, Y H Lee, Carbon-Based Electrochemical Capacitors, ChemSusChem, 2012 5 480-99.
[47] Li Li Zhang, X S Zhao. Carbon-based materials as supercapacitor electrodes. Chem. Soc. Rev., 38, (2009), 2520–2531.

Chapter 7 Conclusion and future work

The EDLC technology is very prospective. In a short time supercapacitors can become viable alternative to batteries. New ways how supercapacitors could be used effectively can also be discovered. Because of the advantages of charging efficiency, long lifetime, fast response, and wide operating temperature range, it is possible to apply EDLCs to any application that requires energy storage. However, the limitations of current technology must be taken into account. Commercial EDLC devices have been available for many years and they are sill improving. As devices of higher energy density and higher power become available on the market, more new applications are found and demand will rise dramatically. Increased levels of interest in the technology then lead to increased development and research efforts, which will result in better devices being manufactured. As manufacturing quantities and demand both increase costs will go down. In this thesis, typical carbon materials have been intensively studied for energy storage applications: cnfs , cnfs /mno$_2$, AC ,CNFS /PVDF POLYEMER AC/CNFS Their electrochemical performances in supercapacitors evaluated individually as detailed in Chapter 3 through to 6

In third chapter, we report a comprehensive experimental study about the use of flexible tape casting of dense carbon nanofiber (CNFs) alone and in hybrid structure with MnO_2 for supercapacitor applications. Different electrolyte concentrations of potassium hydroxide (KOH) were tested and found mild concentrated electrolyte like 9 M KOH provides higher specific capacitance 38 F/g at a scan rate of 5 mV/s. Electrochemical impedance spectroscopy (EIS) measurements explain solution and charge transfer resistance is higher for 3 M KOH and lower for 6 M KOH concentrations. Afterwards a novel, fast and simple method was adopted to achieve a hybrid nanostructure of CNFs/MnO_2 with various $KMnO_4$ ratios. The hybrid supercapacitor having loading mass of 0.0003 g MnO_2 as a thin film delivers a highest specific capacitance of 812 F/g at a scan rate 5 mV/s. Charge/discharge cycling stability at current density of 7.9 A/g

demonstrates larger specific capacitance 606 F/g and stability. Furthermore the hybrid supercapacitor can deliver specific energy (72.4 Wh/kg) at specific power (3.44 kW/kg).

In fourth chapter Symmetric supercapacitors are fabricated by activated carbon (AC) and carbon nanofibers using (Polyvinylidene fluoride) PVDF polymer in similar proportions of 7 wt. % in an aqueous electrolyte. Electrodes are assembled in the cell without current collector. AC carbon provides specific capacitance of 334 F/g and CNFs of 52 F/g at scan rate 5 mV/s. The results indicate that the superior conductivity of CNFs delivers higher specific capacitance and retention up to very fast scan rate of 500 mVs^{-1} in contrast to AC. The measured equivalent series resistance (ESR) shows very small value of (0.28 Ω) for CNFs in comparison to AC (3.72 Ω). CNFs deliver higher specific power (1860 W k/g) whereas AC gives higher specific energy (18.1 Wh k/g). Both CNFs and AC symmetric supercapacitor exhibits an excellent charge discharge stability up to 2500 cycles.

In fivith chapter discussed the impact binder polyvynilidene fluoride (PVDF) concentration (5, 10 and 20 wt%) and pressure force (3, 7, 14 and 20 ton) for the fabrication of electrodes based on Carbon nanofibers (CNFs) for supercapcitors. The surface area, pore size distribution and morphology were characterized by Brunauer–Emmett–Teller (BET) method, SEM and TEM. The specific surface area decreased from 103 to 71 m^2/g and pore volume from 0.41 to 0.35 cm^3/g with increase in PVDF concentration from 5 to 20 wt% at 7 ton pressure force. The assembled electrodes were tested with two electrode system in aqueous electrode. The specific capacitance was 80 F/g for lowest concentration of PVDF (5 wt%) higher than others concentrations at same pressing force 7 ton. In comparing the effect of pressure force on specific capacitance, it increases to 96 F/g for (PVDF, 10 wt%; force, 14 ton) from 59 F/g (PVDF, 10 wt%; force, 7 ton); their corresponding specific power 2285 W/ kg at a specific energy of 5 Wh/kg and 2147 W/ kg at a specific energy of 2.5 Wh/kg. ESR values increase from 0.3 to 1.9 Ω with increase in PVDF and decrease again to 0.5 Ω with increase in pressure force. The results show optimal conditions are 10 wt% of PVDF and higher-pressure force of 14 ton.

In Sixth chapter The specific capacitance of mixture active carbon and carbon nano fibre used as electrode for supercapacitor in this report .the specific capacitance for sample M1(90%AC /10%cnfs) record 207 F/g much higher than sample

M5(10%AC/90%CNF)which record 69 F/g at scan rate 5Mv/s this due to high surface area of sample M1 which record 939m^2/g and 184 m^2/g for sample M5, and the micro volume occupied 71.8% from total volume for sample M1 and 51.8% , 35% , 20 % and 0% for sample M2, M3, M4 and M5 respectively On the other hand, the equivalent series resistance (ESR) contacts resistance are (1.09, 1, 0.7, 0.54 and 0.53 ohms) for samples M1, M2, M3, M4 and M5 respectively. The ESR values decreased as well with increase in CNFs concentrations. This indicate that ESR of all samples are approximation with small differences. The higher ESR related to the sample M1 is due to high quantity of AC is this sample comparing with other samples. This confirms as increase in the CNFs concentration in mixture of these sample ESR decrease due to effectivity of CNFs in sample. At frequency 0.1 Hz specific capacitance is 201,114,100, 64 and 50 F/g for all sampleM1, M2, M3, M4and M5 respectively. When the frequency increases the specific capacitance decrease because as frequency increase the supercapacitors starts works as resistors at high frequency. The phase angles are found to be -78°, -81, -66°, -77° and 78° at low frequency 0.01Hz for sample (M1, M2) and at 0.1 Hz for (M3, M4 and M5). In general, phase angle approach to -90° confirms better capacitive performance and rapid charge discharge process. The sample M1 achieved specific energy of 7.1 Wh/kg and specific power of 3040 W/kg on the other hand sample M5 achieved specific energy 2.3Wh/kg and specific power 3320W/kg at same current density 4 A/g. the relation time constant value ranging from 12.5 s for sample M1 to 1.02 s for sample M5. These results show excellent electrochemical properties of high energy density and power output, therefore very promising for application in the scenarios where high-power output as well as high energy capacity is required.

Future work

Several results reported here need further investigation. Some suggestions for future work are listed below:

1- Investigate the effect of gas flow rate (nitrogen) during carbonization and activation prosses.
2- Study mixture AC/CNFS with solid electrolyte.
3- Investigate the effect of different pore structure and pore size distribution on the electrochemical performance by using solid electrolyte based capacitors.
4- Even though the carbon electrode has a huge surface area, most of the area has not been utilized due to pore size limitation. Future research should be directed to alter the pore size distribution and to engineer an electrode with a pre-determined or controlled pore size.
5- To improve the capacitance utilization. Surface properties of the carbon materials using SEM, TEM and Raman spectroscopic techniques should be studied.
6- Optimize the mass ratio mass positive electrode / mass positive electrode to give better performance such as higher energy density and longer cycle life.
7- Study the self-discharge mechanism, looking for perfect electric isolater to protect self discharge mechanism

Publications referred to in the thesis

The work presented in this thesis is based on the following publicationsin peer-reviewed journals, referred to in the text by their Roman numerals. The papers are appended at the end of the thesis

I. Article 1. Flexible supercapacitors based on low-cost tape casting of high dense carbon nanofibers.
II. Article 2 Impact of PVDF concentration and pressing force on performance of symmetric CNFs based supercapacitors. (Electrochemica Acta)

Contribution to the papers

I. I am the main author of Paper I. Flexible supercapacitors based on low-cost tape casting of high dense carbon nanofibers.

II. I am the main author of Paper II. Impact of PVDF concentration and pressing force on performance of symmetric CNFs based supercapacitors. (Electrochemica Acta)